

Johannes Graspentner, BSc

# **Correlations and Spin-Orbit Coupling in a Two-Band Hexagonal Lattice**

## **MASTER'S THESIS**

to achieve the university degree of

Diplom-Ingenieur

Master's degree programme: Physics

submitted to

**Graz University of Technology**

Supervisor

Assoc.Prof. Dipl.-Ing. Dr.techn. Markus Aichhorn

Institute of Theoretical and Computational Physics



## **AFFIDAVIT**

I declare that I have authored this thesis independently, that I have not used other than the declared sources/resources, and that I have explicitly indicated all material which has been quoted either literally or by content from the sources used. The text document uploaded to TUGRAZonline is identical to the present master's thesis.

---

Date

---

Signature



# Abstract

In 2004 it was possible for the first time to create a two-dimensional material, namely Graphene. Hence, the interest in the physics of such materials increased rapidly. Their possible application in spintronic devices due to topological effects were promising. However, in the one-band model of Graphene the band gap in the topological insulating state is due to second order perturbations and therefore, very small compared to room temperature. Only a two-band model, like passivated Bismuthene, with a local spin-orbit coupling could produce a sufficiently large band gap to be applicable to devices. In this thesis we perform a DFT calculation on passivated Bismuthene, where only the  $p_x$ - and  $p_y$ -orbitals remain at the Fermi level. These two bands are further used as the two-band model where a local SOC term can be applied. The correlations of such a system depending on the interaction are investigated. Furthermore, we compare the method where a local SOC term is added to the Hamiltonian of the DFT calculation, to the method of treating spin-orbit coupling already at the DFT level. Spin-orbit coupling is the reason why non-trivial topological effects appear in two-dimensional materials. Regarding topological aspects, the topological invariant is determined and the prediction that correlations stabilize the topological insulating phase is verified.



# Kurzfassung

Im Jahr 2004 war es erstmals möglich, ein zweidimensionales Material, nämlich Graphen, herzustellen. Im Zuge dessen, hat das Interesse an der Physik derartiger Materialien rasch zugenommen. Ihre mögliche Anwendung in spintronischen Geräten aufgrund topologischer Effekte war vielversprechend. Im Ein-Band-Modell von Graphen ist die Bandlücke des topologischen Isolators jedoch auf Störungen zweiter Ordnung zurückzuführen und daher im Vergleich zur Raumtemperatur sehr gering. Nur ein Zwei-Band-Modell wie passiviertes Bismuthene mit einer lokalen Spin-Bahn-Kopplung könnte eine ausreichend große Bandlücke erzeugen, um für Anwendung zu finden. In dieser Arbeit führen wir eine DFT-Berechnung für passiviertes Bismuthene durch, bei dem nur die Orbitale  $p_x$  und  $p_y$  am Fermi-Niveau verbleiben. Diese zwei Bänder werden in Folge als Zwei-Band-Modell verwendet, dem ein lokaler SOC-Term hinzugefügt werden kann. Die Korrelationen eines solchen Systems in Abhängigkeit von der Wechselwirkung werden untersucht. Darüber hinaus vergleichen wir die Methode, bei der ein lokaler SOC-Term zum Hamiltonian der DFT-Berechnung hinzugefügt wird, mit der Methode bei der Spin-Bahn-Kopplung bereits auf der DFT-Ebene behandelt wird. Spin-Bahn-Kopplung ist der Grund, warum nicht-triviale topologische Effekte in zweidimensionalen Materialien auftreten. Es wird die topologische Invariante bestimmt und die Vorhersage bestätigt, dass topologische Isolatoren durch Korrelationen stabilisiert werden.





# Acknowledgments

I own my gratitude to Prof. Markus Aichhorn, for supervising my thesis and for giving me the opportunity to work on this interesting topic. I am especially thankful for his support and the remarkable clarity of his to answer any kind of questions.

I want to thank Gernot Kraberger and Robert Triebl for their willingness to share all the knowledge they have about DMFT and their support with any kinds of problems I was facing.

I am thankful to Markus Richter for all the fruitful conversations we had and to Hermann Schnait for all the help he provided when I faced problems with certain program codes.

I truly enjoyed working at the Institute of Theoretical and Computational Physics, and want to thank all its members for providing a good working atmosphere at the office. Especially, the interesting discussions during lunch-break, made working here a real pleasure.

I am very grateful to the TRIQS-team for providing such a useful and compact tool to perform DMFT calculations (and more), and making it available to everyone.

Last, but not least I want to thank my family and friends, for their ever lasting support and encouragement. Especially, I want to thank my parents for their financial support and unconditional reassurance.



# Contents

<b>Introduction</b>	<b>1</b>
<b>1 Computational Principles</b>	<b>3</b>
1.1 Density Functional Theory . . . . .	4
1.2 Wannier Functions . . . . .	6
1.2.1 Projection Method . . . . .	6
1.2.2 Maximally localised Wannier functions . . . . .	7
1.2.3 Disentanglement . . . . .	9
1.3 Dynamical Mean Field Theory . . . . .	10
<b>2 Physical Principles</b>	<b>14</b>
2.1 Two-Dimensional Hexagonal Lattice . . . . .	14
2.2 Spin-Orbit Coupling . . . . .	16
2.2.1 SOC in $p_x$ - $p_y$ -orbitals . . . . .	18
2.3 Topology . . . . .	20
2.3.1 Berry Phase and Chern invariant . . . . .	20
2.3.2 Time reversal symmetry . . . . .	23
2.3.3 $\mathbb{Z}_2$ invariant . . . . .	24
2.3.4 Soluyanov-Vanderbilt method to determine the $\mathbb{Z}_2$ invariant . . . . .	26
2.3.5 Topology in interacting systems . . . . .	28
<b>3 One Band Model (Graphene)</b>	<b>31</b>
3.1 DFT + DMFT . . . . .	31
3.1.1 First try: Wien2k + dmftproj . . . . .	32
3.1.2 DFT calculations (VASP) . . . . .	35
3.1.3 Projections . . . . .	37

---

3.1.4	DMFT . . . . .	39
3.2	Results . . . . .	45
<b>4</b>	<b>Two Band Model (Bismuthene)</b>	<b>48</b>
4.1	DFT . . . . .	50
4.1.1	DFT-calculation for Bismuthene . . . . .	51
4.1.2	DFT-calculation for Bismuthene including spin-orbit coupling . . . . .	51
4.2	Projections . . . . .	52
4.2.1	wannier90 for Bismuthene . . . . .	53
4.2.2	Wannier90 for Bismuthene with spin-orbit coupling . . . . .	55
4.3	DMFT . . . . .	56
4.3.1	DMFT for Bismuthene . . . . .	57
4.3.2	DMFT for Bismuthene with spin-orbit coupling included in the DFT calculation . . . . .	62
4.3.3	DMFT for Bismuthene with additional local spin-orbit coupling term . . . . .	71
4.3.4	Z2Pack . . . . .	79
4.3.5	Variation of the interaction parameter $U$ . . . . .	83

# Introduction

In the last years two dimensional materials with their topological properties have attracted a lot of interest. Especially, topologically insulating states have been investigated. A physical key principle to obtain a topological insulator is the spin-orbit coupling. One promising material since it was discovered is Graphene. Kane and Mele have developed a toy model to study topological properties in Graphene. To do so they had to include a next-nearest-neighbour hopping which originates from second order perturbation theory. Therefore, the topological band gap is rather small compared to room temperature. Hence, the possible applications of such a material for spintronic devices are limited.

In order to achieve a larger band gap, the spin-orbit coupling has to come from a direct local SOC term. Such a term can only exist when the major contribution in the bands around the Fermi level comes from the  $p_x$ - and  $p_y$ -orbitals. Hence, a material has to be found where the  $p_z$ -orbitals are shifted away and only  $p_x$ - and  $p_y$ -orbitals remain at the Fermi level. As proposed by Freitas *et al.* a single layer of Bismuth atoms could be passivated with the addition of Hydrogen atoms [1]. Besides from becoming a planar hexagonal material, the  $p_z$ -orbitals are shifted away and it can be treated with an effective two-band model where a local spin-orbit term can be applied. Another method realized by Reis *et al.* would be to put the Bismuthene layer on a SiC substrate which leads to the same result [2].

Since correlations occur due to interaction, it does not suffice to solely perform DFT calculations but one has to use a method that is suited to treat interacting systems, like DMFT. Hence, an approach where DFT and DMFT are combined shows good results for the properties of correlated materials. In this thesis a possible way is investigated to perform DFT+DMFT calculations on the two-band model of an  $sp^2$ -hybrid material. In this process, the difficulties of choosing a correct projection method shall be discussed. Since there are different ways to include spin-orbit coupling in the calculations, two

possible approaches have been performed. The question at hand was if DFT+DMFT calculations, where spin-orbit coupling was already introduced in the DFT level lead to the same results as the DFT+DMFT calculations where a local SOC term is added to the local Hamiltonian after the DFT calculation is converged. Additionally, the possible effect of each method on this topological insulator and its topological invariant is investigated.

A further kind of insulator is the Mott insulator. It results from large on-site interaction energies. To deal with such phenomena again the approach of combining DFT and DMFT is the method of choice for correlated materials. In this thesis, not only the Mott insulator and the topological insulator state are regarded separately, but also the transition from the topological insulating Bismuthene to a Mott insulating material.

# Chapter 1

## Computational Principles

In order to describe molecules and solids, one has to solve the Schrödinger equation

$$\hat{H} |\Psi_\nu\rangle = E_\nu |\Psi_\nu\rangle, \quad (1.1)$$

with the following Hamiltonian, given in atomic units:

$$\hat{H} = -\frac{1}{2} \sum_i \nabla_i^2 - \sum_\alpha \frac{1}{2M_\alpha} \nabla_\alpha^2 - \sum_{\alpha,i} \frac{Z_\alpha}{|\mathbf{r}_i - \mathbf{R}_\alpha|} + \sum_{i<j} \frac{1}{|\mathbf{r}_i - \mathbf{r}_j|} + \sum_{\alpha<\beta} \frac{Z_\alpha Z_\beta}{|\mathbf{R}_\alpha - \mathbf{R}_\beta|} \quad (1.2)$$

Here  $\alpha$  and  $\beta$  denote the indices of the nuclei, and  $i$  and  $j$  are the indices over all electrons considered in the system.  $\mathbf{R}$  and  $\mathbf{r}$  stand for the positions of the nuclei and electrons, respectively, and  $M$  and  $Z$  are the mass and the charge of the nuclei. The first two terms describe the kinetic energy of the electrons and the nuclei. The last three terms describe the nuclei-electron, electron-electron and the nuclei-nuclei Coulomb interaction. Since the exact solution to this problem can only be found for the Hydrogen atom, one has to introduce approximations such as the Born-Oppenheimer-approximation. For this simplification it is taken into account, that the nuclei have way more mass compared to the electrons and are therefore, treated as being fixed with the electrons moving around in the resulting steady potential-surfaces. By doing so the second term in eq. (1.2) drops out and the last term becomes a constant. A constant just gives a shift to the energy levels and can therefore be dropped out. In the end, the Hamiltonian in Born-Oppenheimer-approximation has the following structure:

$$\hat{H} = \underbrace{\frac{1}{2} \sum_i \nabla_i^2}_{\text{kinetic energy}} - \underbrace{\sum_{\alpha,i} \frac{Z_\alpha}{|\mathbf{r}_i - \mathbf{R}_\alpha|}}_{\text{lattice potential}} + \underbrace{\sum_{i<j} \frac{1}{|\mathbf{r}_i - \mathbf{r}_j|}}_{\text{interaction}}. \quad (1.3)$$

Even with this simplification, the electron-electron term is still difficult to treat. However, to describe materials properly it is not possible to simply neglect it, especially if one has to deal with semiconductors or insulators since the free electron model is usually only applicable to metals. The following sections are going to deal with methods to solve this many-body problem.

## 1.1 Density Functional Theory

The following summary on density functional theory is based on the book by Gerd Czycholl [3] and Walter Kohn's nobel lectures [4]. The most common method, nowadays, to calculate the electronic structure of materials is density functional theory. Making use of the Born-Oppenheimer-approximation it does not solve the electron-electron interaction term explicitly but rather treats this phenomenon with an effective one-particle potential. In order to express this potential, only the total electron density is needed. This depends on three variables rather than  $3 * N$ , like it would be necessary for the full many-body-wave function. The dependence on the density only arises from the two Hohenberg-Kohn-theorems [5]. The first theorem states: "*The ground-state energy from Schrödinger's equation is a unique functional of the electron density*". This implies that there is a one-to-one correspondence between the ground-state wave function and the ground-state electron density. In other words, the ground-state electron density defines all properties including the ground-state energy and wave-function. However, the exact form of the energy-density-functional  $E\{n(\mathbf{r})\}$  remains unknown. This functional can be split up into the form of:

$$E\{n(\mathbf{r})\} = T\{n(\mathbf{r})\} + V\{n(\mathbf{r})\} + U\{n(\mathbf{r})\}, \quad (1.4)$$

where the first two parts represent the density-functionals of the kinetic and the potential energy and the last term stands for the density-functional of the exchange energy. Approximating the kinetic part with the one-particle wave function dependence and splitting the exchange-energy functional into a well-known electrostatic exchange term and an unknown exchange-correlation functional, the energy-density-functional can be



written as:

$$E\{n(\mathbf{r})\} = \sum_{i=1}^{N_e} -\frac{\hbar^2}{2m} \int d^3r \psi_i^*(\mathbf{r}) \nabla^2 \psi_i(\mathbf{r}) + \int d^3r V(\mathbf{r}) n(\mathbf{r}) + \frac{e^2}{2} \int d^3r \int d^3r' \frac{n(\mathbf{r}) n(\mathbf{r}')}{|\mathbf{r} - \mathbf{r}'|} + E_{xc}\{n(\mathbf{r})\}, \quad (1.5)$$

with the density being a sum over one-particle densities of the Kohn-Sham orbitals:

$$n(\mathbf{r}) = n_s(\mathbf{r}) = \sum_i |\psi_i(\mathbf{r})|. \quad (1.6)$$

To get the ground state, it is necessary to minimize this functional which is done by a variation with respect to  $\psi_i^*$ . The resulting differential equations are known as the Kohn-Sham-Equations [6]:

$$\left\{ -\frac{\hbar^2}{2m} \nabla^2 + V(\mathbf{r}) + \int d^3r' \frac{e^2}{|\mathbf{r} - \mathbf{r}'|} n(\mathbf{r}') + \frac{\delta E_{xc}\{n(\mathbf{r})\}}{\delta n(\mathbf{r})} \right\} \psi_i(\mathbf{r}) = \epsilon_i \psi_i(\mathbf{r}). \quad (1.7)$$

These equations are exact as long as all the exchange-correlation effects and the exchange parts of the kinetic energy are dealt with in the unknown functional  $E_{xc}\{n(\mathbf{r})\}$ . Since the density we want to know also influences the effective one-particle potential these equations have to be solved in a self-consistent way.

The result of DFT calculations strongly depends on the choice of the exchange-correlation functional, which can only be approximated. There are many different functionals for different applications, however, most popular among them are the local-density-approximation LDA and the generalized-gradient-approximation GGA:

$$E_{xc}^{LDA} = \int d^3r \epsilon_{xc}[n(\mathbf{r})] n(\mathbf{r})$$

$$E_{xc}^{GGA} = \int d^3r \epsilon_{xc}[n(\mathbf{r}), \nabla n(\mathbf{r})] n(\mathbf{r}) \quad (1.8)$$

As can be seen, the LDA approach only depends on the local densities, whereas the generalized-gradient-approximation additionally depends on the gradient of the density. If one is interested in periodic lattices like it is the case in this thesis, then the wave functions can be expressed according to Bloch's theorem as:

$$\psi_{\mathbf{k}\nu}(\mathbf{r}) = e^{i\mathbf{k}\cdot\mathbf{r}} u_{\mathbf{k}\nu}(\mathbf{r}), \quad (1.9)$$

where  $\nu$  denotes the band index of a certain Bloch-band,  $\mathbf{k}$  the crystal momentum inside the Brillouin zone and the  $u_{\mathbf{k}\nu}(\mathbf{r})$  represent lattice-periodic functions.

## 1.2 Wannier Functions

Usually, after performing a DFT calculation the electronic ground state is expressed in terms of Bloch orbitals as mentioned before. Since the translation operator of the crystal commutes with the Hamiltonian in momentum space the Bloch functions are maximally localized in  $\mathbf{k}$ -space. There are, however, issues, such as strong correlation effects, where one needs localization in real space. Therefore, another representation of the ground state is needed. One that might be more useful, is the basis set of Wannier functions (WFs). The following procedure to obtain Wannier functions closely follows the article of Nicola Marzari, David Vanderbilt et al. [7]. The Wannier function for the  $n$ -th band and real-space lattice vector  $\mathbf{R}$  can be obtained by Fourier-transforming the Bloch functions

$$|\omega_{\mathbf{R}in}\rangle = \sum_{\mathbf{k}} e^{i\mathbf{k}\cdot\mathbf{R}_i} \sum_{\nu} U_{\mathbf{k}}^{n\nu} |\psi_{\mathbf{k}\nu}\rangle. \quad (1.10)$$

Here  $U_{\mathbf{k}}^{n\nu}$  stands for a unitary transformation. This unitary transformation is allowed since it changes the states only by a phase factor. Hence, the WFs are not uniquely defined, a fact that can be exploited in generating maximally localized WFs.

### 1.2.1 Projection Method

Tracing back to the analysis of Cloizeaux (1964) [8] is the simple approach of constructing localized WFs with a smooth gauge in momentum space by projection. This is done by starting with  $N$  localized trial orbitals  $t_n(\mathbf{r})$ . These orbitals do not need to represent the wanted WFs well. They can be some analytic functions that only need to roughly be located where the wanted WFs are going to be centred. Via the known Bloch manifold we can project these trial functions to a  $\mathbf{k}$ -formulation which is in general not orthonormal:

$$|\phi_{n\mathbf{k}}\rangle = \sum_{m=1}^N |\psi_{m\mathbf{k}}\rangle \langle\psi_{m\mathbf{k}}|t_n\rangle. \quad (1.11)$$

We define a matrix  $A_{\mathbf{k}}$  with the matrix elements being  $\langle\psi_{m\mathbf{k}}|t_n\rangle$ . With the help of this matrix the overlap matrix  $(S_{\mathbf{k}})_{mn} = \langle\phi_{m\mathbf{k}}|\phi_{n\mathbf{k}}\rangle = (A_{\mathbf{k}}^\dagger A_{\mathbf{k}})_{mn}$  can be computed. This overlap matrix is now used to obtain the orthonormalized Bloch-like states:

$$|\tilde{\psi}_{n\mathbf{k}}\rangle = \sum_{m=1}^N |\phi_{m\mathbf{k}}\rangle (S_{\mathbf{k}}^{-1/2})_{mn}. \quad (1.12)$$

These states are related to the previous Bloch functions via a unitary transformation and yield well localized WFs when inserted in equation (1.10), for the trial states have already been localized where expected.

### 1.2.2 Maximally localised Wannier functions

It is possible to enforce maximum localization. In 1997 Marzari and Vanderbilt [9] developed this procedure to enforce localization by introducing a localization criterion. The localization functional is defined as:

$$\begin{aligned} \Omega &= \sum_n [\langle\mathbf{0}n|r^2|\mathbf{0}n\rangle - \langle\mathbf{0}n|r|\mathbf{0}n\rangle^2] \\ &= \sum_n [\langle r^2 \rangle_n - \bar{\mathbf{r}}_n^2]. \end{aligned} \quad (1.13)$$

It measures the sum of quadratic spreads of the  $N$  WFs around their centres in the home unit cell. In the next step the  $\Omega$  has to be expressed in momentum space, a procedure far from trivial since the position operators are ill-defined in momentum space. How do we get the reciprocal space representation? First, it can be shown, that the localization functional from above can be split into a gauge-invariant and a gauge-dependent part:

$$\Omega = \Omega_I + \tilde{\Omega}, \quad (1.14)$$

with both parts being positive definite:

$$\Omega_I = \sum_n \left[ \langle\mathbf{0}n|r^2|\mathbf{0}n\rangle - \sum_{\mathbf{R}m} |\langle\mathbf{R}m|\mathbf{r}|\mathbf{0}n\rangle|^2 \right] \quad (1.15)$$

$$\tilde{\Omega} = \sum_n \sum_{\mathbf{R}m \neq \mathbf{0}n} |\langle \mathbf{R}m | \mathbf{r} | \mathbf{0}n \rangle|^2. \quad (1.16)$$

The connection between the localization functional and reciprocal space is given by the matrix elements of the position operator shown by Blount (1962):

$$\langle \mathbf{R}n | \mathbf{r} | \mathbf{0}m \rangle = i \frac{V}{(2\pi)^3} \int d\mathbf{k} e^{i\mathbf{k} \cdot \mathbf{R}} \langle u_{n\mathbf{k}} | \nabla_{\mathbf{k}} | u_{m\mathbf{k}} \rangle \quad (1.17)$$

and

$$\langle \mathbf{R}n | r^2 | \mathbf{0}m \rangle = -\frac{V}{(2\pi)^3} \int d\mathbf{k} e^{i\mathbf{k} \cdot \mathbf{R}} \langle u_{n\mathbf{k}} | \nabla_{\mathbf{k}}^2 | u_{m\mathbf{k}} \rangle. \quad (1.18)$$

To determine these matrix elements one uses Bloch orbitals that are defined on a regular  $\mathbf{k}$ -grid as well as finite differences to calculate the derivatives. For any smooth function in  $\mathbf{k}$ -space the gradient takes the form:

$$\nabla f(\mathbf{k}) = \sum_{\mathbf{b}} w_b \mathbf{b} [f(\mathbf{k} + \mathbf{b}) - f(\mathbf{k})] + O(b^2), \quad (1.19)$$

and a similar expression for the squared gradient. Here the  $\mathbf{b}$  vector connects a  $\mathbf{k}$ -point to one of its neighbours,  $w_b$  represents an appropriate geometric factor. In order to calculate the matrix elements, it is only necessary to know the overlaps between the Bloch orbitals at neighbouring  $\mathbf{k}$ -points:

$$M_{mn}^{\mathbf{k}, \mathbf{b}} = \langle u_{m\mathbf{k}} | u_{n, \mathbf{k} + \mathbf{b}} \rangle. \quad (1.20)$$

Knowing this overlap matrix provides all the information needed for the localization process. Hence, no further dependence on the DFT calculation has to be taken into account. There are of course many different functionals that can be used, however, since for this thesis we used wannier90 to get maximally localized Wannier functions, only the expression of Marzari and Vanderbilt (1997) shall be reviewed. With the overlap-matrix, the two parts of the functional can be expressed as:

$$\Omega_I = \frac{1}{N} \sum_{\mathbf{k}, \mathbf{b}} w_b \left( N - \sum_{mn} |M_{mn}^{\mathbf{k}, \mathbf{b}}|^2 \right) \quad (1.21)$$

and

$$\begin{aligned}\tilde{\Omega} &= \frac{1}{N} \sum_{\mathbf{k}, \mathbf{b}} w_{\mathbf{b}} \sum_{m \neq n} |M_{mn}^{(\mathbf{k}, \mathbf{b})}|^2 \\ &+ \frac{1}{N} \sum_{\mathbf{k}, \mathbf{b}} w_{\mathbf{b}} \sum_n \left( -\Im \ln M_{nn}^{(\mathbf{k}, \mathbf{b})} - \mathbf{b} \cdot \bar{\mathbf{r}}_n \right)^2.\end{aligned}\tag{1.22}$$

Now it is time to take a look at the localization procedure. Basically, the minimized functional is found by varying the spread functional from above by an infinitesimal gauge transformation:  $U_{mn}^{(\mathbf{k})} = \delta_{mn} + dW_{mn}^{(\mathbf{k})}$ . With  $dW$  being an anti-hermitian matrix, such that:  $|u_{n\mathbf{k}}\rangle \longrightarrow |u_{n\mathbf{k}}\rangle + \sum_m dW_{mn}^{(\mathbf{k})} |u_{m\mathbf{k}}\rangle$ . To arrive at Marzari and Vanderbilt's definition of the gradient it is necessary to make following definitions:

$$q_n^{(\mathbf{k}, \mathbf{b})} = \Im \ln M_{nn}^{(\mathbf{k}, \mathbf{b})} + \mathbf{b} \cdot \bar{\mathbf{r}}_n\tag{1.23}$$

$$R_{mn}^{(\mathbf{k}, \mathbf{b})} = M_{mn}^{(\mathbf{k}, \mathbf{b})} M_{nn}^{(\mathbf{k}, \mathbf{b})*}\tag{1.24}$$

$$T_{mn}^{(\mathbf{k}, \mathbf{b})} = \frac{M_{mn}^{(\mathbf{k}, \mathbf{b})}}{M_{nn}^{(\mathbf{k}, \mathbf{b})}} q_n^{(\mathbf{k}, \mathbf{b})}.\tag{1.25}$$

Hence, the gradient of the spread-functional takes the form:

$$\begin{aligned}G^{(\mathbf{k})} &= \frac{d\Omega}{dW^{(\mathbf{k})}} \\ &= 4 \sum_{\mathbf{b}} w_{\mathbf{b}} \left( \frac{R_{mn}^{(\mathbf{k}, \mathbf{b})} - R_{mn}^{(\mathbf{k}, \mathbf{b})\dagger}}{2} - \frac{T_{mn}^{(\mathbf{k}, \mathbf{b})} + T_{mn}^{(\mathbf{k}, \mathbf{b})\dagger}}{2i} \right).\end{aligned}\tag{1.26}$$

With this gradient it is straightforward to evaluate the minimal spread and therefore, the maximum localization.

### 1.2.3 Disentanglement

The procedure described so far is performing very well as long as the Bloch bands of interest are separated from the other bands by a certain band gap. However, most of the time, and especially in this thesis, one has to deal with the case where the desired bands lie within the energy-range of other bands. In literature these bands are referred to as entangled bands. In order to be able to perform the localization procedure it is now necessary to specify the Bloch states that can be used to form the  $N$  Wannier

functions. This selection of a subspace is achieved by adapting the projection procedure from the previous subsection. The difference is that now we want to extract a subspace of  $N$  smoothly varying Bloch-like states from a bigger set of  $N_{\mathbf{k}} \geq N$  Bloch bands [10]. Again, one starts from a set of  $N$  trial orbitals  $g_n(\mathbf{r})$  and projects them onto the set of  $N_{\mathbf{k}}$  eigenstates:

$$|\Phi_{n\mathbf{k}}\rangle = \sum_{m=1}^{N_{\mathbf{k}}} |\psi_{m\mathbf{k}}\rangle \langle \psi_{m\mathbf{k}} | g_n \rangle, \quad (1.27)$$

where now the overlap matrix  $(A_{\mathbf{k}})_{mn} = \langle \psi_{n\mathbf{k}} | g_m \rangle$  takes a rectangular form of shape  $N_{\mathbf{k}} \times N$ . After orthonormalizing the wanted  $J$  Bloch-like states the result is:

$$|\tilde{\psi}_{n\mathbf{k}}\rangle = \sum_{m=1}^J |\Phi_{m\mathbf{k}}\rangle (S_{\mathbf{k}}^{-1/2})_{mn}, \quad (1.28)$$

with  $(S_{\mathbf{k}})_{mn}$  being defined as  $\langle \Phi_{m\mathbf{k}} | \Phi_{n\mathbf{k}} \rangle_V = (A_{\mathbf{k}}^\dagger A_{\mathbf{k}})_{mn}$  like in Equation (1.12) but with rectangular matrices  $A_{\mathbf{k}}$ . Usually, this technique suffices the requirements to obtain Wannier functions that represent the Bloch bands quite well. However, by treating Hybrid-states it can be necessary to enforce certain Bloch states to be preserved in the projected manifold. In the Wannier90 code [11] this is referred to as setting an inner frozen window. It is done by defining an energy range where one can be certain that only the wanted states appear.

### 1.3 Dynamical Mean Field Theory

As already mentioned in previous sections, it is necessary to find other ways than DFT to treat strongly-correlated materials in a correct manner. In this thesis, the focus lies on the treatment of the materials with DFT + DMFT, where DMFT stands for dynamical mean field theory which is a quantum mechanical extension of the classical mean-field theory. The summary on the principles of DMFT is based on the PhD thesis of Gernot Kraberger [12] and of Robert Triebl [13], as well as on the review [14].

Since in strongly correlated materials it does not suffice to consider only the electronic hopping between the sites one also has to include interaction terms in the Hamiltonian, leading to the so called Hubbard-model:

$$H = \sum_{\langle mm' \rangle, \sigma} t_{mm'} (c_{m\sigma}^\dagger c_{m'\sigma} + c_{m'\sigma}^\dagger c_{m\sigma}) + U \sum_m n_{m\uparrow} n_{m\downarrow}, \quad (1.29)$$

where the last term denotes the interaction Hamiltonian  $H_{int}$ , which may take different forms in different applications. In equation (1.29) the interaction is only taken into account for one band, which in this thesis is used for the single-band model of Graphene. In the two-band model of Bismuthene a Kanamori-Hamiltonian of following form has to be used:

$$\begin{aligned} H_{int} = & U \sum_m n_{m\uparrow} n_{m\downarrow} + U' \sum_{m \neq m'} n_{m\uparrow} n_{m'\downarrow} + (U' - J_H) \sum_{m < m', \sigma} n_{m\sigma} n_{m'\sigma} \\ & + J_H \sum_{m \neq m'} c_{m\uparrow}^\dagger c_{m'\downarrow}^\dagger c_{m\downarrow} c_{m'\uparrow} + J_H \sum_{m \neq m'} c_{m\uparrow}^\dagger c_{m\downarrow}^\dagger c_{m'\downarrow} c_{m'\uparrow}. \end{aligned} \quad (1.30)$$

In DMFT this Hubbard model is self-consistently mapped onto the Anderson impurity model. The Anderson impurity model describes a strongly correlated impurity that is coupled to a non-interacting bath via hopping. The Hamiltonian describing the Anderson impurity model can be written as:

$$H = \sum_{mm', \sigma} \epsilon_{loc}^{mm'} c_{m\sigma}^\dagger c_{m'\sigma} + H_{int} + \sum_{p, \sigma} \epsilon_{bath}^p a_{p\sigma}^\dagger a_{p\sigma} + \sum_{mp, \sigma} \zeta_{mp} (c_{mp}^\dagger a_{p\sigma} + a_{p\sigma}^\dagger c_{m\sigma}). \quad (1.31)$$

Here, the first two terms represent the local Hamiltonian of the impurity, the third term is the non-interacting Hamiltonian of the bath and the last term stands for the hybridization between the impurity and the bath. Making use of Green's functions one can express the non-interacting Green's function as:

$$G_0^{AIM}(z) = (z - H_0^{AIM})^{-1}. \quad (1.32)$$

In this formulation  $z$  denotes a complex frequency, namely  $z = \omega + i0^+$  or  $z = i\omega_n$  for retarded- or Matsubara Green's function, respectively, with Matsubara frequencies  $\omega_n = (2n + 1)\pi/\beta$  at inverse temperature  $\beta$ . One can not further break down this Green's function into an impurity part and a bath part since these are coupled via the hybridization. However, by effectively integrating out the bath it is possible to obtain the hybridization function  $\Delta(z)$  with the matrix-elements:

$$\Delta^{mm'}(z) = \sum_p \frac{\zeta_{mp}^* \zeta_{m'p}}{z - \epsilon_{bath}^p}. \quad (1.33)$$

Finally, it is possible to explicitly write down the impurity part of the non-interacting Green's function  $G_0^{AIM}$ :

$$G_0(z) = (z - \epsilon_{loc} - \Delta(z))^{-1}. \quad (1.34)$$

By inserting this non-interacting impurity Green's function and an interaction Hamiltonian  $H_{int}$  to an impurity solver like the CTHYB from TRIQS as used in this Thesis, one obtains the interacting impurity Green's function  $G_{imp}(z)$ , which has to fulfill the Dyson equation:

$$(G_{imp}(z))^{-1} = (G_0(z))^{-1} - \Sigma(z). \quad (1.35)$$

In the Dyson equation the Self-energy  $\Sigma(z)$  takes care of all the electron-electron interactions. Until now only the impurity Green's function has been considered. Let us now write down the lattice Green's function, in other words the Green's function of the Hubbard model. Without an interaction the lattice Green's function takes the form:

$$G_{latt,0}(\mathbf{k}, z) = (z - \epsilon_{\mathbf{k}} + \mu)^{-1}, \quad (1.36)$$

where  $\mu$  denotes the chemical potential, adjusted in such a way that it ensures the correct electron filling. Obeying the Dyson equation the interacting lattice Green's function is given by:

$$G_{latt}(\mathbf{k}, z) = (z - \epsilon_{\mathbf{k}} + \mu - \Sigma(\mathbf{k}, z))^{-1}. \quad (1.37)$$

The correctly weighted  $\mathbf{k}$ -sum over the first Brillouin zone gives the local Green's function:

$$G_{loc}(z) = \sum_{\mathbf{k}} G_{latt}(\mathbf{k}, z). \quad (1.38)$$

Until here all considerations have been exact. The approximation done within DMFT is to set the self-energy of the lattice  $\Sigma(\mathbf{k}, z)$  equal to the local self-energy of the Anderson impurity model. However, this leaves the hybridization function  $\Delta(z)$  still unknown. Therefore, one has to iteratively perform a self-consistent calculation, such that the



local Green's function equals the impurity Green's function:

$$G_{loc}(z) = \frac{1}{N_{\mathbf{k}}} \sum_{\mathbf{k}} G_{latt}(\mathbf{k}, z) = G_{imp}(z). \quad (1.39)$$

When Equations (1.35) and (1.39) are combined one gets the connection between the lattice and the impurity model, where an effective non-interacting Green's function  $G_0$ , which is the analogue to the classical Weiss field, can be determined:

$$G_0 = ((G_{loc}(z))^{-1} + \Sigma(z))^{-1}. \quad (1.40)$$

As soon as the  $G_{loc}$  matches  $G_{imp}$  the self-consistency criterion is fulfilled

All the different steps of a DMFT self-consistency cycle summarized:

- Choosing an initial self energy  $\Sigma$ .
- Extracting the local Green's function  $G_{loc}$ , using Eq. (1.37) and Eq. (1.38).
- Using equation (1.40) to map the problem onto the impurity model.
- Calculate a  $G_{imp}$  and an updated  $\Sigma$  with the impurity solver.
- Checking whether Equation (1.39) is fulfilled, if not, perform another iteration starting with the obtained  $\Sigma$ .

# Chapter 2

## Physical Principles

### 2.1 Two-Dimensional Hexagonal Lattice

This section is based on the second chapter (The Atomic Structure of Graphene and Its Few-layer Counterparts) of the book [15].

In order to be able to form a two-dimensional hexagonal lattice, atoms need to have a specific electronic structure. They should provide four valence electrons, where the  $s$ -orbital hybridizes with two of the  $p$ -orbitals forming three  $sp^2$ -orbitals that are at an angle of  $120^\circ$  to each other plus a  $p_z$ -orbital that is perpendicular to the plane spanned by the  $sp^2$ -orbitals. The lattice vectors describing the unit cell are:

$$\mathbf{a}_1 = a \begin{pmatrix} 1 \\ 0 \end{pmatrix} \quad \mathbf{a}_2 = \frac{a}{2} \begin{pmatrix} -1 \\ \sqrt{3} \end{pmatrix}. \quad (2.1)$$

For Graphene,  $a = (2.46 \pm 0.02)\text{\AA}$  and for Bismuthene,  $a = (5.51 \pm 0.02)\text{\AA}$ . From these basis vectors one gets the reciprocal lattice vectors spanning the Brillouin zone:

$$\mathbf{b}_1 = \frac{2\pi}{a} \begin{pmatrix} -1 \\ 0 \end{pmatrix} \quad \mathbf{b}_2 = \frac{4\pi}{a} \begin{pmatrix} 1 \\ \sqrt{3} \end{pmatrix}. \quad (2.2)$$

In the first Brillouin zone the high symmetry points are  $\Gamma$ ,  $K$  and  $M$ ,

$$\mathbf{\Gamma} = \begin{pmatrix} 0 \\ 0 \end{pmatrix} \quad \mathbf{K} = \frac{2\pi}{a} \begin{pmatrix} 1 \\ \sqrt{3} \end{pmatrix} \quad \mathbf{M} = \frac{\pi}{a} \begin{pmatrix} 1 \\ 0 \end{pmatrix}. \quad (2.3)$$

Along the path that is obtained from connecting these points, usually the bandstructure

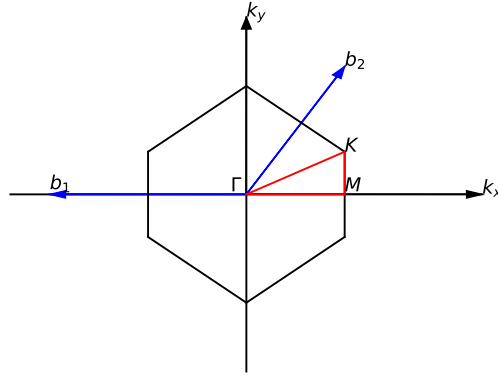


**Figure 2.1:** The first Brillouine zone of a two dimensional hexagonal lattice, including the high symmetry points.

can be evaluated. Among the high-symmetry points the K-points, also known as the Dirac points are by far the most interesting ones. In these points the conduction and the valence bands touch in a linear dispersion relation. This dispersion is a result of massless charge-carriers at the K-points. The unique band structure gives rise to interesting topological effects, which we want to further investigate in this thesis. In Graphene it is the  $p_z$ -orbital that gives rise to the Dirac cone around the Fermi level. Therefore, the calculations of electronic properties break down to a simple one band model. However, with only one band, it is not possible to apply a direct local SOC term in order to investigate non-trivial topological effects. This can be only achieved by considering an imaginary next-nearest-neighbour hopping, as shown by Haldane. The resulting band gap of such a topological insulator is rather small compared to room temperature. Since there is growing interest in two dimensional materials with topological properties and larger bandgaps, materials with higher atomic number attract the attention.

Therefore, in this thesis we want to take a closer look at Bismuthene. It does not only have a higher atomic number, but also provides the possibility to add a direct local SOC term. This spin-orbit term gives rise to a large gap, and hence a stable topological insulator. In order to add a local SOC term, one needs to have at least a two-band model. In Bismuthene all three  $p$ -orbitals contribute at the Fermi level. In order to obtain the wanted two-band model of  $p_x$ - $p_y$ -orbitals, it is essential to shift away the  $p_z$ -orbitals from the Fermi level by some chemical modification. One way to do so, proposed by Liu *et al.* is to passivate Bismuthene with Hydrogen atoms. By shifting away the  $p_z$ -orbitals, it creates a planar two-dimensional hexagonal structure. Since the

$s$ -orbitals are lower in energy and show a smaller bandwidth than in Graphene and the  $p_z$ -orbitals can be assumed to be filled, one only needs to consider the two-band model of  $p_x$ - $p_y$ -bands.

## 2.2 Spin-Orbit Coupling

The following derivation of the spin-orbit coupling term from relativistic quantum mechanics is based on the book of J.Bjorken [16] and the summary in Gernot Krabergers PhD thesis [12].

Of course there are semi-classical models that give a good estimate of spin-orbit coupling. However, its origin is of relativistic nature. Therefore, it is not sufficient to continue with the Schrödinger equation, where the energy-momentum relation is given by  $E = p^2/2m$ , but it is important to use Einstein's relation from special relativity:

$$E^2 = m^2c^4 + c^2p^2. \quad (2.4)$$

Since the energy takes a quadratic form in this relation, a new quantum mechanical equation had to be found, leading to the relativistic Dirac equation:

$$i\hbar\frac{\partial\psi}{\partial t} = \frac{c}{i}\sum_i\alpha_i\frac{\partial\psi}{\partial x_i} + \beta mc^2\psi = H\psi. \quad (2.5)$$

To ensure the dispersion relation from eq. (2.4), the quantities  $\alpha_i$  and  $\beta$  need to obey the following restrictions:

$$\begin{aligned} \alpha_i\alpha_j + \alpha_j\alpha_i &= 2\delta_{ij} \\ \alpha_i\beta + \beta\alpha_i &= 0 \\ \beta^2 &= 1. \end{aligned} \quad (2.6)$$

It can be easily seen that  $\alpha_i$  and  $\beta$  have to be matrices. There are different representations, but here the most common one, namely the Dirac representation will be used:

$$\alpha_i = \begin{pmatrix} 0 & \sigma_i \\ \sigma_i & 0 \end{pmatrix} \quad \beta = \begin{pmatrix} \mathbb{1} & 0 \\ 0 & -\mathbb{1} \end{pmatrix} \quad (2.7)$$

where the  $\sigma_i$  denote the Pauli matrices:

$$\sigma_x = \begin{pmatrix} 0 & 1 \\ 1 & 0 \end{pmatrix} \quad \sigma_y = \begin{pmatrix} 0 & -i \\ i & 0 \end{pmatrix} \quad \sigma_z = \begin{pmatrix} 1 & 0 \\ 0 & -1 \end{pmatrix} \quad (2.8)$$

and  $\mathbb{1}$  is the unity matrix. To derive an expression for the spin-orbit coupling, we are going to use the Dirac equation describing a hydrogen-like atom:

$$H\psi = \left[ c \sum_i \alpha_i p_i + \beta mc^2 + v \right] \psi = \tilde{E}\psi. \quad (2.9)$$

It is useful to break down the four-index Dirac spinors  $\psi$  into a two indexed vector of two-index components:

$$\psi = \begin{pmatrix} \phi \\ \chi \end{pmatrix}. \quad (2.10)$$

Inserting into eq. (2.9) one ends up with two coupled equations of the form:

$$\begin{aligned} c(\boldsymbol{\sigma} \cdot \mathbf{p})\chi &= (E - v)\phi \\ c(\boldsymbol{\sigma} \cdot \mathbf{p})\phi &= (E + 2mc^2 - v)\chi, \end{aligned} \quad (2.11)$$

where  $E = \tilde{E} - mc^2$  represents the energy on top of the rest energy  $mc^2$ . Here, it is assumed that time derivative, kinetic energy and electrostatic energy are small compared to the rest energy. Hence, the  $\phi$  component is approximated as being much larger than the  $\chi$  component. This approximation was first used by Pauli. Therefore, combining the coupled equations leads to the so called Pauli equation:

$$\frac{1}{2m}(\boldsymbol{\sigma} \cdot \mathbf{p})K(\boldsymbol{\sigma} \cdot \mathbf{p})\phi + v(\mathbf{r})\phi = E\phi, \quad (2.12)$$

for the larger  $\phi$  component, with  $K \equiv \left[ 1 + \frac{E-v(\mathbf{r})}{2mc^2} \right]^{-1}$ . This equation can be rewritten by using Einstein's sum convention as well as the relation  $\sigma_i \sigma_j = \delta_{ij}\mathbb{1} + i\epsilon_{ijk}\sigma_k$  in the following form:

$$\left[ \frac{1}{2m}\mathbf{p}K \cdot \mathbf{p} + \frac{i}{2m}\boldsymbol{\sigma} \cdot (\mathbf{p}K \times \mathbf{p}) + v(\mathbf{r}) \right] \phi = E\phi. \quad (2.13)$$

The first term, which is independent of spin, describes the so called scalar-relativistic kinetic energy. The second term, however, is spin dependent and represents the spin-orbit coupling (SOC). Most of the times the  $K$  of eq. (2.13) is just approximated.

Furthermore, the  $K$  of the scalar-relativistic term does not necessarily have to be the same as the  $K$  of the SOC-term.  $K$  can be approximated by an expansion in  $\frac{E-v(\mathbf{r})}{2mc^2}$ , which is a reasonable choice since  $mc^2 \gg E-v(\mathbf{r})$ . If only the zeroth order is considered, the SOC-term would become zero due to the crossproduct of  $\mathbf{p}$ , resulting in the non-relativistic Schrödinger equation. Obviously, the  $K$  needs to be at least expanded to first order  $K \approx 1 - \frac{E-v(\mathbf{r})}{2mc^2}$ , to be able to treat spin-orbit coupling. This leads to the weak relativistic approximation of eq. (2.13):

$$\left[ \frac{\mathbf{p}^2}{2m} - \frac{1}{4m^2c^2} [\mathbf{p}(E - v(\mathbf{r})) \cdot \mathbf{p}] + \frac{i}{4m^2c^2} \sigma \cdot (\mathbf{p}v(\mathbf{r}) \times \mathbf{p}) \right] \phi = [E - v(\mathbf{r})]\phi, \quad (2.14)$$

which can be rearranged further in terms of spin  $\mathbf{s} = \sigma\hbar/2$  and orbital angular momentum  $\mathbf{l} = \mathbf{r} \times \mathbf{p}$ :

$$\left[ \frac{\mathbf{p}^2}{2m} + v(\mathbf{r}) - \frac{\mathbf{p}^4}{8m3c^2} - \frac{1}{4m^2c^2} \frac{dv(r)}{dr} \frac{\partial}{\partial \mathbf{r}} + \frac{1}{2m^2c^2} \frac{1}{r} \frac{dv}{dr} (\mathbf{l} \cdot \mathbf{s}) \right] \phi = E\phi. \quad (2.15)$$

We can see that this represents the Schrödinger equation (first two terms) plus corrections due to relativity. The third term deals with the mass increase, the fourth term is the so called Darwin term, only affecting  $s$ -orbitals and the last term finally denotes the spin-orbit coupling in the well known form. The prefactor of the SOC is usually denoted as  $\lambda$ :

$$\lambda = \frac{1}{2m^2c^2} \frac{1}{r} \frac{dv}{dr} = \frac{Z_N \alpha_F}{2m^2c^2 r^2}, \quad (2.16)$$

with  $\alpha_F$  being the fine-structure constant and the derivative being evaluated like in a hydrogen-like potential:  $\frac{dv}{dr} = \frac{Z_N}{r^2} \alpha_F$ .

### 2.2.1 SOC in $p_x$ - $p_y$ -orbitals

From the previous section it can be observed, that the relativistic eigenvalue equation, derived by Pauli, is approximated by some, most of the times small, energy shifts and an additional SOC-term in the Hamiltonian of the form:

$$H_{SOC} = \lambda \mathbf{l} \cdot \mathbf{s} = \lambda(l_x s_x + l_y s_y + l_z s_z). \quad (2.17)$$

Here, the  $\mathbf{s} = \hbar\sigma/2$  are proportional to the Pauli matrices, eq. (2.8). Since we are here only interested in the spin-orbit coupling for  $l = 1$  orbitals, we start out from a representation in the spherical basis ( $m_l = -1, m_l = 0, m_l = 1$ ). This basis is easily derived from the well known relations:

$$\begin{aligned} l_z |l, m_l\rangle &= \hbar m_l |l, m_l\rangle \\ l_{\pm} |l, m_l\rangle &= \hbar \sqrt{l(l+1) - m_l(m_l \pm 1)} |l, m_l \pm 1\rangle. \end{aligned} \quad (2.18)$$

Via the definition of the ladder operators used in the second relation  $l_{\pm} = l_x \pm il_y$ , we can easily evaluate the matrix representation of the angular momentum operator:

$$l_x^s = \frac{\hbar}{\sqrt{2}} \begin{pmatrix} 0 & 1 & 0 \\ 1 & 0 & 1 \\ 0 & 1 & 0 \end{pmatrix} \quad l_y^s = \frac{\hbar}{\sqrt{2}} \begin{pmatrix} 0 & i & 0 \\ -i & 0 & i \\ 0 & -i & 0 \end{pmatrix} \quad l_z^s = \hbar \begin{pmatrix} -1 & 0 & 0 \\ 0 & 0 & 0 \\ 0 & 0 & 1 \end{pmatrix}, \quad (2.19)$$

where the index  $s$  stands for spherical basis. Since in this thesis the SOC-term is going to be added manually to an existing local Hamiltonian coming from a wannier90 calculation, this additional term needs to be provided in the same basis representation used in wannier90. Therefore, the angular momenta have to be transformed into a cubic basis ( $p_x, p_y, p_z$ ). We use the following transformation:

$$\begin{aligned} p_x &= \frac{1}{\sqrt{2}} (|l=1, m_l=-1\rangle - |l=1, m_l=1\rangle) \\ p_y &= \frac{i}{\sqrt{2}} (|l=1, m_l=-1\rangle + |l=1, m_l=1\rangle) \\ p_z &= |l=1, m_l=0\rangle, \end{aligned} \quad (2.20)$$

which leads to the following cubic matrix representation:

$$l_x^c = \frac{\hbar}{\sqrt{2}} \begin{pmatrix} 0 & 0 & -i \\ 0 & 0 & 0 \\ i & 0 & 0 \end{pmatrix} \quad l_y^c = \frac{\hbar}{\sqrt{2}} \begin{pmatrix} 0 & -i & 0 \\ i & 0 & 0 \\ 0 & 0 & 0 \end{pmatrix} \quad l_z^c = \hbar \begin{pmatrix} 0 & 0 & 0 \\ 0 & 0 & i \\ 0 & -i & 0 \end{pmatrix}, \quad (2.21)$$

with index  $c$  referring to the cubic basis. Evaluating the spin-orbit operator of eq. (2.17) in cubic basis ( $p_z^\uparrow, p_x^\uparrow, p_y^\uparrow, p_z^\downarrow, p_x^\downarrow, p_y^\downarrow$ ) leads to:

$$\mathbf{l} \cdot \mathbf{s} = \frac{\hbar^2}{2} \begin{pmatrix} 0 & 0 & 0 & 0 & -1 & -i \\ 0 & 0 & i & 1 & 0 & 0 \\ 0 & -i & 0 & i & 0 & 0 \\ 0 & 1 & -i & 0 & 0 & 0 \\ -1 & 0 & 0 & 0 & 0 & -i \\ i & 0 & 0 & 0 & i & 0 \end{pmatrix}. \quad (2.22)$$

In neglecting now the  $p_z$  terms since they won't be necessary in our calculations later on we finally arrive at the SOC term of the Hamiltonian for a  $p_x - p_y$  - model:

$$H_{SOC} = \lambda \frac{\hbar^2}{2} \begin{pmatrix} 0 & i & 0 & 0 \\ -i & 0 & 0 & 0 \\ 0 & 0 & 0 & -i \\ 0 & 0 & i & 0 \end{pmatrix}. \quad (2.23)$$

## 2.3 Topology

Topology is a section in mathematics that investigates whether geometric properties of an object can be smoothly deformed or not. The most common picture to explain topology is the mug that can be deformed into a doughnut. Since the mug has only one hole in its surface (the handle) it can obviously be smoothly reshaped into a doughnut. However, it would never be possible to deform a sphere into a torus without ripping an additional hole into its surface. Therefore, the sphere and the torus are distinguished by an integer topological invariant. Those surfaces, which can be transformed into one another without adding any holes, are said to be topological equivalent and share the same topological invariant. Although, this invariant does not play a role in this thesis, the topological invariants treated in the following are going to be quite similar, though more abstract. This section is based on chapter 1 (Topological Band Theory and the  $\mathbb{Z}_2$  invariant) of the book [17].

### 2.3.1 Berry Phase and Chern invariant

The quantum-mechanical wave functions are well defined up to an arbitrary phase that is physically meaningless since it drops out in the expectation values. However, in topological band theory, a so called Berry phase arises due to the intrinsic phase



ambiguity of a wave function. Berry has shown in 1984 that this geometric phase appears when a system is transformed adiabatically and it can induce observable effects [18] [19].

The following derivation is based on the review of Yoichi Ando [19]. The Schrödinger equation for a given Hamiltonian  $H$  depending on a set of parameters  $\mathbf{a}$  which change adiabatically from the  $t = 0$  value  $\mathbf{R}_0$  is given by:

$$H[\mathbf{a}(t)] |n, \mathbf{a}(t)\rangle = E_n[\mathbf{a}(t)] |n, \mathbf{a}(t)\rangle, \quad (2.24)$$

where  $|n, \mathbf{a}(t)\rangle$  denotes the  $n$ th eigenstate. This state evolves in time following:

$$H[\mathbf{a}(t)] |n, \mathbf{a}_0\rangle (t) = i\hbar \frac{\partial}{\partial t} |n, \mathbf{a}_0\rangle (t). \quad (2.25)$$

Therefore, a state at time  $t$  can be expressed as:

$$|n, \mathbf{a}_0\rangle (t) = \exp \left\{ \frac{i}{\hbar} \int_0^t dt' (i\hbar \dot{\mathbf{a}}(t') \langle n, \mathbf{a}(t') | \nabla_{\mathbf{a}} |n, \mathbf{a}(t')\rangle - E_n[\mathbf{a}(t')]) \right\} |n, \mathbf{a}(t)\rangle. \quad (2.26)$$

The second term of the phase factor denotes the well known dynamical phase factor which is not explicitly time dependent. The first term is called the Berry phase  $\gamma_n$  and it is a non-trivial phase that appears when the parameters  $\mathbf{a}$  change adiabatically.

If the parameters  $\mathbf{a}$  move on a closed loop  $C$  for evolving time from 0 to  $T$ , then the Berry phase can be defined as:

$$\begin{aligned} \gamma_n[C] &\equiv i \int_0^T dt \dot{\mathbf{a}}(t) \langle n, \mathbf{a}(t) | \nabla_{\mathbf{a}} |n, \mathbf{a}(t)\rangle \\ &= i \oint_C d\mathbf{a} \cdot \langle n, \mathbf{a}(t) | \nabla_{\mathbf{a}} |n, \mathbf{a}(t)\rangle \\ &= - \oint_C d\mathbf{a} \cdot \mathbf{A}_n(\mathbf{a}) \\ &= - \int_S d^2\mathbf{a} \cdot \mathbf{F}_n(\mathbf{a}), \end{aligned} \quad (2.27)$$

where the definition  $\mathbf{A}_n(\mathbf{a}) \equiv -i \langle n, \mathbf{a}(t) | \nabla_{\mathbf{a}} |n, \mathbf{a}(t)\rangle$  is the so called Berry connection, from which one can obtain the Berry curvature  $\mathbf{F}_n(\mathbf{a}) \equiv \nabla_{\mathbf{a}} \times \mathbf{A}_n(\mathbf{a})$  via Stokes' theorem. To sum up, the Berry phase represents an accumulated phase factor additional to the dynamical one after completing a closed path in parameter space  $\mathbf{a}$ . Like the vector

potential for electromagnetic fields in real space, the Berry connection plays the role of a gauge field in parameter space.

To describe topological insulators, there is a topological invariant called the Chern number. Its definition for the  $m$ -th band is given by [20]:

$$\begin{aligned} C_m &\equiv \frac{1}{2\pi} \int_{BZ} d^2\mathbf{k} \cdot \mathbf{F}_m(\mathbf{k}) \\ &= \frac{1}{2\pi} \oint_{\partial BZ} d\mathbf{k} \cdot \mathbf{A}_m(\mathbf{k}) \\ &= \frac{1}{2\pi} \gamma_m[\partial BZ], \end{aligned} \quad (2.28)$$

where we have used the relations  $\mathbf{A}_m(\mathbf{k}) = i \langle u_{m\mathbf{k}} | \nabla_{\mathbf{k}} | u_{m\mathbf{k}} \rangle$  and  $\mathbf{F}_m(\mathbf{k}) = \nabla_{\mathbf{k}} \times \mathbf{A}_m(\mathbf{k})$ . Here the  $|u_{m\mathbf{k}}\rangle$  states represent the Bloch states and the wave vector  $\mathbf{k}$  spans the set of parameters that are changed adiabatically. Of course the closed path described by the parameters  $\mathbf{k}$  is given by the edge of the Brillouin zone. Therefore, the Chern number equals the Berry phase up to a factor of  $2\pi$ .

For individual bands the Chern number may not be unique. For degenerate bands it may vary by a gauge. The total Chern invariant is given as the sum of Chern numbers of all occupied bands [21]:

$$C = \sum_m^{\text{occupied}} C_m. \quad (2.29)$$

As long as the gap between the occupied states and the empty bands remains finite this total Chern invariant is a uniquely defined integer.

For the better understanding the simplest model of a two band Hamiltonian can be investigated [17]. The Hamiltonian expressed in terms of Pauli matrices  $\sigma$  takes the form:

$$H_m(\mathbf{k}) = \mathbf{h}_m(\mathbf{k}) \cdot \sigma = \begin{pmatrix} h_z & h_x - ih_y \\ h_x + ih_y & h_z \end{pmatrix}. \quad (2.30)$$

The corresponding eigenvalues are given by  $\pm|\mathbf{h}|$  and therefore the normalized vectors are:  $\hat{\mathbf{h}} = \mathbf{h}/|\mathbf{h}|$ . The vector  $\hat{\mathbf{h}}$  defines a point on a sphere  $S^2$ . Berry has shown in [18] that the Berry phase for a closed loop  $C$  on the surface  $S^2$  is given by  $\gamma_C = \frac{1}{2}(\text{Solid angle swept out by } \hat{\mathbf{h}}(\mathbf{k}))$ .

Since we know the connection between the Berry phase and the Chern number we can

write down the expression for the Chern invariant [17]:

$$C_m = \frac{1}{4\pi} \int d^2k \left[ \frac{\partial \hat{\mathbf{h}}_m(\mathbf{k})}{\partial k_x} \times \frac{\partial \hat{\mathbf{h}}_m(\mathbf{k})}{\partial k_y} \right] \cdot \hat{\mathbf{h}}_m(\mathbf{k}), \quad (2.31)$$

where the Berry curvature is given by half the solid angle element for the mapping  $\hat{\mathbf{h}}(\mathbf{k})$ :  $\mathbf{F}_m(\mathbf{k}) = \frac{1}{2} \left[ \frac{\partial \hat{\mathbf{h}}_m(\mathbf{k})}{\partial k_x} \times \frac{\partial \hat{\mathbf{h}}_m(\mathbf{k})}{\partial k_y} \right] \cdot \hat{\mathbf{h}}_m(\mathbf{k})$ . In words, the Chern invariant describes the number of times  $\hat{\mathbf{h}}(\mathbf{k})$  wraps around the  $S^2$  as a function of  $\mathbf{k}$ .

The Chern number describes classes of Bloch bands when the time reversal symmetry is broken. Details on the time reversal symmetry are provided in the next subchapter. When there is a band gap at the Fermi level and the total Chern number doesn't vanish it is showed in the work of Thouless, Kohmoto, Nightingale and Nijs (TKNN) in 1980 [22], that an integer quantum hall effect can be observed as well as gapless chiral edge states at the boundary of the system. The derivation of this TKNN invariant can be looked up in the review by Yoichi Ando [19] and won't be provided here since in this thesis the  $\mathbb{Z}_2$  invariant plays the major role.

### 2.3.2 Time reversal symmetry

When reversing time, the spin  $\mathbf{S}$  receives a minus sign for it behaves like an angular momentum. The time symmetry  $T$  is represented by an anti-unitary operator  $\Theta$ , which can be represented as [17]:

$$\Theta = e^{-i\pi S_y/\hbar} K = e^{-i\pi \sigma_y/2} K = -i\sigma_y K, \quad (2.32)$$

for spin 1/2 particles.  $S_y$  denotes the spin operator and  $K$  is the operator for complex conjugation. Therefore, when considering the spin 1/2 electrons,  $\Theta$  shows the property  $\Theta^2 = -1$ . Due to this property one faces a constraint known as the Kramer's theorem, that states: A Hamiltonian that is  $T$  invariant, describing a system with an odd number of electrons, possesses energy eigenvalues that are at least two fold degenerate. This can be proven via contradiction: If a non degenerate state  $|\psi\rangle$  would exist, then  $\Theta|\psi\rangle = c|\psi\rangle$  for any constant  $c$ . This would, however, due to the properties of  $\Theta$  imply  $\Theta^2|\psi\rangle = |c|^2|\psi\rangle$ , which is not possible since  $|c|^2 \neq -1$ . This Kramer's degeneracy is simply expressed in the degeneracy of up and down spins for systems without spin-orbit interaction. However, as soon as a spin-orbit interaction is present, non-trivial consequences can be observed.

The Hamiltonian for a system that preserves time reversal symmetry has to satisfy:

$$H(-\mathbf{k}) = \Theta H(\mathbf{k}) \Theta^{-1}. \quad (2.33)$$

Hence, the Bloch waves for momentum  $\mathbf{k}$  have the same energy as for momentum  $-\mathbf{k}$ . If  $\mathbf{k}$  and  $-\mathbf{k}$  are equivalent points in the Brillouin zone, then the bands show a degeneracy at these points. These momenta are also known as time reversal invariant momenta (TRIM).

### 2.3.3 $\mathbb{Z}_2$ invariant

It was already mentioned that the Chern number describes the integer quantum Hall effect. However, a system that shows zero Hall conductivity may still have a non-zero spin Hall conductivity  $\sigma_{xy}^s = \frac{1}{2}(\sigma_{xy}^\uparrow - \sigma_{xy}^\downarrow)$  for an existing spin current  $\mathbf{J}_s \equiv (\hbar/2\pi)(\mathbf{J}_\uparrow - \mathbf{J}_\downarrow)$  [23]. Same as for the Hall conductivity, the spin Hall conductivity can only be a multiple of  $\frac{e}{2\pi}$ , where the multiplication factor is the negative spin Chern number [24]:

$$C^s = \sum_{\sigma} \sigma C^{\sigma} = (C^{\uparrow} - C^{\downarrow})/2. \quad (2.34)$$

The spin Chern number modulo 2 defines the  $\mathbb{Z}_2$  invariant  $\nu$  which describes all the topological spin properties of a system [21]:

$$\nu = C^2 \pmod{2}. \quad (2.35)$$

In order to achieve further insight into the physical meaning of the  $\mathbb{Z}_2$  invariant, consider the definition given by Fu and Kane in their original work [25] for a one dimensional periodic Hamiltonian  $H$  with lattice constant  $a$ . In addition, the Hamiltonian changes adiabatically depending on a periodic pumping parameter  $t$  that is odd under time reversion  $\Theta$ .

$$H[t + T] = H[t] \quad (2.36)$$

From previous chapters we know the expression for the Berry connection:  $\mathbf{A}_m(\mathbf{k}) = -i \langle u_{m\mathbf{k}} | \nabla_{\mathbf{k}} | u_{m\mathbf{k}} \rangle$  as well as the connection between the Wannier functions and the Bloch functions:  $\langle \mathbf{R}n | \mathbf{r} | \mathbf{0}m \rangle = -\frac{V}{(2\pi)^3} \int d\mathbf{k} e^{i\mathbf{k}\cdot\mathbf{R}} \langle u_{n\mathbf{k}} | \nabla_{\mathbf{k}} | u_{m\mathbf{k}} \rangle$ . Obviously, the Berry phase can be connected to the position operator in the Wannier basis. Hence, it is

reasonable to describe the topological properties of the system in terms of Wannier charge centres (WCCs). In the case of the one dimensional model the polarisation  $P^n$  is expressed as:

$$P^n \equiv \langle 0n|x|0n \rangle = \frac{i}{2\pi} \int_{-\pi}^{\pi} dk \langle u_{nk} | \partial_k | u_{nk} \rangle = C_n, \quad (2.37)$$

which denotes the first Chern number  $C_n$ . By summing up all the  $P^n$  one gets the total charge polarization  $P_\rho$ . For adiabatic changes of  $H(t)$  from  $t_1$  to  $t_2$  the change of the charge polarization is given by:

$$P_\rho[t_1] - P_\rho[t_2] = \frac{1}{2\pi} \int_{-\pi}^{\pi} dk (A(t_1, k) - A(t_2, k)). \quad (2.38)$$

This can be expressed in terms of the Berry curvature if one treats  $k$  and  $t$  as two independent coordinates of a two dimensional system:

$$P_\rho[t_1] - P_\rho[t_2] = \frac{1}{2\pi} \int_{-\pi}^{\pi} dk \int_{t_1}^{t_2} F(k, t). \quad (2.39)$$

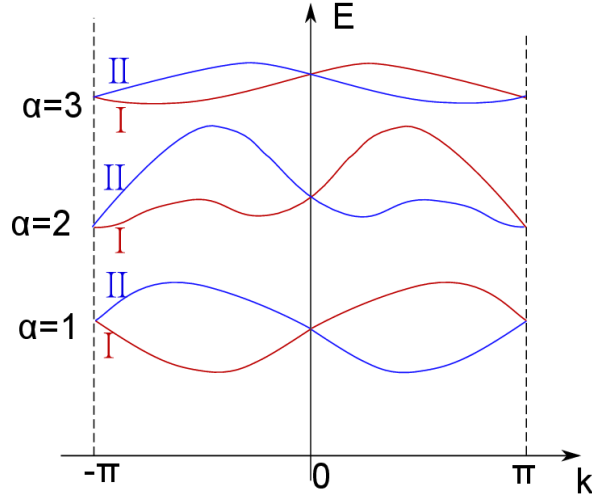


**Figure 2.2:** Kramers pairs of a one dimensional time reversal invariant system. Each level  $\alpha$  consists of two pairs  $I$  and  $II$

Since  $H$  is invariant under time reversion the integration over a full period gives zero and hence the Chern number becomes trivial. Due to the presence of Kramers pairs in a time reversal symmetric system it is sufficient to only evaluate a half period to describe it. These Kramers pairs are obtained through the proposition made by Fu and Kane [25] to separate the total charge polarization in two parts namely up and down

parts. As shown in figure 2.2 each Kramers pair is further distinguished by the label  $s = I, II$ . Hence, the relation between the Bloch waves within one band is:

$$|u_{\alpha,-k}^I\rangle = -e^{i\chi_{\alpha,k}\Theta} |u_{\alpha,-k}^{II}\rangle. \quad (2.40)$$

As a consequence it is possible to split the total charge polarization into the sum of partial polarizations  $P_\rho = P^I + P^{II}$ , with

$$P^s = \frac{1}{2\pi} \int_{-\pi}^{\pi} dk A^s(k) \quad (2.41)$$

$$A^s(k) = i \sum_{\alpha=1}^N \langle u_{\alpha,k}^s | \partial_k | u_{\alpha,k}^s \rangle. \quad (2.42)$$

Even though, for the system at hand the total charge polarization represented by the Chern number turns out to be zero, there is still a way to define a topological invariant in order to describe the topological spin effects. To do so the time reversal polarization needs to be defined as the difference between the partial polarizations:

$$P_\theta \equiv P^I - P^{II}. \quad (2.43)$$

Since it is sufficient to integrate over half a period at the presence of time reversal symmetry the  $\mathbb{Z}_2$  invariant can be defined as:

$$\nu \equiv P_\theta[T/2] - P_\theta[0] \pmod{2}. \quad (2.44)$$

Kane and Fu also provided a method to determine the  $\mathbb{Z}_2$  invariant. However, there is more robust method by Soluyanov and Vanderbilt [26] which is also used in this thesis.

### 2.3.4 Soluyanov-Vanderbilt method to determine the $\mathbb{Z}_2$ invariant

Although, in the original paper [26] the parametrization  $(k, t)$  is used, we are going to stick to the notation  $(k_x, k_y)$ , that Robert Triebl used in his Master thesis [27]. The reason to do so, is that I am only going to investigate two dimensional systems. Hence, to describe the Wannier charge centres we need a hybrid Wannier function, where only one coordinate is transformed from momentum to position space:

$$|R_x k_x n\rangle = \frac{1}{2\pi} \int_{-\pi}^{\pi} dk_x e^{-iR_x k_x} |\psi_{n\mathbf{k}}\rangle. \quad (2.45)$$

As already mentioned, the WCC is given by:

$$\bar{x}_n(k_y) = \langle 0k_y n | \hat{X} | 0k_y n \rangle, \quad (2.46)$$

where  $\hat{X}$  is the x component of the position operator. The expression of the WCC can be further rewritten by taking the connection between the Berry curvature and the Wannier transformation:

$$\bar{x}_n(k_y) = \frac{i}{2\pi} \int_{-\pi}^{\pi} dk_x \langle u_{n\mathbf{k}} | \partial_{k_x} | u_{n\mathbf{k}} \rangle, \quad (2.47)$$

which of course represents the polarization in the  $x$  direction. Inserting into equation (2.44) leads to the  $\mathbb{Z}_2$  invariant:

$$\nu = \sum_{\alpha} [\bar{x}_{\alpha}^I(\pi) - \bar{x}_{\alpha}^{II}(\pi)] - \sum_{\alpha} [\bar{x}_{\alpha}^I(0) - \bar{x}_{\alpha}^{II}(0)]. \quad (2.48)$$

At the points  $k_y = 0$  and  $k_y = \pi$ ,  $\bar{x}_{\alpha}^I$  equals  $\bar{x}_{\alpha}^{II}$  as a consequence of Kramers degeneracy. As already mentioned in previous sections the Wannier functions are not uniquely defined but rather possess a freedom of unitary gauge transformations. This gauge freedom can be used to exploit maximally localized WCCs which is achieved via the same functional as given in (1.15) [7]. The correct transformation of the Bloch bands is finally given by:

$$|\tilde{u}_{mk}\rangle = \sum_n U_{mn}(k) |\tilde{u}_{nk}\rangle. \quad (2.49)$$

Since we are dealing with a periodic lattice, it is possible to relate  $|\tilde{u}_{m0}\rangle$  and  $|\tilde{u}_{m2\pi}\rangle$  via a unitary matrix  $\Lambda$ :

$$|\tilde{u}_{m2\pi}\rangle = \sum_n \Lambda_{mn} |\tilde{u}_{n0}\rangle, \quad (2.50)$$

it is allowed to express the eigenvalues of  $\Lambda$  in terms of complex phases  $\lambda_n = e^{-i\phi_n}$ , where  $|\tilde{u}_{n0}\rangle$  picks up the total phase  $\phi_n$  while evolving from  $k_x = 0$  to  $k_x = 2\pi$  with  $k_y$  still remaining a constant. This phase has a direct relation to the WCC:

$$\bar{x}_n(k_y) = \frac{\phi_n}{2\pi}, \quad (2.51)$$

where the properties of the curves  $\bar{x}_n(k_y)$  represent all the topological properties of the band structures.

To sum up, one simply has to follow the WCC for all Kramers pairs from  $k_y = 0$  to  $k_y = \pi$ . If the same branches intersect again one is dealing with a topologically trivial system. However, a Kramers pair is said to be non trivial for the case that the WCCs at  $k_y = 0$  and  $k_y = \pi$  belong to a different branch. One major drawback is, that due to the discretization of the  $k_y$  values it can be hard to track the WCCs. Therefore, Soluyanov and Vanderbilt [26] proposed to follow the maximum interspace  $z(k_y)$  between the WCCs rather than the curves themselves. Hence, the  $\mathbb{Z}_2$  invariant can be defined as the number of discontinuities of  $z(k_y)$  between 0 and  $\pi$ .

$$\nu = \text{number of discontinuities of } z(k_y) \text{ in } [0, \pi] \quad \text{mod } 2 \quad (2.52)$$

This is a much easier approach since the jump at a discontinuity takes exactly the value 1/2 for two bands whereas the crossing of two bands needs a pretty good resolution to be made out.

### 2.3.5 Topology in interacting systems

In this section we are going to deal with topological invariants in interacting systems. The expression for the Chern number previously mentioned cannot be used for interacting systems, because it is calculated using Bloch states. The first approach to deal with this problem was given by Niu, Thouless and Wu in 1984 [22]. In their definition, they utilize a change of the ground state  $|\psi_0\rangle$  while the boundary conditions are altered. Let's consider a 2D many body system to get further insight. This system should obey general boundary conditions defined by phase shifts  $\phi_x$  and  $\phi_y$ , such that:

$$\psi_0(\dots, x_i + n_x L_x, y_i + n_y L_y, \dots) = e^{i(n_x \phi_x + n_y \phi_y)} \psi_0(\dots, x_i, y_i, \dots). \quad (2.53)$$

Under these circumstances, the Chern number is defined as [22]

$$C = \int_0^{2\pi} \int_0^{2\pi} \frac{d\phi_x d\phi_y}{2\pi i} \left( \left\langle \frac{\partial \psi_0}{\partial \psi_y} \middle| \frac{\partial \psi_0}{\partial \psi_x} \right\rangle - \left\langle \frac{\partial \psi_0}{\partial \psi_x} \middle| \frac{\partial \psi_0}{\partial \psi_y} \right\rangle \right), \quad (2.54)$$

where it is again possible to distinguish between spins to get the  $\mathbb{Z}_2$  invariant or the



spin Chern number. Therefore, the Chern number for the spin combinations takes the form [24]:

$$C^{\sigma\sigma'} = \int_0^{2\pi} \int_0^{2\pi} \frac{d\phi_x^\sigma d\phi_y^{\sigma'}}{2\pi i} \left( \left\langle \frac{\partial\psi_0}{\partial\phi_y^{\sigma'}} \middle| \frac{\partial\psi_0}{\partial\phi_x^\sigma} \right\rangle - \left\langle \frac{\partial\psi_0}{\partial\phi_x^\sigma} \middle| \frac{\partial\psi_0}{\partial\phi_y^{\sigma'}} \right\rangle \right), \quad (2.55)$$

from which the total Chern number  $C = \sum_{\sigma\sigma'} C^{\sigma\sigma'}$  and spin Chern number  $C = \sum_{\sigma\sigma'} \sigma C^{\sigma\sigma'}$  can easily be evaluated.

However, expressions like that may turn out to be hard to calculate. The good news is that by using a formulation of Green's functions it is possible to get another expression of equation (2.54) in terms of a single particle Green's function [22] [28]:

$$C = \frac{\epsilon^{\mu\nu\rho}}{24\pi^2} \int dk_0 \int d^2k \text{Tr}[G\partial_\mu G^{-1}G\partial_\nu G^{-1}G\partial_\rho G^{-1}], \quad (2.56)$$

with  $k_0$  being the real frequencies  $k_0 \equiv \omega \in \mathbb{R}$  and  $G = G(i\omega, \mathbf{k})$  referring to the Matsubara Green's functions taking on the form of matrices. Of course the Greek letters take the integer values  $[0, 1, 2, 3]$  and are summed over according to Einstein's convention. With this formulation a good qualitative measure for topology is ensured even though the numerical evaluation can be demanding, since the derivatives of the Green's functions have to be well known in order to ensure an accurate integration.

Fortunately, Zhong Wang *et al.* came up with a much simpler method where only the Green's function evaluated at  $\omega = 0$  is needed [29] [30] [31]. For  $\omega = 0$  the eigenfunction for a Green's function is:

$$G^{-1}(\omega = 0, \mathbf{k}) |\alpha(\omega = 0, \mathbf{k})\rangle = \mu_\alpha(\omega = 0, \mathbf{k}) |\alpha(\omega = 0, \mathbf{k})\rangle. \quad (2.57)$$

One can see that this expression is similar to the Schrödinger equation with the hamiltonian being substituted by the inverse of the Green's function. Therefore, the Chern numbers are calculated via:

$$C_\alpha = \frac{1}{2\pi} \int_{BZ} d^2\mathbf{k} \cdot \mathbf{F}_\alpha(\mathbf{k}) = \frac{1}{2\pi} \oint_{\partial BZ} d\mathbf{k} \cdot \mathbf{A}_\alpha(\mathbf{k}), \quad (2.58)$$

where as before the Berry curvature is given as  $\mathbf{F}_\alpha(\mathbf{k}) = \nabla_{\mathbf{k}} \times \mathbf{A}_\alpha(\mathbf{k})$  and  $\mathbf{A}_\alpha(\mathbf{k}) = -i \langle \alpha(0, \mathbf{k}) | \nabla_{\mathbf{k}} | \alpha(0, \mathbf{k}) \rangle$  denotes the so called Berry connection, directly determined from the eigenvectors of the interacting system. So rather than Bloch bands, here we have used the eigenfunctions  $|\alpha(\mathbf{k})\rangle$  of the inverse Green's function  $G^{-1}(\omega = 0, \mathbf{k})$  to evaluate the topology of the system. In the work of Wang *et al.* it is shown, that summing up

the  $C_\alpha$ , which belong to the positive eigenvalues results in the same total Chern number as defined in equation (2.29)

$$C = \sum_{\alpha \in R\text{-space}} C_\alpha, \quad (2.59)$$

where R-space presents all the positive eigenvalues  $\mu_\alpha > 0$ .

In other words: Where for non-interacting systems one uses the negative eigenvalues of the Hamilton matrix  $H(\mathbf{k})$  to calculate the topological invariants, in the interacting case these values are determined by the positive eigenvalues of the inverse Green's function  $G^{-1}(\omega = 0, \mathbf{k})$ . Therefore by defining a topological Hamiltonian:

$$H_t(\mathbf{k}) = -G^{-1}(\omega = 0, \mathbf{k}), \quad (2.60)$$

the problem takes an equivalent form and all the methods described for the non-interacting calculation can now be used on the interacting system taking advance of the topological Hamiltonian  $H_t(\mathbf{k})$ .

# Chapter 3

## One Band Model (Graphene)

As already mentioned Graphene won't be able to show any non-trivial effects due to a direct local SOC-term. Nonetheless, it is useful to first start out with this two-dimensional material as a one band model and gain some insight in the calculations before proceeding with the more sophisticated two band model.

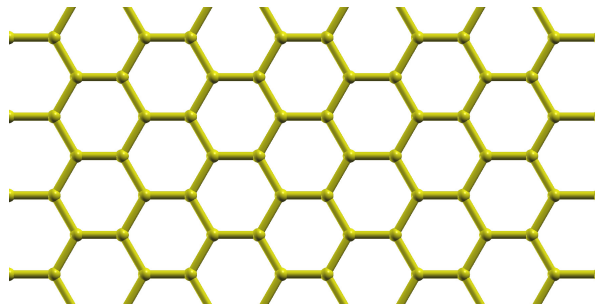


**Figure 3.1:** Structure of a Graphene layer.

### 3.1 DFT + DMFT

Contrary to the tight-binding model, we want to perform ab-initio calculations of Graphene's electronic properties and then proceed with a dynamical mean field calculation after having done a projection onto the  $p_z$ -orbitals which are the most interesting ones as already mentioned. The DFT-codes that are going to be tested are plane wave codes with periodic boundary conditions. That is particularly useful for the calculation of solids since one has periodically repeated unit cells. In the cases present where two dimensional materials are treated, it is important to ensure a sufficiently large vacuum

gap between the atomic planes so that the result correctly represents a mono-layer atomic sheet rather than a bulk. The first approach to do these calculations was to use Wien2k for the band structure calculations and then create the projectors via dmftproj to be able to use TRIQS for the DMFT calculations. While Wien2k did a pretty good job on calculating the Graphene structure, the determination of the structure of Bismuthene exceeded the computational capacities. This is due to the fact that Wien2k other than VASP does not approximate the region around the atoms with pseudo potentials. When it comes to the determination of the projectors, using dmftproj raised another problem. The main issue with dmftproj was that one can only project onto the  $s$ -orbitals or the  $p$ -orbitals as they are. There is no way of taking into account that the orbitals of Graphene (as well as Bismuthene) undergo a  $sp^2$  hybridization and we are only interested in the  $p_z$ -orbitals. This led to wrong fillings in the bands and wrong densities. To solve the problem one is left with two options, either adapt the dmftproj procedure so that it is able to treat  $sp^2$ -hybrid and  $p_z$ -orbitals separated or use wannier90 to create maximally localized Wannier functions. The latter was the method of choice since there is already an existing interface between the finally chosen VASP code and the wannier90 program.

### 3.1.1 First try: Wien2k + dmftproj

In computational material science the most promising way of treating strongly correlated materials is the approach of combining DFT and DMFT. One can do this in a so called single shot manner, where the DFT calculation is performed and the final result is obtained by further application of a DMFT code. However, it is important not to forget that the DMFT calculation may produce corrections in the charge distribution. Therefore, a self-consistent DFT+DMFT loop would be preferable. Hence, the first approach in this thesis was to use Wien2k and dmftproj to generate the Wannier functions, since, other than with wannier90, it would be possible to easily extend the calculation to a self-consistent cycle.

In Wien2k the only input file that needs to be provided is the structure file. The structure of Graphene was taken as a .cif file from the ICSD homepage [32] and converted to the Graphene.struct file.

```

Graphene
H  LATTICE,NONEQUIV.ATOMS  1  194  P63/mmc
MODE OF CALC=RELA  unit=bohr
4.667624  4.667624  30.000000  90.000000  90.000000 120.000000
ATOM  -1: X=0.33333333 Y=0.66666667 Z=0.00000000
MULT= 2          ISPLIT= 4
      -1: X=0.66666667 Y=0.33333333 Z=0.00000000
C  0+          NPT= 781  R0=.000100000 RMT= 1.34      Z:  6.00000
LOCAL ROT MATRIX:  1.0000000  0.0000000  0.0000000
                   0.0000000  1.0000000  0.0000000
                   0.0000000  0.0000000  1.0000000

```

**Listing 3.1:** Graphene.struct file to provide the atomic structure for the Wien2k code.

With the existing .struct file one can make further specifications by running `init_lapw`. Among them, the specification of the muffin-tin radius `RMT` is fundamental for the (L)APW method in order to determine where the plane waves connect to the spherical harmonics describing the atomic spheres. An exchange correlation potential needs to be selected (PBE in the present case [33]) as well as an energy to separate the valence states from the core states. Finally, one has to determine the `RKMAX` value, determining the size of the basis set, and the k-points grid on which the problem is evaluated. A grid of  $49 \times 49 \times 1$  has proven to be more than sufficient to obtain reasonably converged results. After the initialization is completed, the DFT calculation is started via `run_lapw`. The following programs start in a self-consistent loop :

- `x lapw0`: calculates the exchange-correlation potential
- `x lapw1`: solves the Kohn-Sham equations
- `x lapw2`: calculates the charge density
- `x lcore`: calculates the core states
- `x mixer`: mixes the old and the new charge densities

With a converged DFT-cycle the band structure is easily calculated. First, set up the preferred k-path and save it in the `.klist_band` file. Run `x lapw0` and `x lapw1 -band` to solve the Kohn-Sham equations on the new k-path. The `x lapw2 -band` command

should be executed after having prepared the .insp file that deals with several plot specifications. To conclude the band structure calculation x spaghetti needs to be run in order to obtain the bands in dependence of the k points, which can be plotted as figure 3.2. The Wien2k DMFT calculation was performed with the WIEN2k code [34].

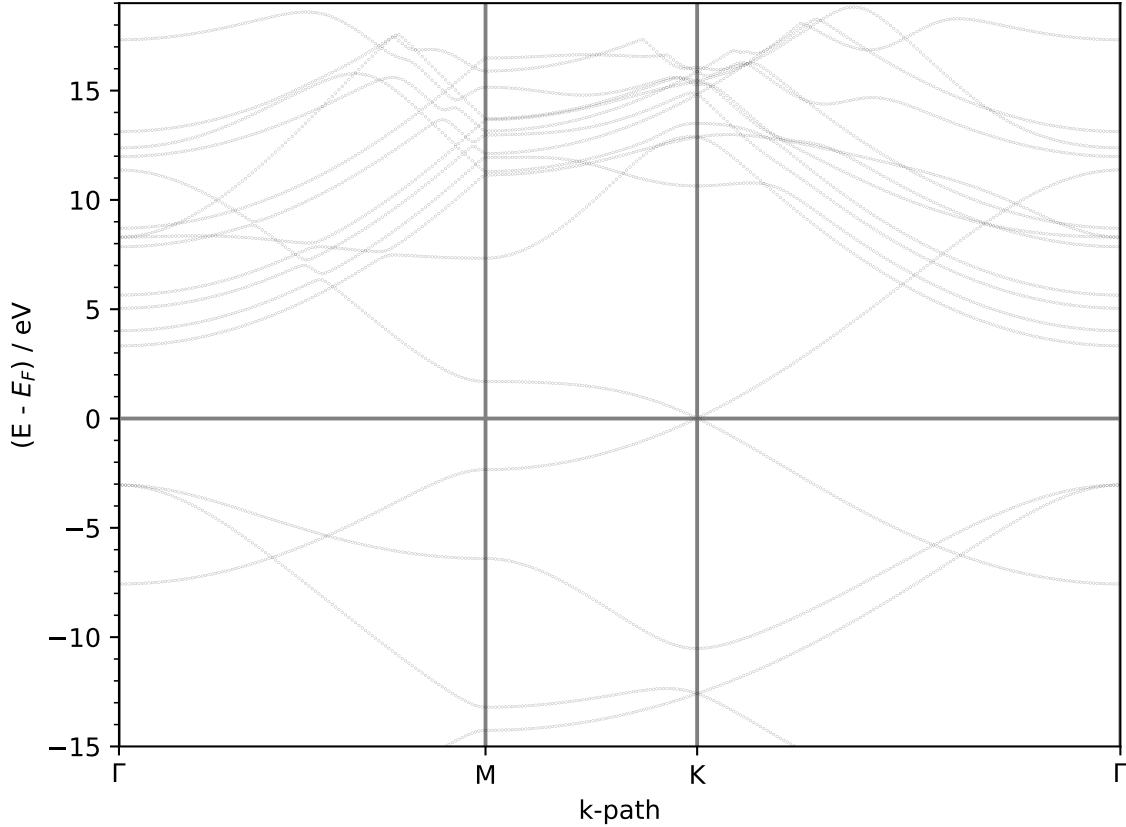


**Figure 3.2:** Band structure of Graphene determined with Wien2k.

With the electronic structure obtained from a Wien2k calculation, one can use dmftproj to generate projective Wannier functions. This means to calculate the projection matrix  $P_{m\nu}(\mathbf{k})$ , such that it satisfies:

$$G_{mn}^{0,\alpha}(i\omega_n) = \sum_{\mathbf{k}} \sum_{\nu} P_{m\nu}^{\alpha}(\mathbf{k}) \frac{1}{i\omega_n - \epsilon_{\mathbf{k}\nu} + \mu} P_{n\nu}^{\alpha*}(\mathbf{k}), \quad (3.1)$$

where  $G_{mn}^{0,\alpha}(i\omega_n)$  is the non-interacting Green's function depending on the Matsubara frequencies  $i\omega_n$ . To write all the necessary quantities into an input file the command x lapw2 -almd has to be invoked. In addition, a .indmftpr file should be provided in order

to determine the local orbitals for the projection. All the necessary files provided, the projectors are calculated by invoking the command `dmftproj`. These projectors could already be converted to run a `dmft` code. However, due to the way the orbitals are implemented in this code, it is not possible to apply it on a Graphene calculation. The problem arises when specifying for which orbitals projections should be generated. In Graphene as well as in Bismuthene, which will be treated later, the  $s$ -orbital hybridizes with the  $p_x$ - and the  $p_y$ -orbitals. Unfortunately, in the `.indmftpr` file one can only choose between the  $s$ -orbitals and/or all  $p$ -orbitals rather than distinguish them. One way to solve this problem, is to modify the code to obtain a linear combination of the orbitals in such a way that the  $sp^2$ -hybrid is guaranteed.

Since the Wien2k calculation was rather time consuming compared to a VASP calculation and due to the fact that in this thesis only single-shot DFT+DMFT calculations need to be done, the obvious step was to execute the DFT calculation with VASP and use `wannier90` to construct the maximally localized Wannier functions since in this code the  $sp^2$ -hybrid is already implemented.

### 3.1.2 DFT calculations (VASP)

The following DFT calculations have been performed using the ab-initio total-energy and molecular-dynamics program VASP (Vienna ab-initio simulation program) developed at the Institut für Materialphysik of the Universität Wien [35] [36].

Since VASP calculations are performed with periodic boundary conditions as already mentioned, one can use Bloch's theorem from eq. (1.9). Writing all cell periodic functions as sum of plane waves leads to the following structure of the wave functions:

$$\psi_{\mathbf{k}\nu}(\mathbf{r}) = \frac{1}{\sqrt{\Omega}} \sum_{\mathbf{G}} c_{\mathbf{G}\mathbf{k}\nu} e^{i(\mathbf{G}+\mathbf{k})\mathbf{r}} \quad (3.2)$$

where one has to choose an energy cut-off  $\frac{\hbar^2}{2m_e} |\mathbf{G} + \mathbf{k}|^2 < E_{cutoff}$  to make the sum over the  $\mathbf{G}$ -vector finite. For two dimensional materials this cut-off has to be chosen rather large in order to have enough plane waves to deal with the vacuum gap. The usage of plane waves is simply due to computational reasons, since the evaluation of  $H|\psi\rangle$  becomes very efficient using Fast Fourier transform (FFT).

Even though there is the limit of an energy cut-off, the number of plane waves would become highly impractical as the atomic number increases. Therefore, instead of exact potentials, VASP uses pseudo-potentials. These treat the core electrons as a frozen

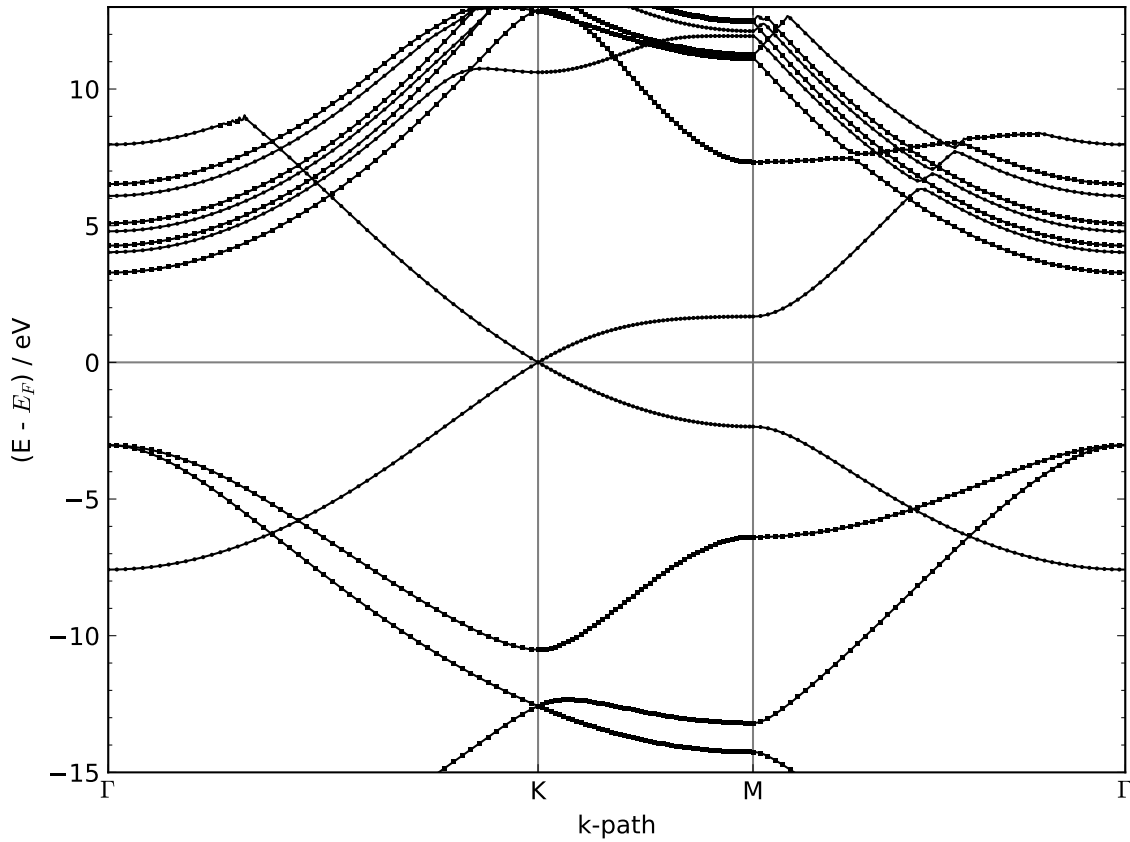


**Figure 3.3:** Band structure of Graphene determined with Vasp.

ensemble, providing a potential for the valence electrons. Hence, VASP was chosen over Wien2k since this saves a lot of computational time.

To run the calculations four files need to be prepared: INCAR, KPOINTS, POSCAR and POTCAR. In the INCAR file one specifies all the different parameters essential for a calculation like the energy cut-off that needs to be set to 700 eV in order to be able to deal with the vacuum gap between the sheets. The KPOINTS file sets the k-points for the calculation which should be sufficiently large in order to get smooth results. In case of the Graphene calculations a Gamma-centred grid of  $49 \times 49 \times 1$  has been used. The POTCAR file contains the pseudopotentials that are used for the different atoms of the material and the POSCAR file includes the information of the atomic structure.

```
Graphene_Vasp
```

```
1.0
```

```
2.4700000000
```

```
0.0000000000
```

```
0.0000000000
```



```

-1.2350000000    2.1390827473    0.0000000000
0.0000000000    0.0000000000    25.0000000000
2
Direct
0.666670000    0.333330000    0.000000000    !C
0.333340000    0.666670000    0.000000000    !C

```

**Listing 3.2:** POSCAR file for Graphene calculations in VASP

In addition, it is necessary to set the LWANNIER90-tag as well as the LWRITE\_MMN\_AMN-tag to TRUE in the INCAR file. Otherwise, one would not be able to perform the wannier90 projections. After convergence was reached a second run was started on a given K-path in order to check the band structure of Graphene, figure 3.3.

Comparing the bandstructure obtained from the Wien2k calculation figure 3.2 with the one of VASP figure 3.3, one can see the perfect agreement for the filled bands. At the energy of 10 eV one can see that VASP kinks the  $p_z$ -orbital, whereas Wien2k depicts all the orbitals as expected. This is probably due to the fact that the energy cut-off for the VASP calculation was chosen smaller than necessary in order to save computational time.

### 3.1.3 Projections

With the Bloch states obtained from the DFT calculations one can proceed by transforming them into Wannier functions using wannier90 [11]. The essential file to be prepared is the wannier90.win file. This is created already in the VASP run because of the LWANNIER90-tag. However, it is important to add some additional information, otherwise wannier90 would not be able to determine which projections should be done.

```

search_shells = 70

num_wann = 2 ! set to NBANDS by VASP
num_bands = 24

fermi_energy = -3.06267351

dis_conv_window = 4
dis_conv_tol = 1.0E-10

```

```

dis_win_min = -15.6
dis_win_max = 9.4

dis_froz_min = -5.9
dis_froz_max = -0.2

Begin Projections
C:pz
End Projections

hr_plot = TRUE

bands_plot = TRUE
begin kpoint_path
G 0.000000 0.000000 0.000000   K 0.333333 0.333333 0.000000
K 0.333333 0.333333 0.000000   M 0.500000 0.000000 0.000000
M 0.500000 0.000000 0.000000   G 0.000000 0.000000 0.000000
end kpoint_path

```

**Listing 3.3:** wannier90.win file for Graphene

For Graphene the important bands are the  $p_z$ -orbitals of the Carbon-atoms. This is defined in the section between Begin and End Projections. The number of bands `num_bands` is taken from the number of Bloch bands obtained in the DFT run, whilst `num_wann` represents the number of Wannier functions to be obtained (two in our case). To further improve the calculation it is possible to define an energy-window in which the wanted bands are expected as well as a frozen window, that represents an energy-range where solely the bands of interest can be found.

As can be seen, there is also a `kpoint_path` defined. Along this path the Wannier Hamiltonian is printed, figure 3.4.

At the Gamma point, the band structures do not match perfectly. The differences near this point are due to the kink from the VASP calculation. Here, wannier90 tries to follow the bands of the DFT results while at the same time orthonormality of the Wannier states should be ensured. However, at the K-points, the interesting physics happens and since we have a maximally localized presentation now there won't be any influence

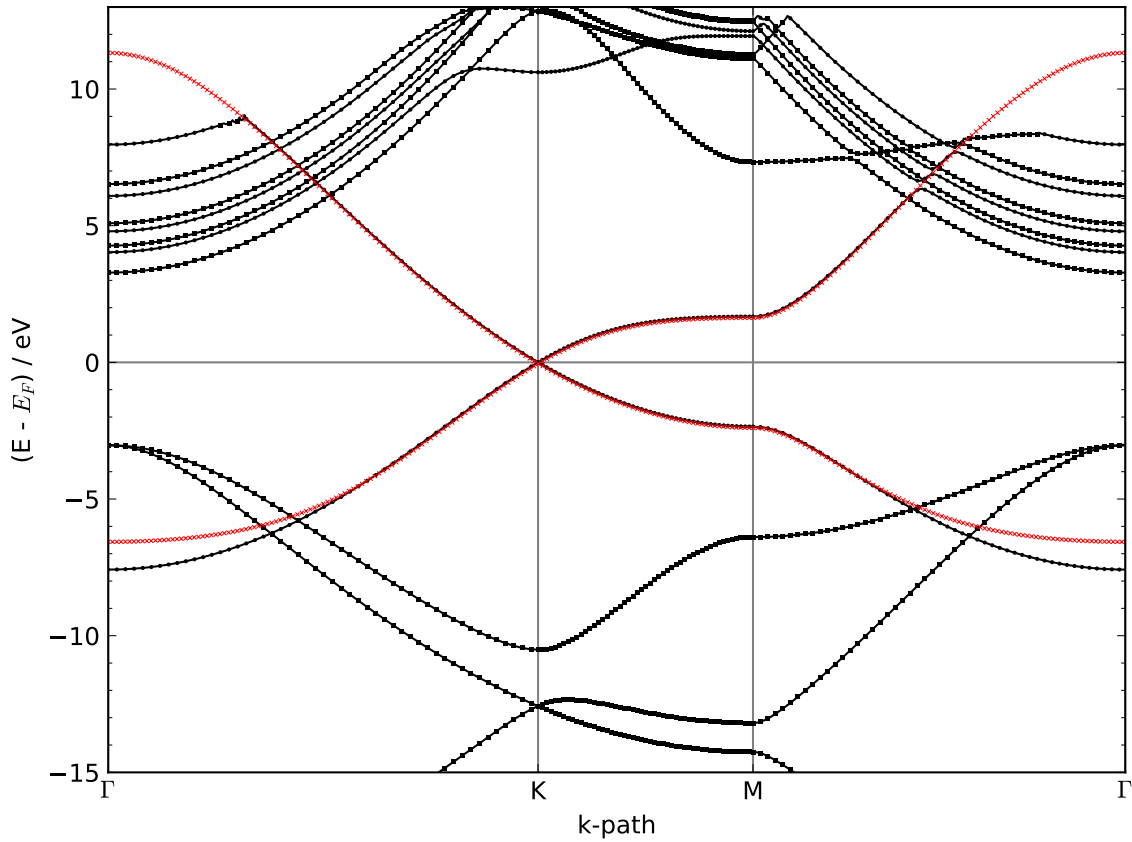


**Figure 3.4:** Band structure of Graphene. The black lines depict the Bloch bands obtained from the VASP DFT calculation. In red the Wannier bands are shown. Around the K-point they match perfectly.

due to discrepancies at the origin of the Brillouin zone.

With setting the `hr_plot`-tag `TRUE` a file is written at the end of the calculation which includes the local Hamiltonian. This is the essential file needed to be passed on to the TRIQS code for running DMFT-calculations.

### 3.1.4 DMFT

The DMFT calculations were carried out with the TRIQS toolbox [37], where the DFT-Tools applications [38] have been used to combine the VASP calculation with the DMFT runs. To create the input HDF5 file one has to provide the `wannier90_hr.dat` file along with a `wannier90.inp` file.

```
0 49 49 1      # specification of the k-mesh
```

```

2.0          # electron density
2           # number of atoms
0 0 1 1 0 0  # atom, sort, l, dim, SO, irep
1 0 1 1 0 0  # atom, sort, l, dim, SO, irep

```

**Listing 3.4:** wannier90.inp file for Graphene

In this file it is crucial to correctly define the correlated shell structure. The SO flag can in a way be ignored. To use calculations with spin-orbit coupling, one has to modify the HDF5 file once it is written. The HDF5 file is obtained via the short script:

```

from pytriqs.applications.dft.converters import
    Wannier90Converter
Converter = Wannier90Converter(seedname = 'wannier90')
Converter.convert_dft_input()

```

**Listing 3.5:** Code to invoke the Wannier90 converter

In order to later on achieve correct results, it is beneficial to add the Fermi energy to the hopping matrix in the HDF5 file, since it is dropped out during the wannier90 calculation. Finally, it is save to perform the DMFT run, as follows:

There are several basic modules that need to be imported to run a TRIQS code:

```

from pytriqs.gf.local import *
from pytriqs.operators import *
from pytriqs.operators.util import *
from pytriqs.archive import *
from pytriqs.archive import HDFArchive
import numpy as np
import pytriqs.utility.mpi as mpi
import os

```

**Listing 3.6:** Modules needed to run a TRIQS DMFT cycle on top of a DFT calculation

Furthermore, the SumkDFT class has to be initialized. This class contains all the basic routines to perform k-space-summation in order to obtain local quantities:

```

from pytriqs.applications.dft.sumk_dft import *
SK = SumkDFT(hdf_file = filename+'.h5')

```

**Listing 3.7:** Initialization of the SumkDFT class

In addition, it is essential to setup an impurity solver, where one has different solvers from which can be chosen. In this case the most suitable solver is the CTHYB solver, that solves the generic problem of an impurity embedded in a conduction bath. However, to do so the structure of the Green's functions needs to be defined. Since we only have the  $p_z$ -orbitals they take a diagonal form of a  $2 \times 2$  matrix with entries for the 'up' and the 'down' spin.

```
gf_struct = {'up': [0], 'down': [0]}
```

**Listing 3.8:** Structure of the Green's functions

```
from pytriqs.applications.impurity_solvers.cthyb import *
S = Solver(beta = beta, gf_struct = gf_struct)
```

**Listing 3.9:** Initialization of the Solver class

In order to perform the self-consistent DMFT loop some further parameters need to be set.

```
filename = 'wannier90'

beta = 40          # Inverse temperatur
n_loops = 15      # Number of cycles to be performed
measure = 25000   # Number of measurements to be made per cycle
dc_type = 1       # Type of formula to treat double-counting
U_min = 6         # Minimum value of the interaction range
U_max = 9         # Maximum value of the interaction range
n_orb = SK.corr_shells[0]['dim']          # Number of orbitals
orb_names = [i for i in range(0,n_orb)]  # Names of the orbitals
orb_hyb = True    # Hybridization of the orbitals
l = SK.corr_shells[0]['l']                # Correlated shells
spin_names = ['up', 'down']              # Names of the spins
```

**Listing 3.10:** Global parameters to be set in order to run a DMFT cycle

Since Graphene is only a one-band model the interaction Hamiltonian is simply obtained by:

```
h_int = Operator()
h_int += U * (n('up',0) * n('down',0))
```

**Listing 3.11:** Interaction Hamiltonian

With all the initializations done the DMFT loop can be set up with the self-consistency condition:

```

for k in range(1, n_loops+1):
    SK.set_Sigma([S.Sigma_iw])
    chemical_potential = SK.calc_mu
    S.G_iw << SK.extract_G_loc()[0]
    G_loc = S.G_iw

    S.G0_iw << S.Sigma_iw + inverse(S.G_iw)
    S.G0_iw << inverse(S.G0_iw)

    G0_tau = S.G_tau.copy()
    for name, g in S.G0_iw:
        G0_tau[name] << InverseFourier(g)
        G0_tau[name].data[:, :, :] =
            np.real(G0_tau[name].data[:, :, :])
        S.G0_iw[name] << Fourier(G0_tau[name])

    S.solve(h_int = h_int,
            length_cycle = 10,
            n_warmup_cycles = 5000,
            n_cycles = measure,
            **p)

    S.G_iw['up'] = 0.5*(S.G_iw['up']+S.G_iw['down'])
    S.G_iw['down'] = S.G_iw['up']
    S.Sigma_iw['up'] = 0.5*(S.Sigma_iw['up']
        + S.Sigma_iw['down'])
    S.Sigma_iw['down'] = S.Sigma_iw['up']

```

**Listing 3.12:** The DMFT loop for Graphene

In the first section the self energy as well as the chemical potential are set and a local Green's function is extracted. This local Green's function is also saved as `G_loc`.

Next, the Dyson equation is applied in order to obtain an effective non-interacting Green's function.

Before solving the impurity problem to obtain the impurity Green's function as well as an updated self energy, the positive imaginary part of the non-interacting Green's function is set to be the same as the inverse negative imaginary part. Due to this enforcement of antisymmetry, numeric errors won't result in failures of the code.

When the impurity problem is solved, spin 'up' and spin 'down' parts are forced to be equal since it is a paramagnetic ordering that is expected. At the end of one cycle the local Green's function is extracted and depending on the convergence a new loop is started or the problem is considered as being solved.

For high frequencies the Green's functions usually show a lot of noise in the data and therefore, need to be fitted. This is done via a tail fit provided by Gernot Kraberger.

```

fit_min_n = f_min[U-2]
fit_max_n = f_max[U-2]
fit_max_moment = 4
if FIT == True:
    fit_known_moments = {}
    for name, g in S.Sigma_iw:
        fit_known_moments[name]
            = TailGf(len(g.indicesL),
                    len(g.indicesR),0,0)
    for name, sig in S.Sigma_iw:
        try:
            S.Sigma_iw[name].fit_tail(
                fit_known_moments[name],
                fit_max_moment,
                -S.Sigma_iw[name].mesh.
                    last_index()-1,
                -fit_min_n-1,
                fit_min_n,
                S.Sigma_iw[name].mesh.
                    last_index(),
                error_omega=2.0)
        except TypeError:

```

```

        S.Sigma_iw[name].fit_tail(
            fit_known_moments[name],
            fit_max_moment,
            -fit_max_n-1,
            -fit_min_n-1,
            fit_min_n,
            fit_max_n)

    S.G_iw[name].tail
        = inverse(inverse(S.G0_iw[name].tail)
            - S.Sigma_iw[name].tail )

```

**Listing 3.13:** Tailfit for Green's functions according to Gernot Kraberger

To take care of double counting, the density needs to be known. The double counting energy along with the chemical potential is written into the SumkDFT class:

```

dm = S.G_iw.density()
SK.calc_dc(dm, U_interact = U, J_hund = J, orb = 0,
           use_dc_formula = dc_type)
SK.save(['chemical_potential', 'dc_imp', 'dc_energ'])

```

**Listing 3.14:** Writing the results into an HDF5 file

Finally, the results need to be saved in a HDF5 file. The structure is such that the Green's functions are saved for every iteration.

```

if mpi.is_master_node():
    with HDFArchive("results_"+filename+"_U{:1d}.h5"
                   .format(U), 'a') as A:
        if 'DMFT_results' not in A:
            A.create_group('DMFT_results')
        if 'Iterations' not in A['DMFT_results']:
            A['DMFT_results'].
                create_group('Iterations')
        A1 = A['DMFT_results']['Iterations']
        if k < 10:
            A1['Giw_it{:1d}'].format(k) = S.G_iw
            A1['Gloc_it{:1d}'].format(k) = G_loc

```



```

A1[ 'G0_iw_it{:1d}'.format(k)] = S.G0_iw
A1[ 'Sigma_it{:1d}'.format(k)]
    = S.Sigma_iw
A1[ 'Gtau_it{:1d}'.format(k)] = S.G_tau
else :
A1[ 'Giw_it{:2d}'.format(k)] = S.G_iw
A1[ 'Gloc_it{:2d}'.format(k)] = G_loc
A1[ 'G0_iw_it{:2d}'.format(k)] = S.G0_iw
A1[ 'Sigma_it{:2d}'.format(k)]
    = S.Sigma_iw
A1[ 'Gtau_it{:2d}'.format(k)] = S.G_tau
A[ 'DMFT_results' ][ 'iteration_count' ] = k

```

**Listing 3.15:** Writing the results into an HDF5 file

## 3.2 Results

Since Graphene as an effective one band material was more or less only a model to test the performance of the programs when calculating correlation effects for ab-initio two dimensional structures, no further physical measurements besides the determination of the Green's function and the self energy have been made. The final impurity Green's function for Graphene takes the form of figure 3.5.

The self energy obtained from the DMFT calculations also satisfies the wanted shape, with negative values for positive Matsubara frequencies. In figure 3.6 there is a small spike in the curve. This is a result of the tail fit not being perfect.

Taking a look at the Fourier transform of the impurity Green's function, figure 3.7, namely  $G(\tau)$  one can see that the bands are half filled as expected since  $G(0) = G(\beta) = -\frac{1}{2}$ .

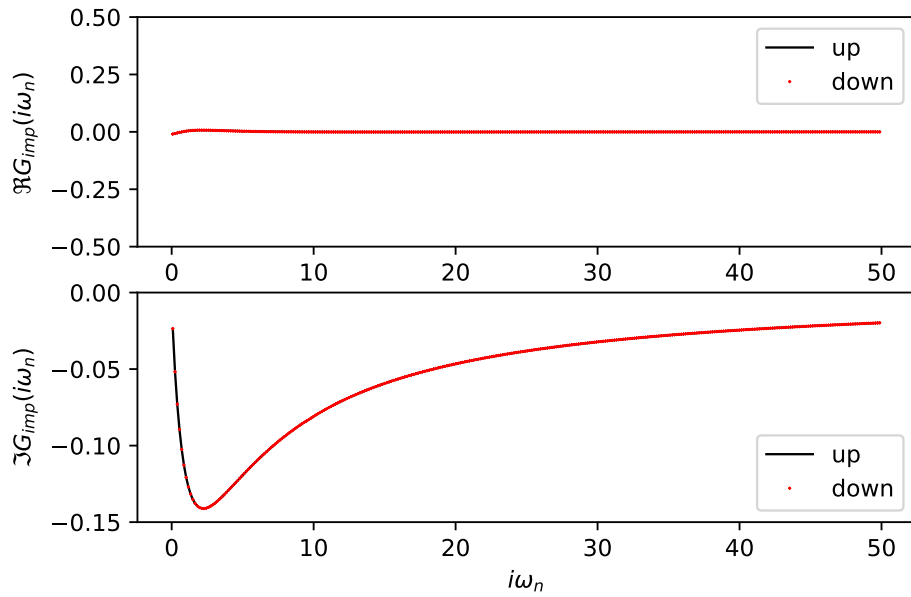


**Figure 3.5:** The real and imaginary part of the Green's function of Graphene. Up and down spin are degenerate as can be seen. Interaction value  $U = 2$ .

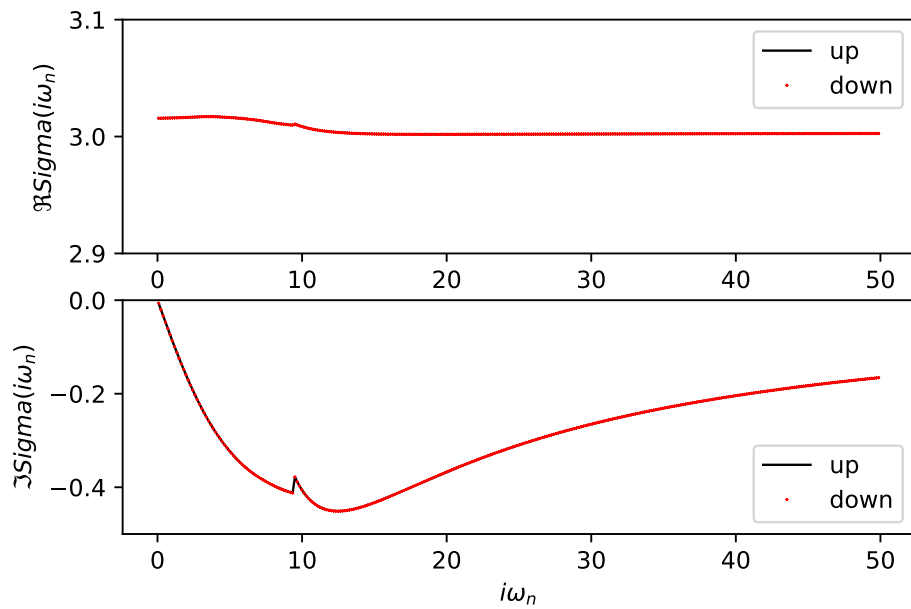


**Figure 3.6:** The real and imaginary part of the self energy function of Graphene. Up and down spin are degenerate as can be seen. Interaction value  $U = 2$ .

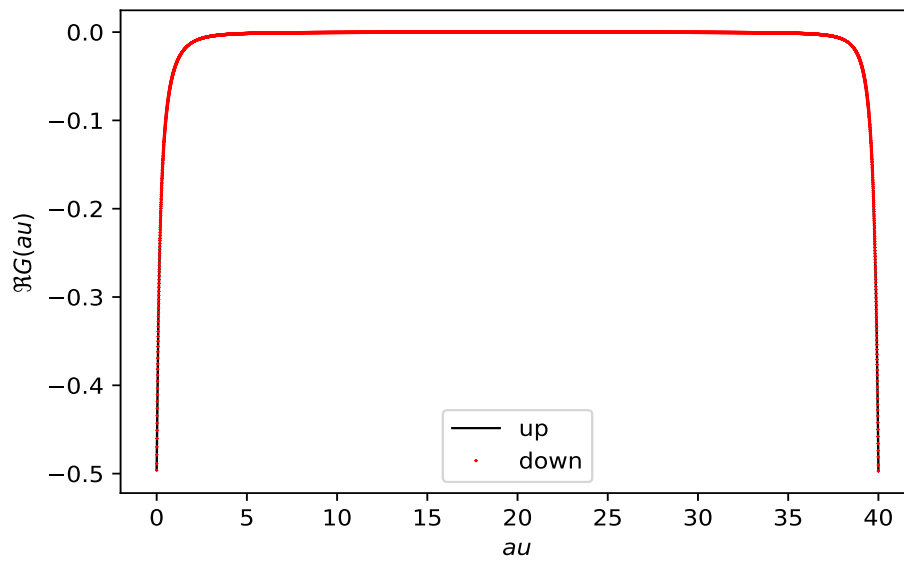


**Figure 3.7:** The real part of the Fourier transform of the impurity Green's function of Graphene. Up and down spin are degenerate as can be seen. The  $\tau$  values go from 0 to the defined beta value 40. Interaction value  $U = 2$ .

# Chapter 4

## Two Band Model (Bismuthene)

Bismuth has one more valence electron than Carbon, therefore, it forms a hexagonal lattice, that is buckled, with all the  $p$ -orbitals being near the Fermi edge. When passivating this sheet of Bismuth atoms with either a suitable substrate or hydrogen, not only the buckling vanishes and it becomes planar, but also the  $p_z$ -orbitals are shifted away from the Fermi energy. This happens because the Hydrogen atom binds with the excess valence electron, resulting in Dirac cones at the K-points for the  $p_x$ - and the  $p_y$ -orbitals, which gives an effective two band model. In the Science paper [2] on Bismuthene the authors used SiC as a substrate to get rid of the  $p_z$ -orbitals. In this thesis, the approach of adding Hydrogen atoms to the Bismuthene sheet like it is done in the paper of Freitas *et al.* [1] is used, figure 4.1. Here the H-atoms are attached chair-like as they called it in the paper. This means, that for neighbouring Bismuth atoms one Hydrogen is attached top- and one down-side of the sheet, figure 4.2. Due to the rather high atomic number of Bismuth, it is said to open a rather large band gap when considering spin-orbit coupling. Since in the passivated Bismuthene we are left with two bands, it is possible to add a local spin-orbit term to the Hamiltonian. This term should give rise to non-trivial topology.

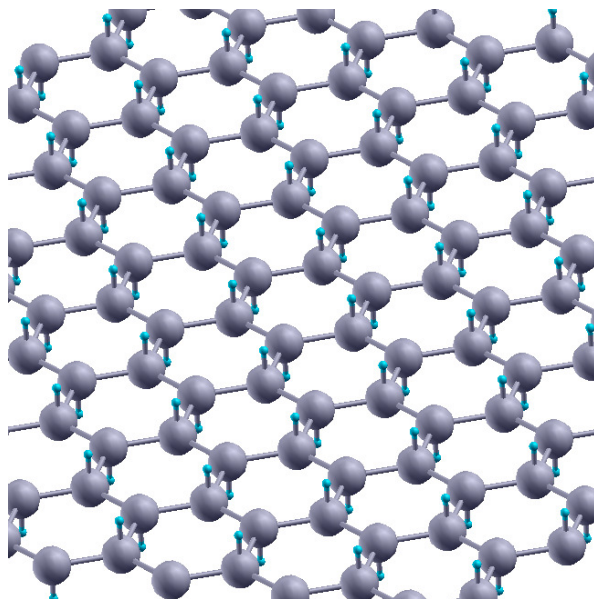


**Figure 4.1:** Passivated Bismuthene viewed from an angle in order to make out the structure and the H-atoms of the passivation.

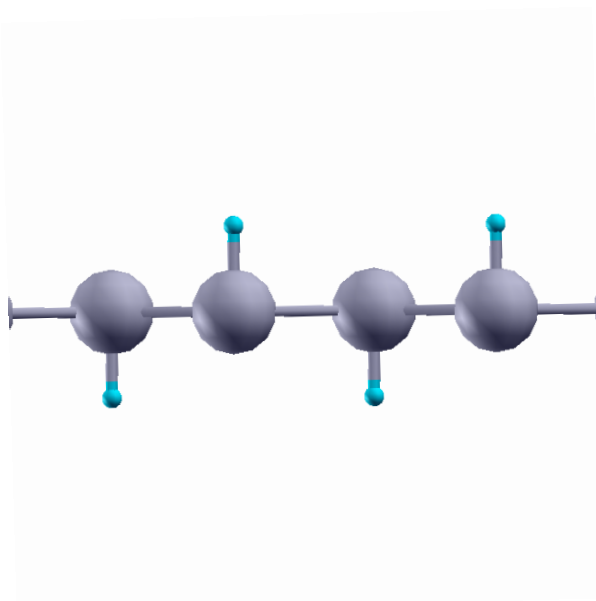


**Figure 4.2:** Passivated Bismuthene viewed from  $x$ -direction. The hydrogen atoms are arranged alternately on top and bottom of the Bismuth atoms.

## 4.1 DFT

As was done for Graphene, the electronic structure of Bismuthene was calculated using VASP. The atomic structure is similar to Graphene, but the atomic distances were taken from the paper of Freitas *et al.* [1]. Therefore, the POSCAR file takes the following form:

```
Bismuthene
1.0000000000000000
5.5059967041000002      0.0000000000000000      0.0000000000000000
-2.7529983521000001     4.7683330188999999     0.0000000000000000
0.0000000000000000      0.0000000000000000     32.9177017211999967
Bi   H
2    2
Direct
0.3333333429999996     0.6666666919999997     -0.0009766590231054
0.6666666730000017     0.3333333460000034     0.0009766590231054
0.3333333429999996     0.6666666919999997     0.0336044968170526
0.6666666730000017     0.3333333460000034     0.9663955251829494

0.00000000E+00  0.00000000E+00  0.00000000E+00
0.00000000E+00  0.00000000E+00  0.00000000E+00
0.00000000E+00  0.00000000E+00  0.00000000E+00
0.00000000E+00  0.00000000E+00  0.00000000E+00
```

**Listing 4.1:** POSCAR file for all the VASP calculations of Bismuthene.

A  $\Gamma$ -centred k-point grid of  $27 \times 27 \times 1$  turned out to be sufficient. Since Bismuthene consists of two atom sorts, two different POTCAR files need to be provided, namely the ones for Hydrogen and Bismuthene. In the INCAR files it was sufficient to set ENCUT to 200 eV. Of course the flags LWANNIER90 = .TRUE. LWRITE\_MMN\_AMN = .TRUE. need to be included in order to be able to perform wannier90 calculations later on. Depending on whether spin-orbit coupling is included or not, the corresponding flag needs to be set too (LSORBIT=.TRUE.).

### 4.1.1 DFT-calculation for Bismuthene

The DFT calculation for Bismuthene results in the band structure, figure 4.3

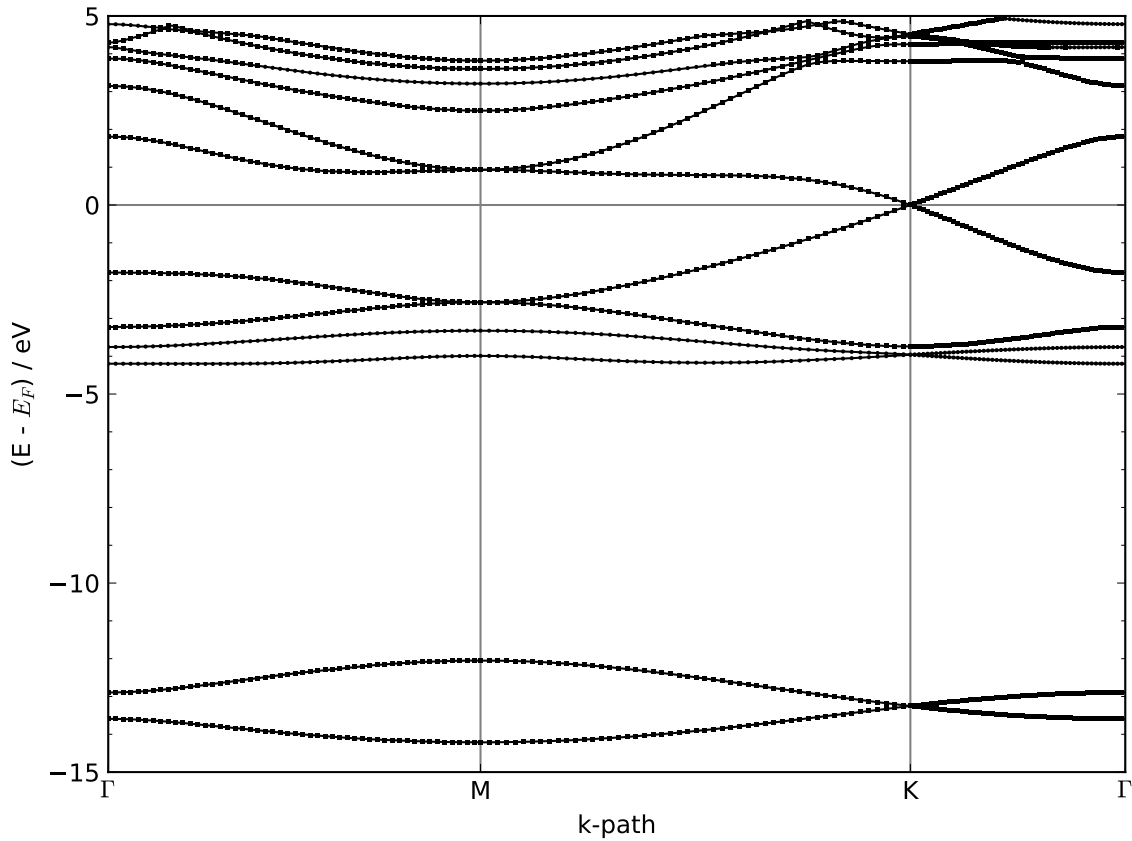


**Figure 4.3:** Bandstructure of Bismuthene determined with VASP. The two lowest bands with the crossing at the K-point are the  $p_z$ -orbitals that are shifted away from the Fermi level.

In figure 4.3 one can see the prominent Dirac cone at the K-point. At the Fermi level the cone is formed by the  $p_x$ - and  $p_y$ -bands. The  $p_z$ -bands, the two lowest bands in figure 4.3 are shifted away from the Fermi level due to the passivation with hydrogen atoms.

### 4.1.2 DFT-calculation for Bimuthene including spin-orbit coupling

When performing the DFT-calculation with the spin-orbit flag set true, the bands split up with respect to their spin resulting in a band gap 4.4

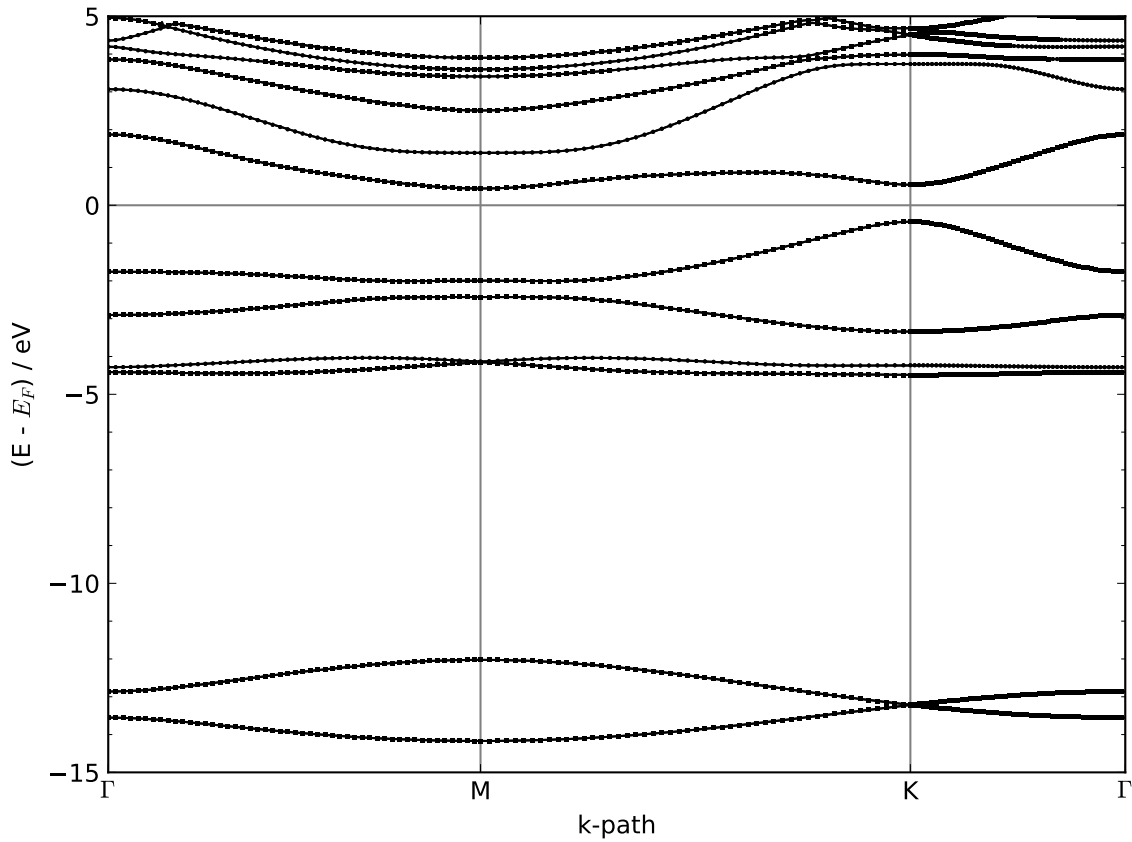


**Figure 4.4:** Bandstructure of Bismuthene with the inclusion of spin-orbit coupling determined with VASP. At the Fermi level, the  $p_x$ - and the  $p_y$ -orbitals open up a gap, while there is no gap in the bands coming from the  $p_z$ -orbitals (lowest energy bands).

## 4.2 Projections

Same as for Graphene, maximally localized Wannier functions are created, in order to perform the DMFT calculations. Since we have four bands now, we need to prepare a new wannier90.win file, determining for which Blochbands a projection should be made. In addition, we have to distinguish between the Bismuthene calculations with and without spin-orbit coupling, because spin-orbit coupling doubles the bands. The possibility of spin-orbit coupling is not implemented in the wannier90-Converter and therefore, some matrices need to be doubled by hand.



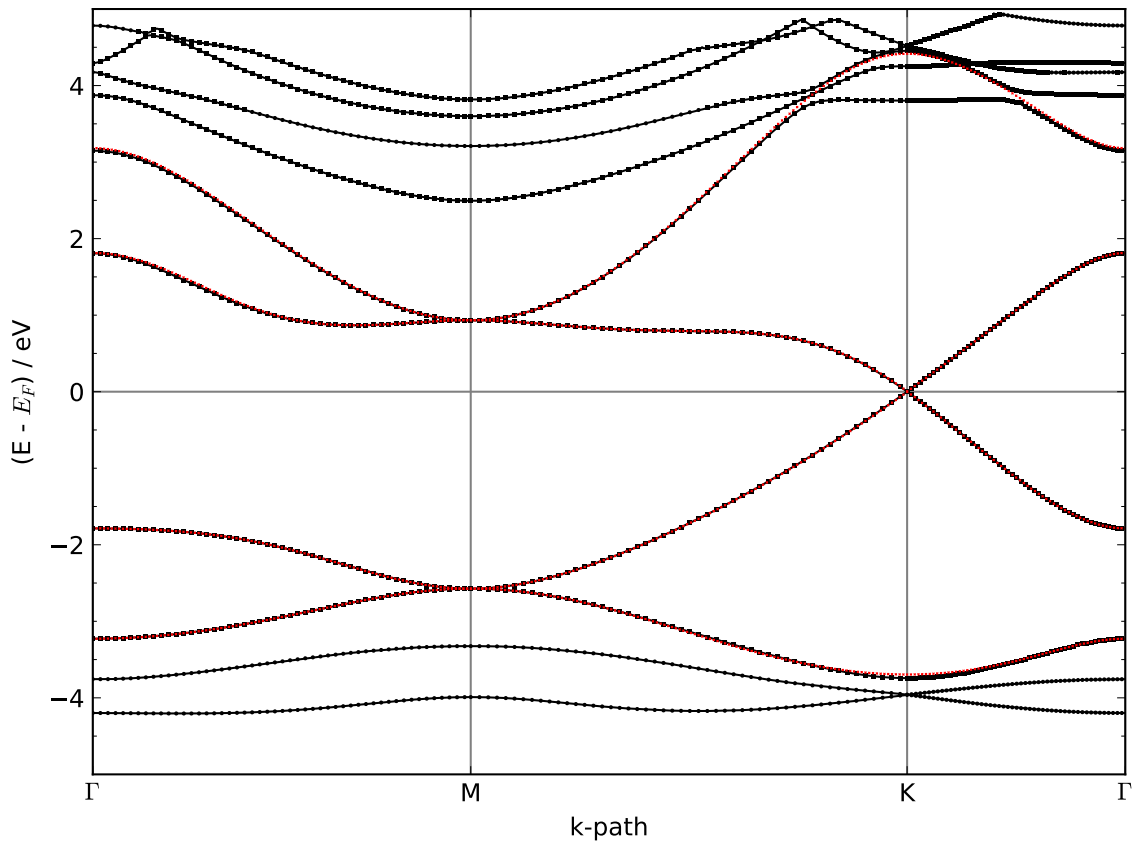


**Figure 4.5:** Band structure of Bismuthene. In red are the Wannier functions, which match the black Bloch functions of the DFT calculation pretty well.

### 4.2.1 wannier90 for Bismuthene

As a result of the VASP calculation with the LWANNIER90-tag set true, a wannier90.win file is generated:

```
search_shells = 100

num_wann = 4
num_bands = 24

dis_mix_ratio = 0.5

dis_conv_window = 4
dis_conv_tol = 1.0E-10
```

```
dis_win_min = -11.6
dis_win_max = 9.4
dis_froz_min = -5.6
dis_froz_max = -2.1

Begin Projections
Bi:px,py
End Projections

hr_plot = TRUE

bands_plot = TRUE
begin kpoint_path
M 0.500 0.000 0.000   G 0.000 0.000 0.000
G 0.000 0.000 0.000   K 0.333 0.333 0.000
K 0.333 0.333 0.000   M 0.500 0.000 0.000
end kpoint_path

begin unit_cell_cart
5.5059967      0.0000000      0.0000000
-2.7529984     4.7683330      0.0000000
0.0000000     0.0000000     32.9177017
end unit_cell_cart

begin atoms_cart
Bi      -0.0000000      3.1788888      32.8855524
Bi       2.7529984      1.5894444       0.0321494
H       -0.0000000      3.1788888       1.1061828
H       2.7529984      1.5894444     31.8115196
end atoms_cart

mp_grid =      27      27      1
```

**Listing 4.2:** wannier90.win file for Bismuthene without spin orbit coupling

Besides from determining four bands that are projected onto the  $p_x$  and the  $p_y$  orbital, it is also essential to set the energy window where the orbitals are to be found (`dis_win_min` and `dis_win_max`). In addition, it is possible to choose a so called frozen window. In this energy region only the bands we want to project onto are present and therefore, it is easier to do the transformation. In listing 4.2 not only the command to generate the local Hamiltonian is defined, but also a path of k-points. Therefore, the output is the local Hamiltonian along with a file that allows plotting the band structure as shown in figure 4.5

As can be seen in figure 4.5, the projections are in perfect accordance with the Bloch bands. Hence, we can further proceed to perform the DMFT calculations.

### 4.2.2 Wannier90 for Bismuthene with spin-orbit coupling

In the case of Bismuthene with spin-orbit coupling the `wannier90.win` file has the same form as without spin-orbit coupling apart from some minor changes. It has the same structure as 4.2 but the following parameters have been modified:

```
num_wann = 8

dis_win_min = -6.5
dis_win_max = 2.7

dis_froz_min = -6.5
dis_froz_max = -2.1

spinors = .true.
```

**Listing 4.3:** changes in the `wannier90.win` file from the case of Bismuthene to Bismuthene with spin-orbit coupling

The most important difference is the doubling of the bands according to the spins. Since the different spins are treated individually it is useful to set the `spinors-tag` to `true`. Besides, it is essential to define new energy windows. This is important because `wannier90` does not take care of Fermi energy and therefore, one needs to determine the windows according to a different Fermi level. The Wannier functions have been determined with the `wannier90` code [11]. In figure 4.6, the gained Wannier functions are again checked against the Bloch functions from the DFT calculation.

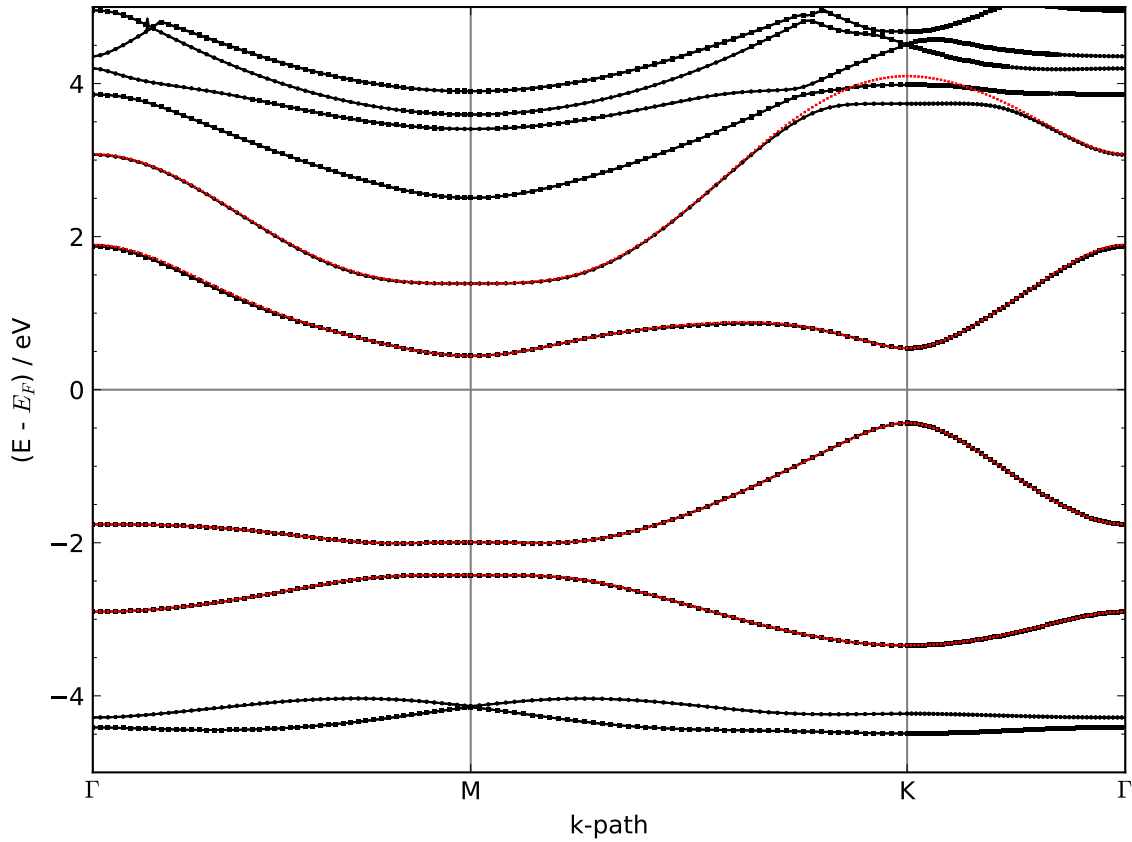


**Figure 4.6:** Band structure of Bismuthene with spin-orbit coupling. In red are the Wannier functions, which are in perfect accordance to the black Bloch bands.

It can be easily seen that the constructed Wannier functions are nearly identical to the Bloch bands. There is only one minor difference for the highest Wannier bands at the K-point, which will not affect the physics near the Fermi level. Hence, they can be used to perform DMFT cycles without doubt.

### 4.3 DMFT

Finally, all the prerequisites to perform the calculations that take correlation effects into account are provided. These DMFT calculations are again performed with the TRIQS code using the DFTTools package [38] and a CTHYB solver [37]. The main code has already been discussed in the subsection of Graphene. In the following subsections of Bismuthene with and without spin-orbit coupling only the relevant changes for the

specific cases are to be reviewed.

### 4.3.1 DMFT for Bismuthene

Same as for Graphene, the results of Bismuthene wannier90 calculations need to be converted and written to an HDF5 file. The corresponding wannier90.inp file takes the form:

```
0 27 27 1      # specification of the k-mesh
4.0           # electron density
2            # number of atoms
0 0 1 2 0 0   # atom, sort, l, dim, SO, irep
1 0 1 2 0 0   # atom, sort, l, dim, SO, irep
```

**Listing 4.4:** wannier90.inp file for Bismuthene conversion

In comparison to the one orbital Graphene here we have dimension 2 from  $p_x$  and  $p_y$  and therefore, an electron density of four electrons in the unit cell. Together with the wannier90\_hr.dat file these two files form the input for the wannier90Converter that creates the HDF5 file. As previously already mentioned, wannier90 does not take the Fermi energy into account. Therefore, it needs to be fixed before performing a DMFT cycle in order to obtain correct results of the chemical potential.

```
import numpy as np
from pytriqs.archive import *

filename = 'wannier90'
ar = HDFArchive(filename+'.h5', 'a')
dft_in = ar['dft_input']
hopping = dft_in['hopping']
for fer in range(8):
    hopping[:, :, fer, fer] = hopping[:, :, fer, fer]
    + 3.01604113
dft_in['hopping'] = hopping

del ar
```

**Listing 4.5:** Programm to ensure the Fermi level is set correctly

At the beginning of the python file containing the actual DMFT code, the same modules are loaded as in listing 3.6. Again the SumkDFT class needs to be initialized :

```
from pytriqs.applications.dft.sumk_dft import *
SK = SumkDFT(hdf_file = filename+'.h5' ,use_dft_blocks = True)
SK.block_structure.approximate_as_diagonal()
gf_struct = {'up_0': [0], 'up_1': [0],
             'down_0': [0], 'down_1': [0]}
```

**Listing 4.6:** SumkDFT initialization with enforcement of a diagonal block structure

With the structure of the Green's functions at hand, the solver class can be initialized like it is done in listing 3.9. Same as for Graphene (listing 3.10) the global variables are defined before setting up an interaction Hamiltonian and the self consistent cycle. Since we no longer treat a one band model the interaction Hamiltonian needs to take on a more sophisticated form. Here, we use the density interaction Hamiltonian constructed with U matrices from the function `U_matrix_kanamori`. The Hund's coupling J is going to be a tenth of the interaction value U.

```
Umat, Upmat = U_matrix_kanamori(n_orb=n_orb, U_int=U, J_hund=J)
h_int = h_int_density(spin_names, orb_names,
                     map_operator_structure = SK.sumk_to_solver[0],
                     U=Umat, Uprime=Upmat)
```

**Listing 4.7:** Construction of the interaction himltonian

This setup at hand, allows to perform the DMFT cycle until self-consistency is achieved:

```
for k in range(1,n_loops+1):
    SK.set_Sigma([S.Sigma_iw])
    chemical_potential = SK.calc_mu()
    S.G_iw << SK.extract_G_loc()[0]
    SK.symm_deg_gf(S.G_iw,0)

    S.G_iw['up_0'] =
        0.25*(S.G_iw['up_0']+S.G_iw['down_0']
            + S.G_iw['up_1']+S.G_iw['down_1'])
    S.G_iw['down_0'] = S.G_iw['up_0']
    S.G_iw['up_1'] = S.G_iw['up_0']
```

```

S.G_iw['down_1'] = S.G_iw['up_0']

G_loc = S.G_iw

S.G0_iw << S.Sigma_iw + inverse(S.G_iw)
S.G0_iw << inverse(S.G0_iw)

G0_tau = S.G_tau.copy()
for name, g in S.G0_iw:
    G0_tau[name] << InverseFourier(g)
    G0_tau[name].data[:, :, :] =
        np.real(G0_tau[name].data[:, :, :])
    S.G0_iw[name] << Fourier(G0_tau[name])

S.solve(h_int = h_int,
        length_cycle = 10,
        n_warmup_cycles = 5000,
        n_cycles = measure,
        random_seed = 34788 + 928374 * mpi.rank,
        move_double = True,
        **p)

```

**Listing 4.8:** Self-consistent DMFT loop for Bismuthene

In listing 4.8 it is easily observed that it hardly differs from the one-band model. The only major difference is the symmetrization done at the beginning, where all the bands available are set equal since this expected property of the two band model should be enforced at any time. In addition, for the solver the `move_double` parameter is activated which is important for multi-band calculations. The tail fitting for higher frequencies as well as the treatment of the double counting and finally the saving of the results is exactly the same as for the Graphene case, see listings 3.13, 3.14 and 3.15.

As already expected the Green's function is spin degenerate, figure 4.7. The  $p_x$ - and  $p_y$ -orbitals however, differ just a little bit. Since they already differ in  $G_0$  the self energy, figure 4.8 is equal for both orbitals. The kink at Matsubara frequency  $i\omega = 15$  comes from the choice of tailfit parameters.

Inspecting the Fourier transform of the impurity Green's function, namely  $G(\tau)$  one can see that averaging over all bands gives half filling as expected, since  $G(0) = G(\tau) = -0.5$ . However, taking a closer look at the bands separately, one can see that the individual bands are not half filled.

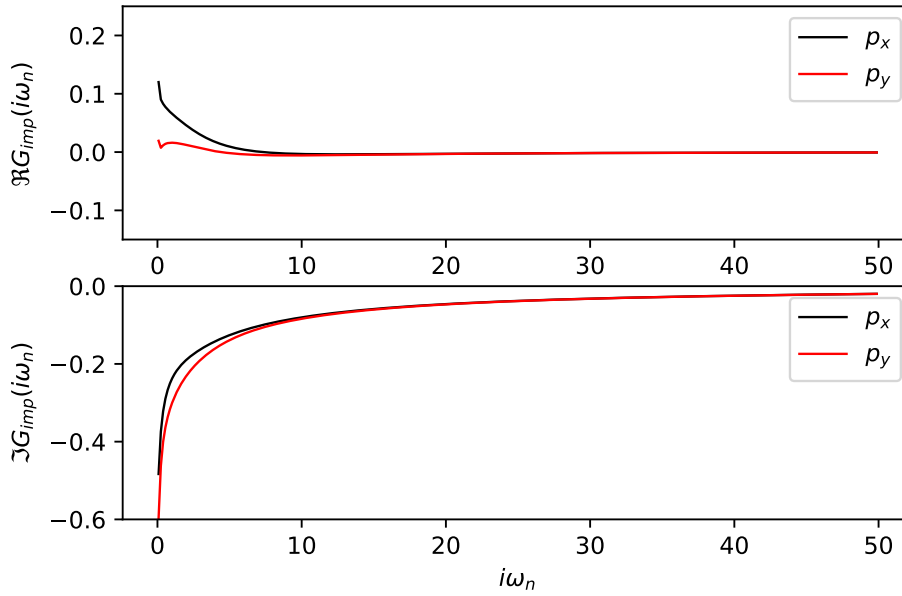


**Figure 4.7:** The real and imaginary part of the Green's function of Bismuthene.  $U = 2$  and  $J = 0.2$ . Up and down spin are degenerate as can be seen. However, the  $p_x$ - and the  $p_y$ -orbital vary slightly.



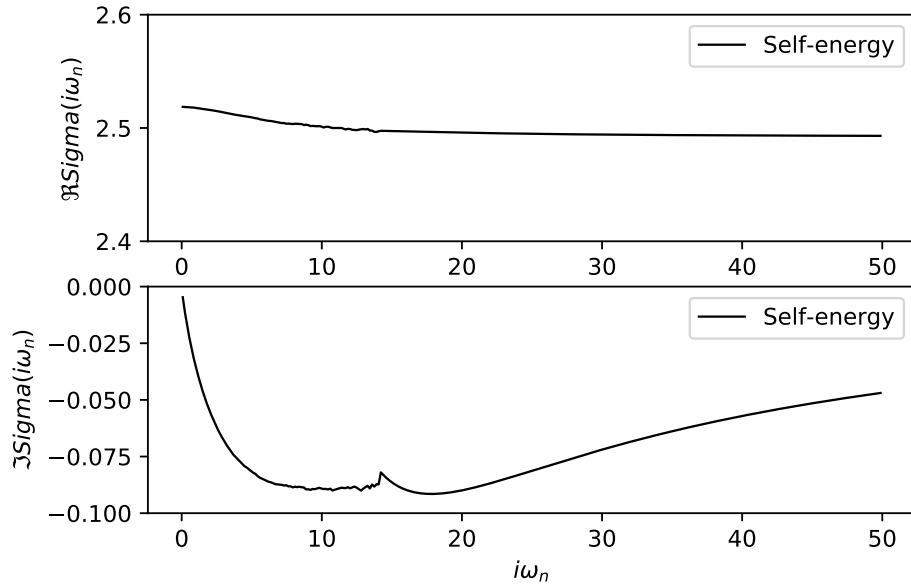


**Figure 4.8:** The real and imaginary part of the self energy function of Bismuthene.  $U = 2$  and  $J = 0.2$ . Up and down spin are degenerate as well as the  $p_x$ - and  $p_y$ -orbitals.

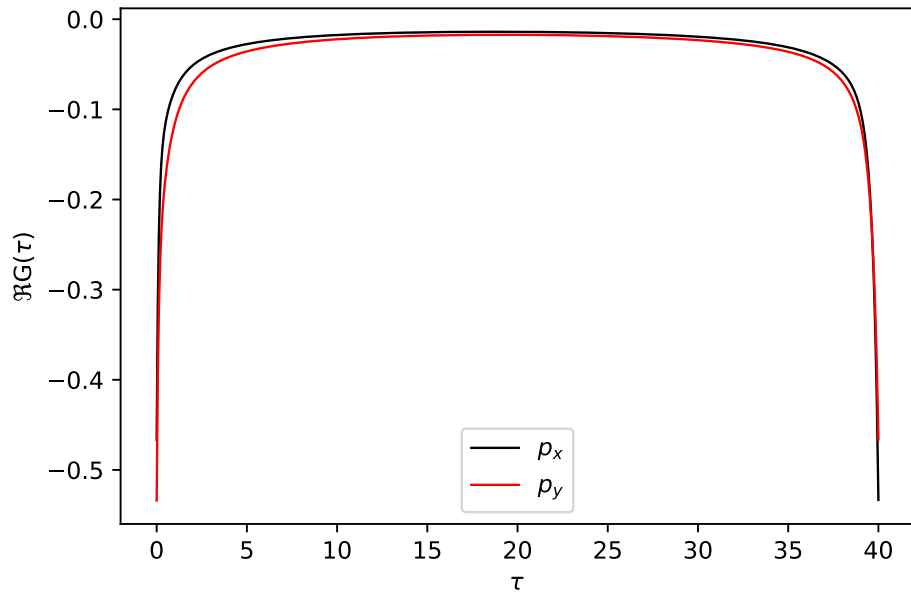


**Figure 4.9:** The real part of the Fourier transform of the impurity Green's function of Bismuthene.  $U = 2$  and  $J = 0.2$ . Again the four bands available are degenerate. The  $\tau$  values go from 0 to the defined beta value 40.

### 4.3.2 DMFT for Bismuthene with spin-orbit coupling included in the DFT calculation

The DMFT cycle of Bismuthene with spin-orbit coupling is based on the one of plain Bismuthene without SOC. However, there are some changes that need to be made in order to make the program work properly. To begin with, the conversion from the wannier90 output to a HDF5 file is done the same way as before, but since w90-Converter does not allow spin-orbit coupling some changes to the HDF file need to be made. Hence, in a small program the HDF5 file is loaded and the specific values are modified:

```

from itertools import *
import numpy as np
from pytriqs.archive import *
from pytriqs.applications.dft.sumk_dft_tools import *

filename = 'wannier90'

def double_size(M):
    # doubles the size of an np.array M
    # a copy on M is in each diagonal block
    sh = M.shape
    M_new = np.zeros((sh[0]*2, sh[1]*2), np.complex_)
    M_new[:sh[0], :sh[1]] = M
    M_new[sh[0]:, sh[1]:] = M
    return M_new

#read necessary data:
ar = HDFArchive(filename+'.h5', 'a')
dft_in = ar['dft_input']
SO = dft_in['SO']
SP = dft_in['SP']
n_k = dft_in['n_k']
n_corr_shells = dft_in['n_corr_shells']
charge_below = dft_in['charge_below']

```

```

density_required = dft_in['density_required']
n_orbitals = dft_in['n_orbitals']
corr_shells = dft_in['corr_shells']
shells = dft_in['shells']
hopping = dft_in['hopping']
proj_mat = dft_in['proj_mat']
T = dft_in['T']
rot_mat = dft_in['rot_mat']

# change data:
SP = 1
SO = 1
n_spin_blocks = 1+SP-SO

for sh in shells:
    sh['dim'] = sh['dim'] * 2

for csh in corr_shells:
    csh['SO'] = 1
    csh['dim'] = csh['dim'] * 2

proj_mat = np.append(proj_mat, np.zeros(np.shape(proj_mat)),
                    axis = 3)
proj_mat[:, :, :, 2:4, 4:8] = proj_mat[:, :, :, 0:2, 0:4]

for fer in range(8):
    hopping[:, :, fer, fer] = hopping[:, :, fer, fer] + 2.85129687

for k, s, ind1, ind2 in range(n_k, n_spin_blocks, 8, 8):
    if abs(np.real(hopping[k, s, ind1, ind2])) < 0.001:
        hopping[k, s, ind1, ind2] = 0 +
            np.imag(hopping[k, s, ind1, ind2])*1j

for k, s, ind1, ind2 in range(n_k, n_spin_blocks, 8, 8):

```

```

        if abs(np.imag(hopping[k,s,ind1,ind2])) < 0.001:
            hopping[k,s,ind1,ind2] =
                np.real(hopping[k,s,ind1,ind2]) + 0

T = [double_size(TT) for TT in T]

rot_mat = [double_size(ro) for ro in rot_mat]

# write data
dft_in['SO'] = SO
dft_in['SP'] = SP
dft_in['charge_below'] = charge_below
dft_in['density_required'] = density_required
dft_in['n_orbitals'] = n_orbitals
dft_in['shells'] = shells
dft_in['corr_shells'] = corr_shells
dft_in['hopping'] = hopping
dft_in['proj_mat'] = proj_mat
dft_in['T'] = T
dft_in['rot_mat'] = rot_mat
del ar

```

**Listing 4.9:** Additional changes in order to treat the spin-orbit coupling of the DFT calculations correctly

In this program, the necessary values are read from the existing HDF5 file. Then spin polarization and spin orbit coupling are set true. Since the bands double with spin orbit coupling, so do all the matrices. Therefore, a function to double matrices is defined and applied to the projection matrix as well as the rotation and the transposition matrix. the only matrix that need not be doubled is the hopping matrix, since it is already made up of eight bands as wanted. However, some changes need to be ensured even for the hopping matrix. First of all, the Fermi energy has to be included. This time however, it is essential to only add it to the diagonal since we have off-diagonal terms due to spin orbit coupling. Furthermore, all the elements in the hopping matrix smaller than  $10^{-3}$  are set to zero in order to avoid numerical problems later on. In the end the

changes are again written into the HDF5 file, which can now be used as an input for the DMFT calculation.

At first, nearly the same code as for Bismuthene without SOC was used, however, it soon turned out to produce a severe sign problem because of the off-diagonal terms. Hence, the basis in which the solver operates needs to be rotated into a diagonal form. Thus we import the `matrix_dict.py` written by Gernot Kraberger as well as the following function to transform an operator:

```
def transform_operator(O_in, T, fops_from, fops_to):
    O_out = Operator(0)

    for monomial in O_in:
        coefficient = monomial[-1]
        new_monomial = Operator(1)

        for single_operator in monomial[0]:
            new_single_operator = Operator(0)
            daggered = single_operator[0]
            i = fops_from.index(single_operator[1])
            for j in range(len(fops_to)):
                new_single_operator += (T[j, i]
                                         * c_dag(*fops_to[j]))
                if daggered
                else (T[j, i].conjugate()
                     * c(*fops_to[j]))
            new_monomial *= new_single_operator

        O_out += new_monomial * coefficient

    return O_out
```

**Listing 4.10:** transform operator function

When initializing the `SumkDFT` class, now we need to define two structures of Green's functions. One structure representing the initial problem (`gfs_from`) and one diagonal structure (`gfs_diag`).

```

from pytriqs.applications.dft.sumk_dft import *
SK = SumkDFT(hdf_file = filename+'.h5' , use_dft_blocks = True)
gfs_from = SK.block_structure
gfs_diag = SK.block_structure.copy()
#gfs_diag.approximate_as_diagonal()

```

**Listing 4.11:** Initializing the SumkDFT class for Bismuthene with spin-orbit coupling

In this code the SK-basis is always going to be the original basis with the off-diagonal terms. The solver however, only operates in the diagonal representation. Hence the initial self-energy, the local Green's function, the chemical potential and the double counting are determined as before in listing 4.8. To obtain a diagonal basis, the eigenvalues of the local Hamiltonian needs to be evaluated as well as a rotation matrix 'V\_full' be defined:

```

Hloc = eff_atomic_levels_solver(first_G_loc)
e,V = Hloc.diagonalize(hermitian = True)
V_full = V.to_full_matrix(gfs_from.sumk_to_solver[0])

```

**Listing 4.12:** Determination of the diagonal basis

Having this rotation matrix at hand one can set up the solver in the diagonal basis as well as pass on the rotated self-energy and the first local Green's function. Though a rotation has been performed, there could still be some off-diagonal terms in the solver basis due to the hybridization with the bath. If these are small, one can use the `approximate_as_diagonal()` function to ignore off-diagonals. The code was tested with and without applying this function and gave the same results.

```

from pytriqs.applications.impurity_solvers.cthyb import *
S = Solver(beta = beta , gf_struct =
          gfs_diag.gf_struct_solver[0])
S.Sigma_iw << rotate_and_convert_gf(first_Sigma , V_full ,
          gfs_from , gfs_diag , beta=beta)
S.G_iw << rotate_and_convert_gf(first_G_loc , V_full ,
          gfs_from , gfs_diag , beta=beta)

```

**Listing 4.13:** Initializing the solver in the diagonal basis

The rest of the DMFT cycle is the same as without spin-orbit coupling. Only, in the end one has to rotate back all the wanted results into the original basis with off-diagonal

terms.

The resulting impurity Green's function is shown in figures 4.10 and 4.11

The real part as well as the imaginary part of the impurity Green's function has the same Green's function in the diagonal. the complex off-diagonal terms coupling the  $p_x$ - and the  $p_y$ -orbital differ by a minus sign as they do in 2.23. The other off-diagonals are zero as expected. In the self energy one can see the diagonal parts are at the Hartree energy, whereas the off-diagonals have zero real value, figure 4.12.

The imaginary part depicts a similar structure as the impurity Green's function, where again the off diagonal parts that couple the  $p_x$ - and  $p_y$ -orbitals are nonzero, figure 4.13. The self-energy gives a measure of how much the local non-interacting Green's function differs from the interacting Green's function. Therefore, it represents the degree of electron-electron interactions, especially the correlations. The imaginary part of the self-energy in 4.13 has only a small diagonal part. Also the off-diagonals representing the interaction between the  $p_x$ - and  $p_y$ -orbitals are very small. Hence, the correlations within the two-band model are hardly present. Since the other off-diagonals coupling up and down parts are zero, one can derive that there is no interaction between the spin up and the spin down block at all.

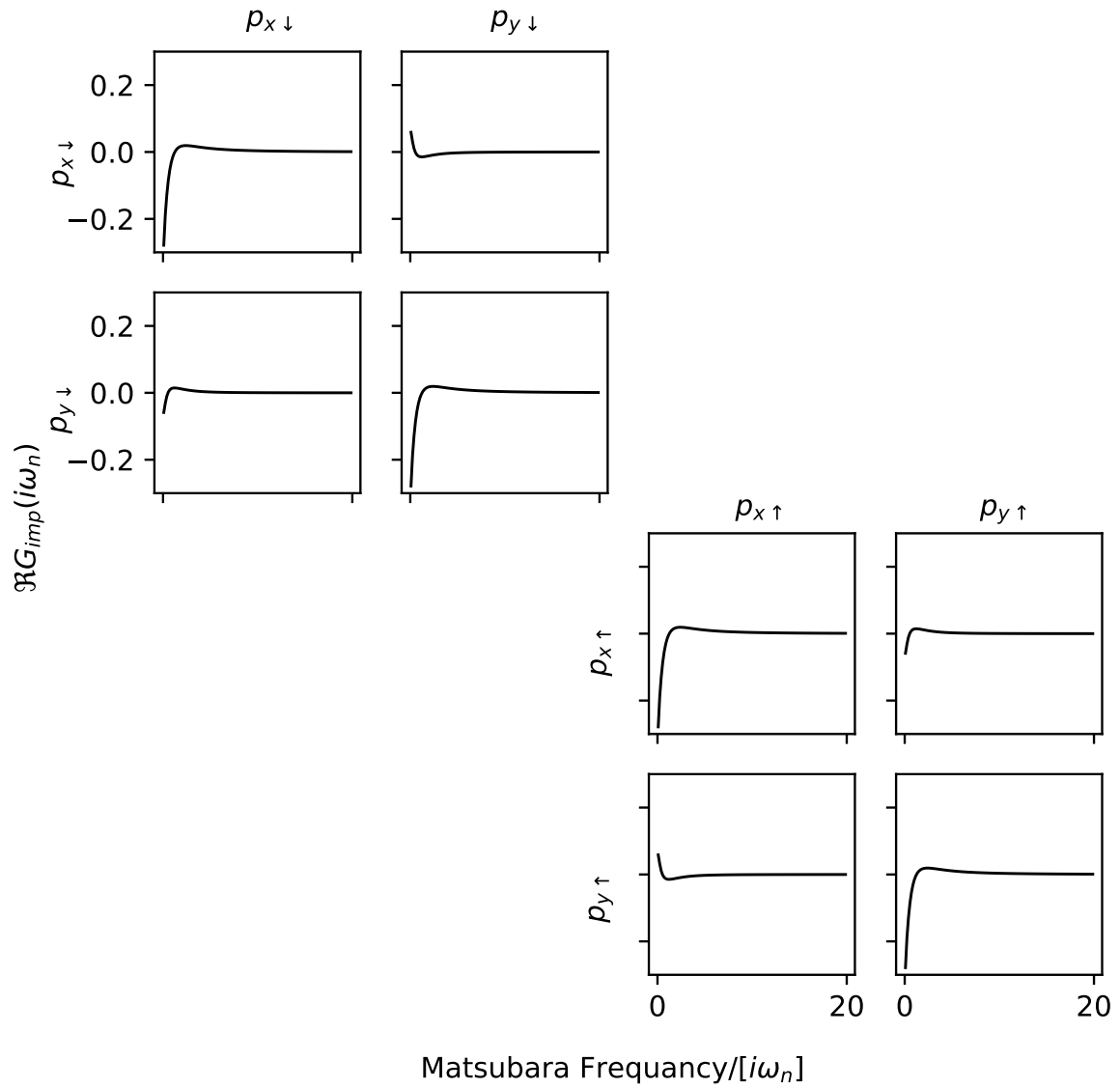


**Figure 4.10:** The real part of the Green's function of Bismuthene with spin-orbit coupling added at DFT level. For  $U = 2$  and  $J = 0.2$



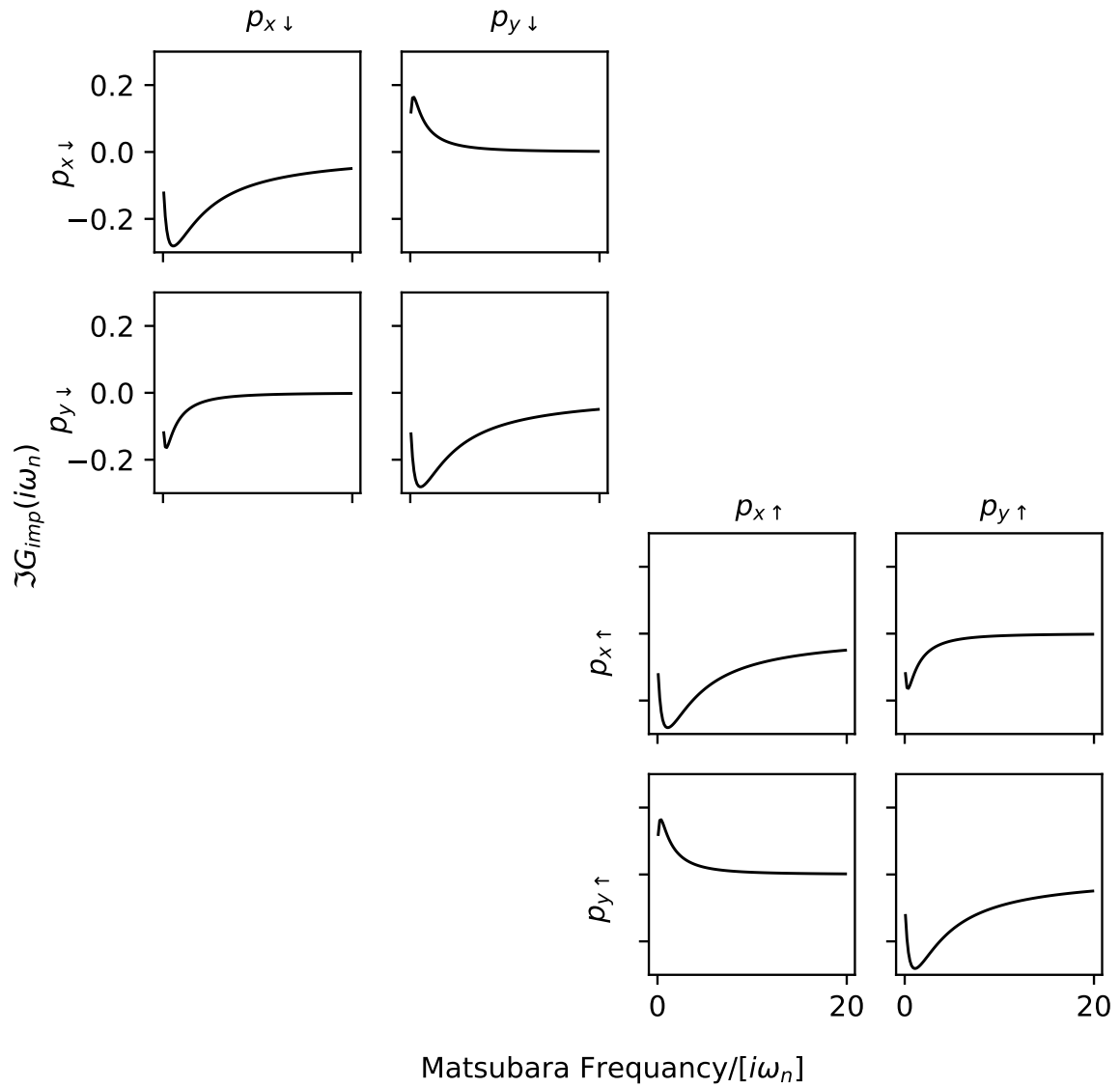


**Figure 4.11:** The imaginary part of the Green's function of Bismuthene with spin-orbit coupling added at DFT level. For  $U = 2$  and  $J = 0.2$

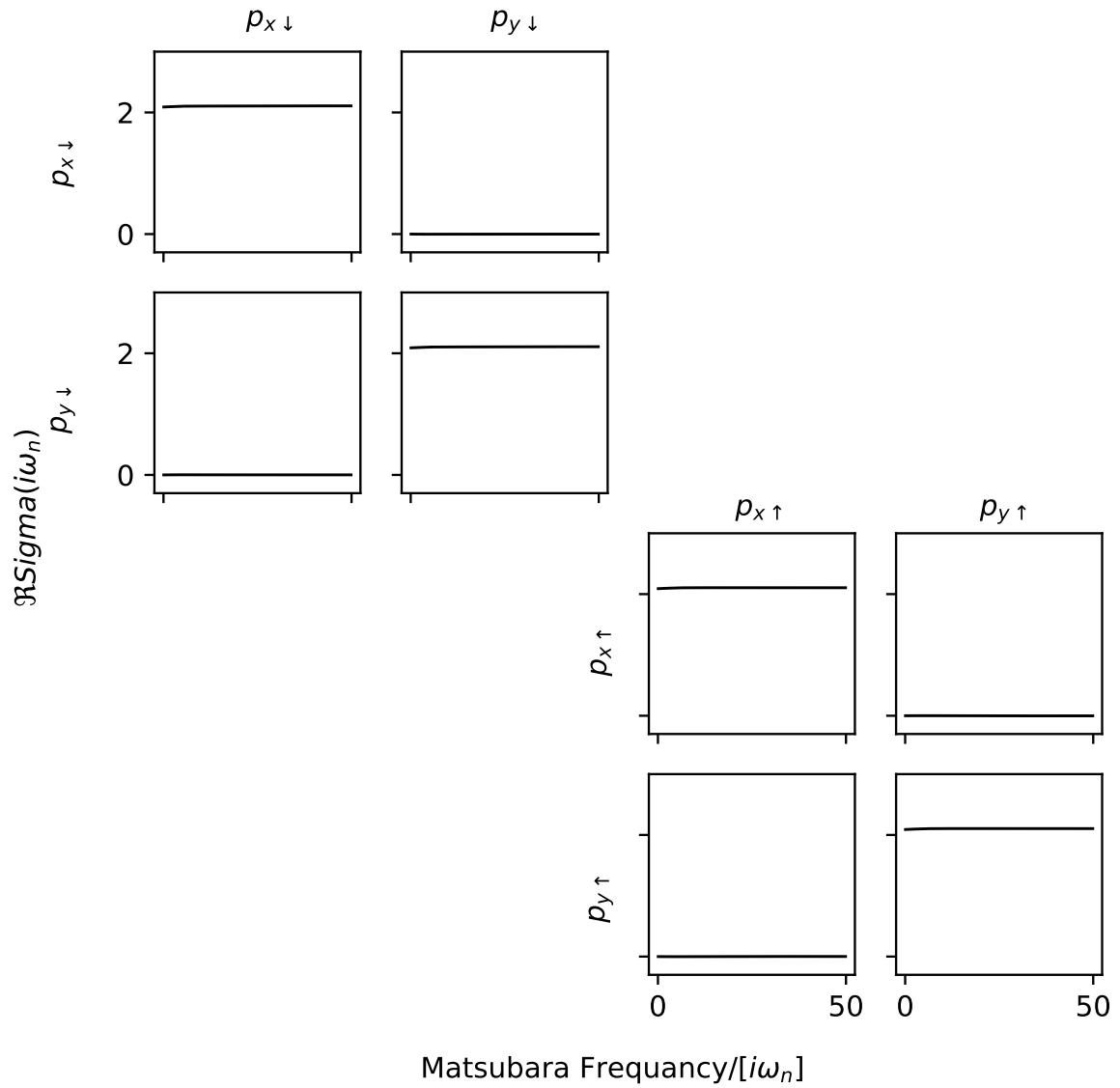


**Figure 4.12:** The real part of the self energy of Bismuthene with spin-orbit coupling added at DFT level. For  $U = 2$  and  $J = 0.2$

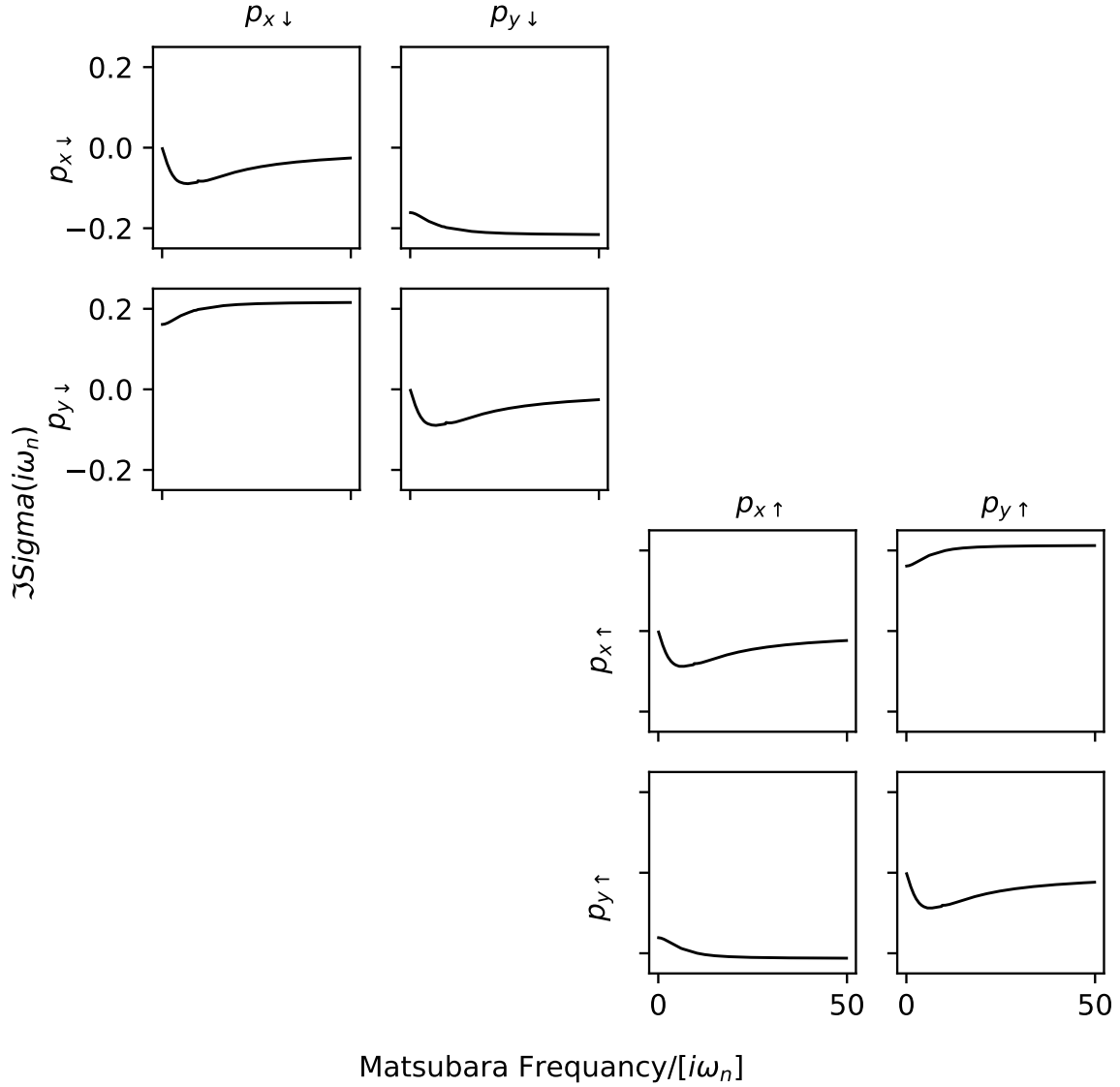


**Figure 4.13:** The imaginary part of the self energy of Bismuthene with spin-orbit coupling added at DFT level. For  $U = 2$  and  $J = 0.2$

### 4.3.3 DMFT for Bismuthene with additional local spin-orbit coupling term

Besides from performing the spin-orbit coupled calculation already in the DFT code and then proceeding to the DMFT run, it is also possible, to add a local spin orbit term to the non-SOC Hamiltonian of Bismuthene. Therefore, the local Hamiltonian of the wannier90 calculation of Bismuthene without SOC is taken and converted as before,

but to the resulting HDF5 file some major changes need to be made. Some changes are similar to the one for the case of Bismuthene where spin-orbit coupling is already included in DFT, however in addition now also the hopping matrix needs to be doubled and the SOC term derived in 2.23 has to be added.

Since the doubling of the matrices and saving of the new values was already treated in listing 4.9 we will not review them at this point. However, it is essential to take a look at the changes done to the hopping matrix:

```
lambda_so = 0.435
n_orbitals = n_orbitals * 2

# pauli matrices
sx=np.array([[0,1],[1,0]])
sy=np.array([[0,-1j],[1j,0]])
sz=np.array([[1,0],[0,-1]])

# angular momentum matrices for p-orbitals

ldx = np.zeros((3,3), dtype=np.complex)
ldx[0,2] = -1j
ldx = ldx + ldx.conjugate().T
ldy = np.zeros((3,3), dtype=np.complex)
ldy[0,1] = -1j
ldy = ldy + ldy.conjugate().T
ldz = np.zeros((3,3), dtype=np.complex)
ldz[1,2] = 1j
ldz = ldz + ldz.conjugate().T

LS = np.kron(sx, ldx) + np.kron(sy, ldy) + np.kron(sz, ldz);
LS = LS[:, [1, 2, 4, 5]];
LS = LS[[1, 2, 4, 5], :];

ls = np.zeros((8,8), dtype=np.complex)
ls[0:2, 0:2] = LS[0:2, 0:2]
ls[2:4, 2:4] = LS[0:2, 0:2]
```

```

ls [4:6 ,4:6] = LS [2:4 ,2:4]
ls [6:8 ,6:8] = LS [2:4 ,2:4]

LS = -0.5*ls

hopping = np.array ([[ double_size (hopping [k, s]) + lambda_so*LS
                        for s in range (n_spin_blocks)] for k in range (n_k)])

```

**Listing 4.14:** Adding the local spin-orbit coupling term to the local Hamiltonian of a DFT calculation without SOC.

The value chosen for the spin-orbit coupling is taken from [2], where they have determined it via treating the problem with a tight binding model. Since spin-orbit coupling splits the spin bands the number of bands needs to be doubled. The expression of the SOC-term in equation 2.23 is derived following the formula 2.17. In the end the local spin-orbit term is added to a doubled hopping matrix.

As expected, the local SOC term gives rise to a band gap at the Fermi level. In figure 4.14 it is shown that for applying a  $\lambda$ -parameter of  $0.435eV$  the band gap pretty much equals the band gap obtained from DFT calculations where SOC was already included. Especially at the K-point, where the interesting physics takes place the bands match well. Hence, it is shown that the spin-orbit term can also be added by hand after the DFT cycle and be used as an input for the DMFT calculations. SOC is shown to be mainly local here.

For the dynamical mean-field theory calculations, exactly the same code as for the Bismuthene calculation with SOC from DFT is used. The only difference are some names of up and down blocks. Apart from that, again the Sumk basis needs to be rotated to obtain a diagonal solver basis in order to not run into a sign problem.

And of course the resulting Green's function and self energy are similar to the ones shown before in figures 4.10, 4.11, 4.12 and 4.13. However, the complex off diagonal parts in the impurity Green's function have exactly the opposite sign as the ones where SOC has been treated in DFT. However, this shall not pose any problems, since it just switches the ordering of the spin up and the spin down block.

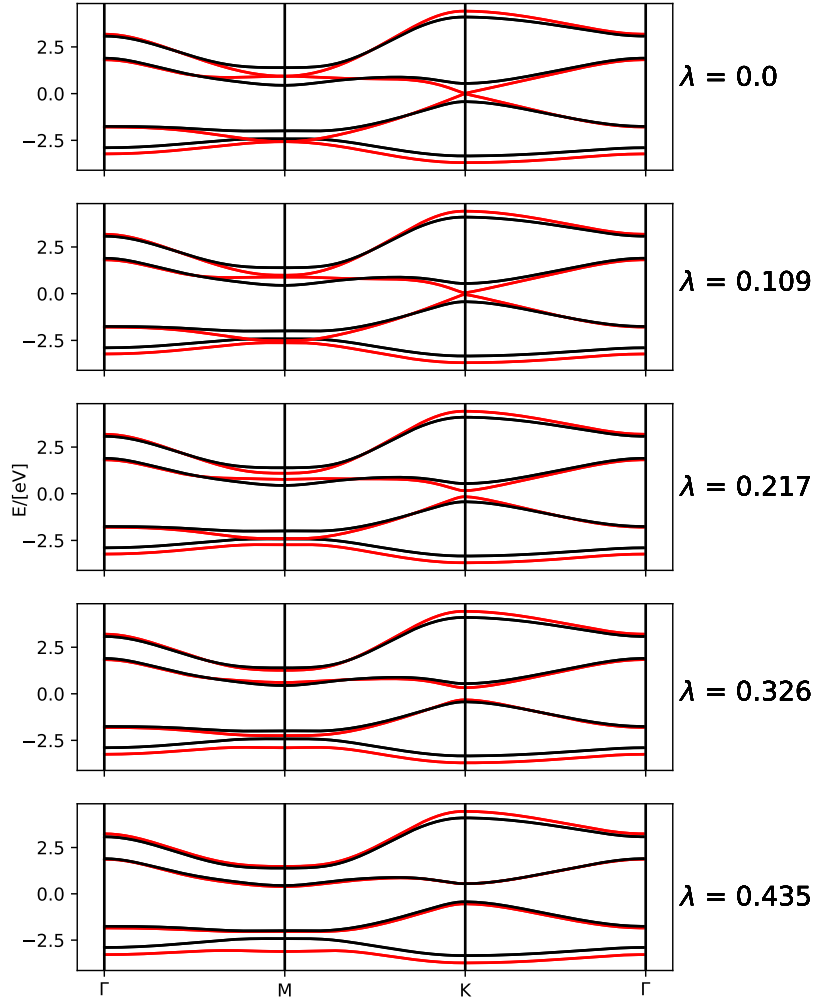


**Figure 4.14:** The band structure of Bismuthene. The black lines depict the band structure of Bismuthene gained from spin-orbit coupling included DFT-calculations. The red lines show the band structure of Bismuthene, where the DFT calculations have been performed without SOC, but a local spin-orbit coupling term is added with values for  $\lambda$  from 0 to 0.435.

Due to the SOC-term (2.23) the local Hamiltonian has off-diagonal terms. Therefore, when interactions are present also the self energy gets off-diagonals as shown in figures 4.12 and 4.13. In the eigenbasis of the local Hamiltonian,

$$\begin{aligned}
 |p_{\pm}^{\uparrow}\rangle &= \frac{1}{\sqrt{2}} (|p_x^{\uparrow}\rangle \pm i |p_y^{\uparrow}\rangle) \\
 |p_{\pm}^{\downarrow}\rangle &= \frac{1}{\sqrt{2}} (|p_x^{\downarrow}\rangle \pm i |p_y^{\downarrow}\rangle),
 \end{aligned}
 \tag{4.1}$$

where the eigenvalues are  $\pm\lambda/2$ , the self-energy is diagonal, too, with  $\Sigma_{+}^{\uparrow} = \Sigma_{-}^{\downarrow}$  and

$\Sigma_-^\uparrow = \Sigma_+^\downarrow$ . In this basis it is possible to expand the self energy as:

$$\Sigma = \frac{1}{2} \left( \Sigma_+^\uparrow + \Sigma_-^\uparrow \right) \mathbb{1} + \left( \Sigma_+^\uparrow - \Sigma_-^\uparrow \right) \mathbf{1} \cdot \mathbf{s}. \quad (4.2)$$

With this relation one can express an effective spin-orbit coupling as

$$\lambda_{eff} = \lambda + \left( \Sigma_+^\uparrow(\omega) - \Sigma_-^\uparrow(\omega) \right) \Big|_{\omega \rightarrow 0}. \quad (4.3)$$

Since the diagonal elements of the Hamiltonian, proportional to the unity matrix, have no influence on topological effects, only the effective SOC influences the topology of the system. The imaginary part of the off diagonal  $\Sigma_{yx}$  shown in figure 4.17 is equivalent to the real part of  $\Sigma_+^\uparrow - \Sigma_-^\uparrow$ . It is positive for all Matsubara frequencies  $i\omega$  and therefore, correlations effectively enhance the spin-orbit coupling. As a result, interactions stabilize the topological phase, as we will see in the next subchapter where different interaction parameters were tested.

In figure 4.18 the imaginary part of the Self energy of the two different ways of calculating the two band model with spin orbit coupling are compared. In the diagonal part the red line of Bismuthene with added local SOC-term exactly matches the black line of Bismuthene with spin-orbit coupling already included at the DFT level. As discussed before, due to a small interaction parameter  $U = 2$ , the self energies are small as are the correlations within the bands. Interestingly, the off-diagonals coupling the  $p_x$ - with the  $p_y$ -orbitals show the same behaviour but with different amplitudes. It seems like the electron-electron interaction in the case of the added local SOC-term is smaller than for Bismuthene with SOC included in DFT by a factor of two. Therefore, the  $p_x$ - and the  $p_y$ -bands interact more when SOC is already included in the DFT calculations. As a consequence, the effective SOC contribution from the self energy is smaller when a local SOC term is added, than it is when the SOC was already treated at the DFT level. Hence, the effective value of the SOC-parameter is increased when using a Hamiltonian where SOC was already treated at the DFT level, compared to adding the SOC term to a Hamiltonian by hand. The real parts are not depicted since they perfectly match for any element of the Self energy matrix.

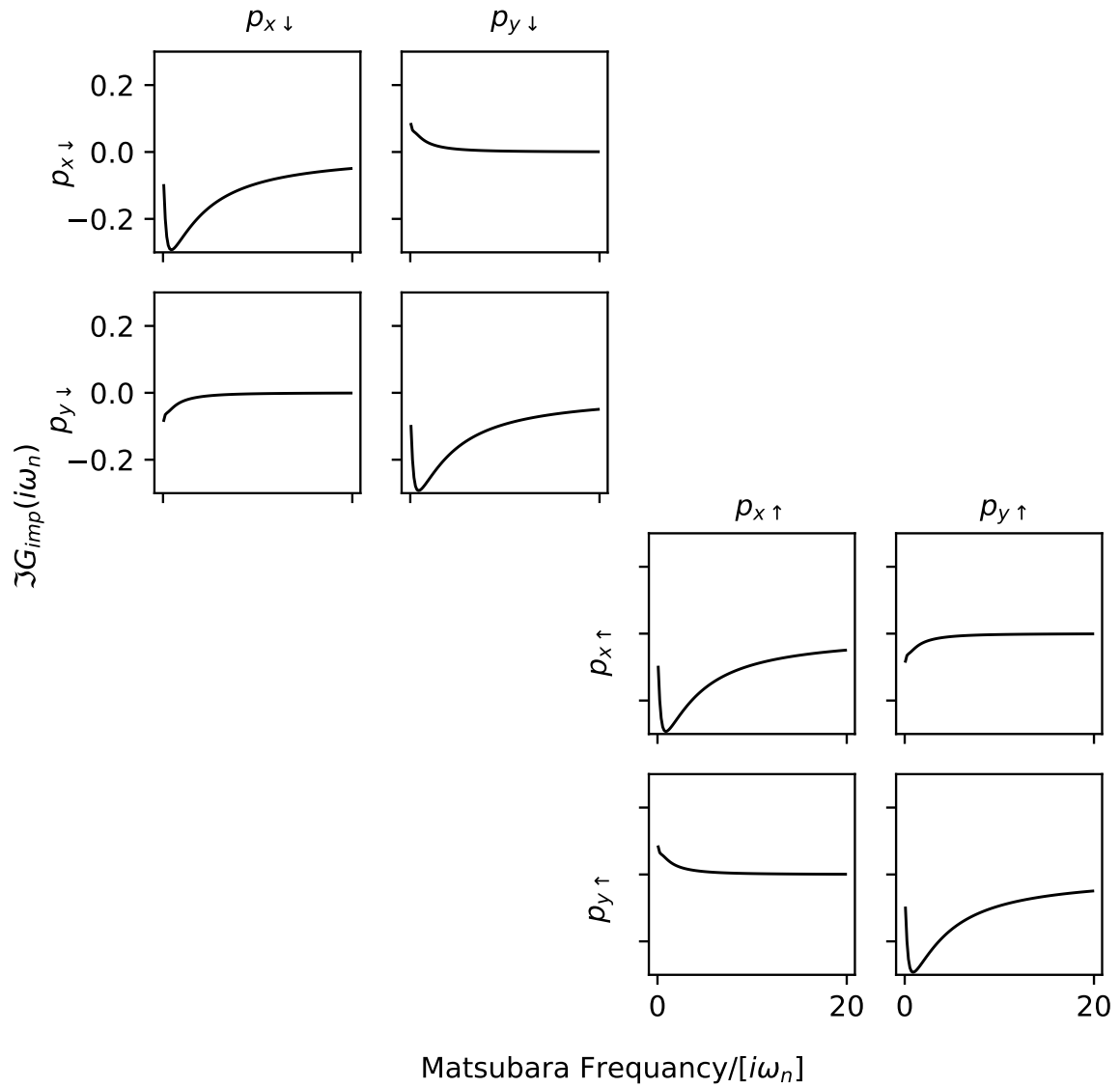


**Figure 4.15:** The imaginary part of the Green's function of Bismuthene with local SOC term added after the DFT calculations were performed.  $U = 2$  and  $J = 0.2$ .



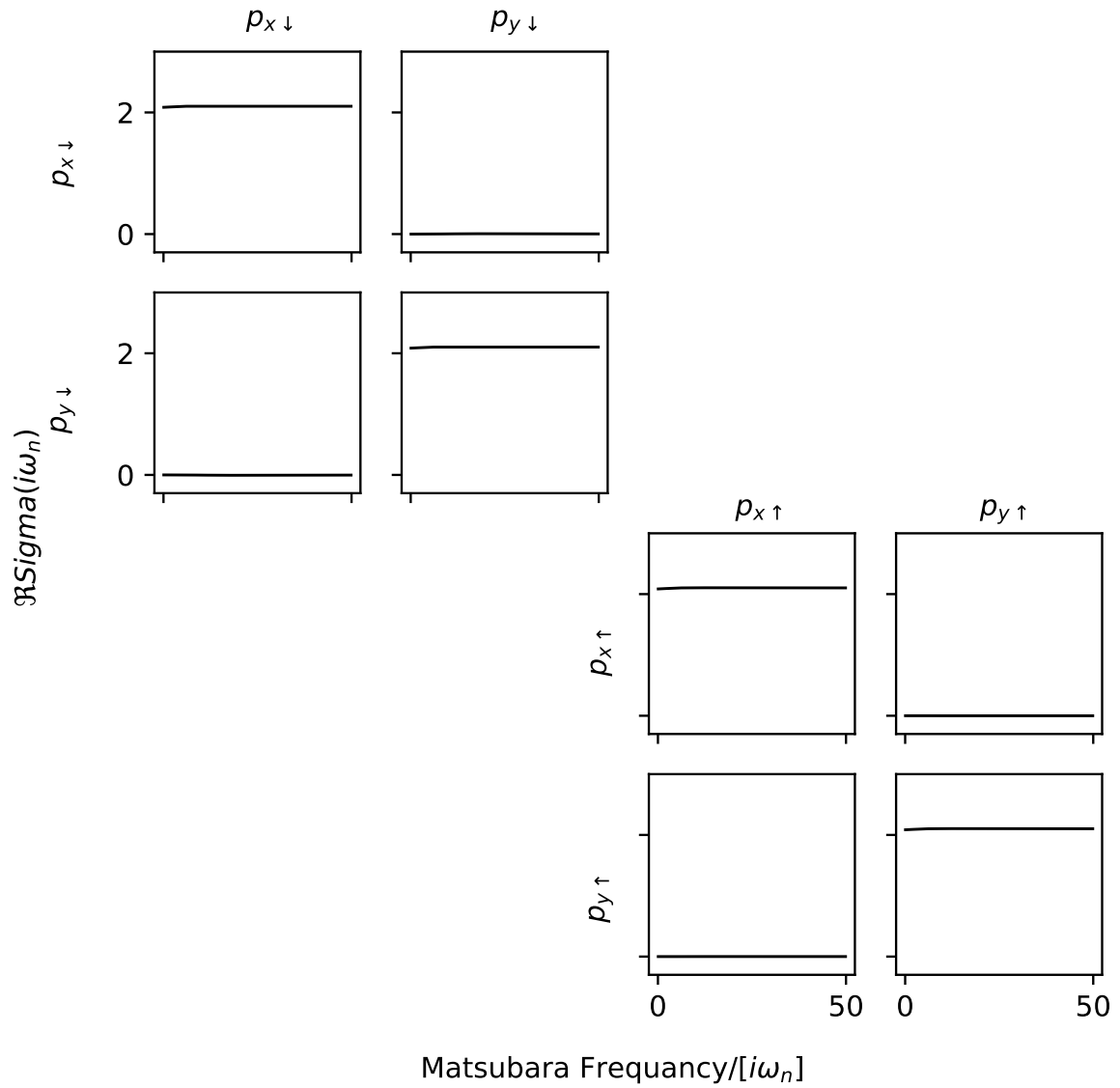


**Figure 4.16:** The real part of the self energy of Bismuthene with spin-orbit coupling added to a given local Hamiltonian.  $U = 2$  and  $J = 0.2$ .

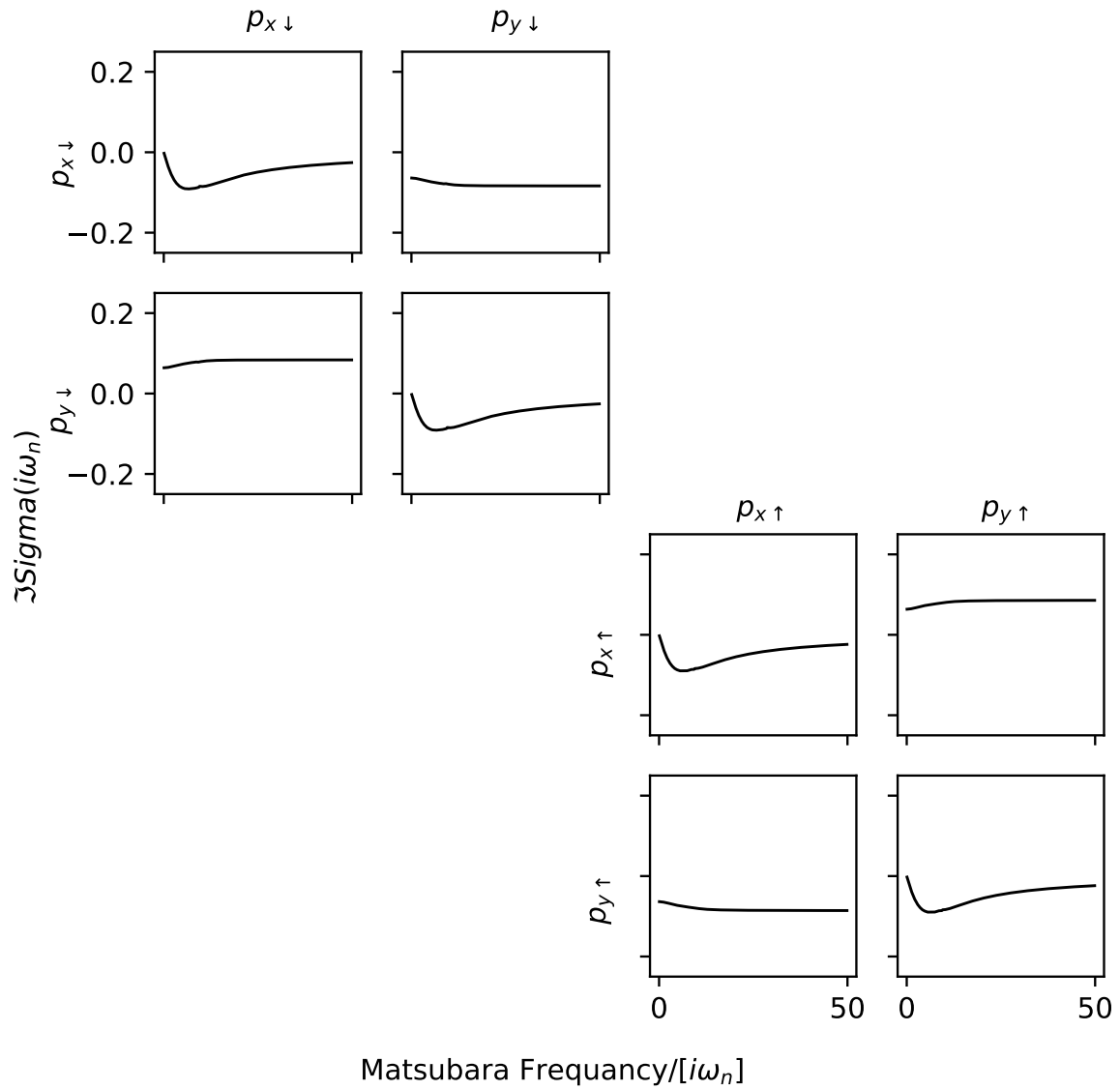


**Figure 4.17:** The imaginary part of the self energy of Bismuthene with spin-orbit coupling added to a given local Hamiltonian.  $U = 2$  and  $J = 0.2$ .

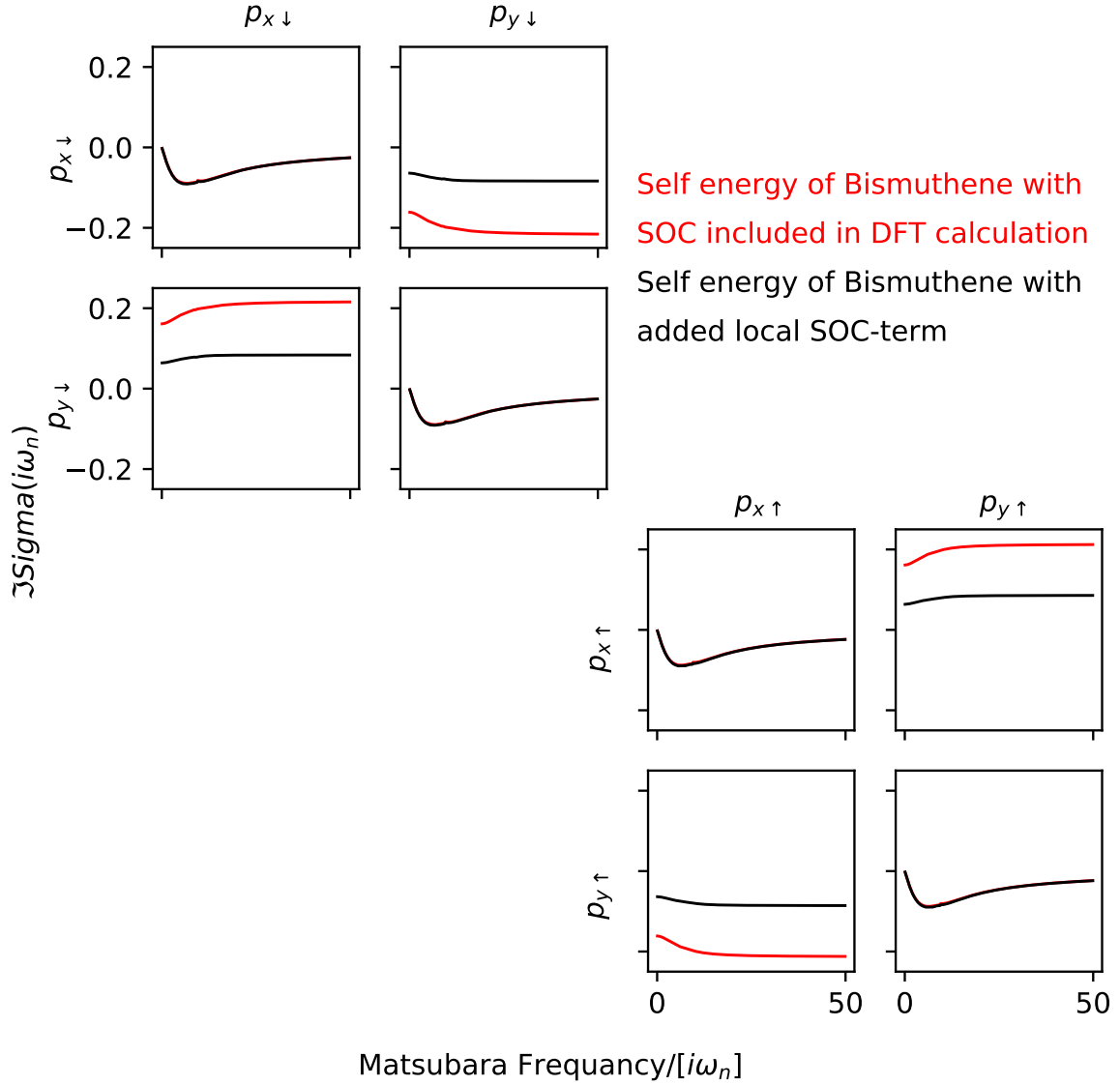


**Figure 4.18:** Comparison of the imaginary part of the self energy of Bismuthene in cubic basis with spin-orbit coupling included at the DFT level (black graphs) and Bismuthene with an added local SOC term.  $U = 2$  and  $J = 0.2$ .

#### 4.3.4 Z2Pack

In this last subsection, the presence of a non-trivial insulator is investigated. As seen in previous band structures, the spin-orbit coupling in Bismuthene gives rise to the opening of a band gap at the Fermi level. Therefore, it is interesting to determine now the Chern number as well as the  $\mathbb{Z}_2$  invariant. To do so the Z2pack is used [39] [40]. It

is a simple tool that calculates topological invariants from a given Hamiltonian. Just for simplicity the topological invariants of the  $p_x$ - $p_y$ -model without spin-orbit coupling are determined even though we obviously expect them to be zero any ways. This is a good way to check whether the written code works or not. There are two possible ways to provide the Hamiltonian. The first method is to Fourier transform the local Hamiltonian resulting from the wannier90 calculation:

```
nrpt = np.load('datnrpt.npy')
Rvec = np.load('datRvec.npy')
Rdeg = np.load('datRdeg.npy')
HR = np.load('datHR.npy')

norb = 4
twopi = 2* np.pi

def hamiltonian(k):
    HK = np.zeros((norb, norb), dtype=np.complex)

    for ir in np.arange(0, nrpt):
        rdotk = twopi * np.dot(k[:], Rvec[ir, :])
        factor = (math.cos(rdotk) + 1j
                  * math.sin(rdotk)) / \
                  float(Rdeg[ir])
        HK[:, :] += factor * HR[ir][:, :]

    return HK
```

**Listing 4.15:** Construction of a k-dependent Hamiltonian via Fourier transform of the local Hamiltonian of the wannier90 calculations

At the beginning, the different values of the wannier90\_hr.dat file are loaded. They have been saved separately with a python2 script since the wannier90Converter only works in python2 while the Z2pack only operates in python3. The Hamiltonian is simply the Fourier transform of the given local Hamiltonian.

The second possibility of generating a k-dependent Hamiltonian is via the negative inverse of the local Green's function at zero frequency as mentioned in equation (2.60).

To do so, one has to first Fourier transform the Green's function at zero frequency into local space only to Fourier transform it later back as a  $k$ -dependent Hamiltonian. To obtain the Green's functions value at zero frequency one needs to fit the function and evaluate it at  $i\omega = 0$ . The negative inverse of the outcome is saved again and called upon in the python3 script, which is exactly the same as listing 4.15

In this thesis both ways have been used as an input to the Z2pack which only consists of a few lines:

```
system = z2pack.hm.System(hamiltonian, bands = [0, 1],
                          hermitian_tol = None)
result = z2pack.surface.run(system = system,
                           surface = lambda t1, t2: [t1/2, t2, 0],
                           pos_tol=0.01, gap_tol=0.8, move_tol=0.3,)
print(z2pack.invariant.chern(result))
print(z2pack.invariant.z2(result))
z2pack.plot.wcc(result)
plt.show()
```

**Listing 4.16:** The code used to calculate the topological invariants for Bismuthene without SOC

One important fact to be mentioned: If one determines the invariants with the first method of the local Hamiltonian the filled bands are the first two bands (four bands if SOC is included). However, when using the method with the Green's function the order of the orbitals gets mixed up and one has to take the zeroth and the second band (zeroth, second, fifth and seventh band for SOC), in order to get the correct result. As expected this calculation gives a trivial Chern and  $\mathbb{Z}_2$  number. The plot of the Wannier charge centres as well as the largest gap between them while pumping in one direction obviously depicts only straight lines and is therefore not shown.

More interesting is the case of Bismuthene with spin-orbit coupling. Here, the self energy at zero frequency needs to be added to the local Hamiltonian before performing the Fourier transform in order to obtain an interacting Hamiltonian. The Z2pack calculations are performed for both methods as well as for both ways of adding spin-orbit coupling. Fortunately, in all four cases the Chern number turns out to be zero whereas the  $\mathbb{Z}_2$  invariant becomes one since time reversal symmetry is broken. When taking a look at the Wannier charge centres all four figures depict a similar behaviour with only numerical deviations:

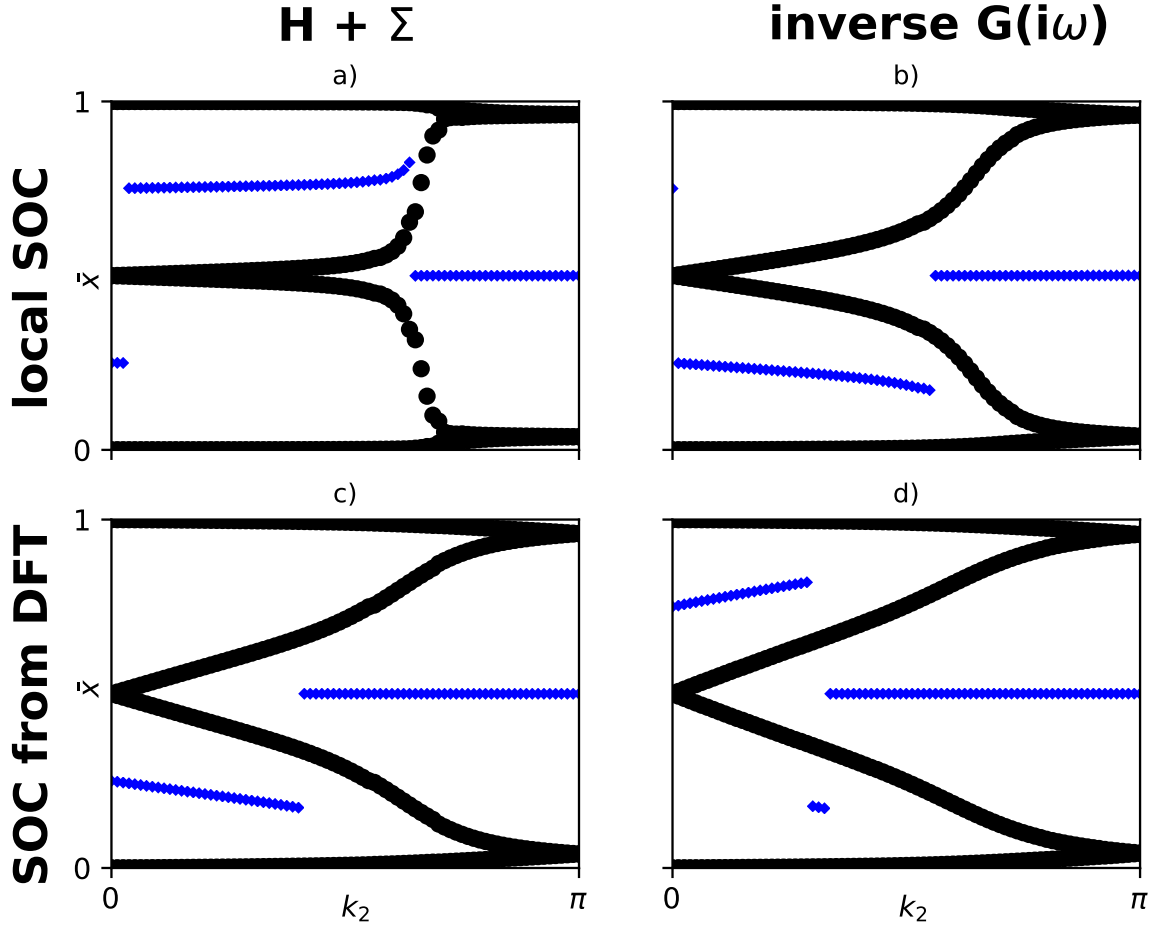


**Figure 4.19:** The Wannier charge centres of Bismuthene with spin-orbit coupling. a) and b) depict the result for Bismuthene where the local SOC term was added after the DFT calculation was solved. With a) being gained from the local Hamiltonian plus the self energy and b) being the result of the inverse Green's function method. c) and d) are shown the cases for Bismuthene with spin-orbit coupling included at DFT level. c) again arises from the local Hamiltonian with added self energy, whereas d) is the product of the inverse Green's function method. The self energies and the Green's functions have been obtained from DMFT calculations with  $U = 2$  and  $J = 0.2$ . The black dots represent the Wannier charge centres, the blue crosses stand for the largest gap between the WCCs.

In figure 4.19 the Wannier charge centres are shown. All four of them have a similar structure and the largest gap between the Wannier charge centres only performs a jump of 0.25 once between 0 and  $\pi$ . The blue lines do not take exactly the same form in the different cases which is a result of numerical errors and the symmetry at hand. The distance between the Wannier charge centres at the beginning is nearly the same in the lower half of the plot compared to the upper half. However, small numerical deviations

make it hard for the code to decide where the biggest gap is. As a result the blue line performs a jump of 0.5 in a), which of course has no influence on the topological invariants.

### 4.3.5 Variation of the interaction parameter $U$

This subsection deals with the physics arising due to increasing interaction energy in a topological insulator. With increasing interaction energy  $U$  a Mott transition takes place. Hence, a conducting material becomes insulating. Bismuthene, especially the  $p_x$ - $p_y$  two band model, without spin orbit coupling is a conducting material as can be seen in its band structure 4.3. Its density of states for zero interaction is similar to Graphene where the density goes to zero for zero frequency. However, there is no actual band gap since the filled states touch the empty states in the K-points of the Brillouin zone. The effect of an increasing  $U$  is shown in figure 4.20. It was essential to determine the density of states, since it best depicts the effects of a change in the  $U$  parameter. Unfortunately, the post-processing tools of TRIQS were not applicable to the results generated from the wannier90 calculations. Therefore,  $\sum_{\mathbf{k}}(\omega - H(\mathbf{k}))^{-1}$  was calculated and evaluated at frequencies  $\omega + i0^+$ , for the non-interacting case. The Hamiltonian  $H(\mathbf{k})$  is simply the hopping matrix from the DMFT input file. To take the interaction into account the real frequency self energy needs to be added to the Hamiltonian  $\sum_{\mathbf{k}}(\omega - H(\mathbf{k}) - \Sigma)^{-1}$ . To get the real-frequency self energy the Matsubara frequency self energy needs to be analytically continued. This procedure is done with the maxent-code provided by Kraberger, Triebl, Zingl and Aichhorn [41]. The maximum entropy method provides a good estimate of the self energy, however one can never be sure whether it provides the correct solution or not. After determining the best suited parameters the density of states can be plotted. From the evolution of density of states with increasing interaction parameter a Mott transition can be observed. In the DMFT-calculations, the Hund's coupling  $J$  was set to  $0.2U$  since it reduces the critical interaction parameter.

In figure 4.20 it can be seen that for increasing values of  $U$  the filled states and the empty states come closer to one another. When the interaction takes a critical value of roughly  $U = 14$ , the transition takes places and an insulating gap opens. For  $U = 14$  an additional small peak arises at zero frequency, however, since it is not possible to further improve the resolution, one cannot exactly tell whether this has a physical meaning or is just a numerical artefact

In the case of Bismuthene with spin-orbit coupling, the material already starts from a

band-insulating state. The procedure to determine the density of states is the same as before. With increasing interaction energy the material changes from being a topological insulator to becoming a Mott insulator. As observed in the trivial case, the states get closer to one another for increasing  $U$  and at a critical point the Mott transition takes place. Due to the non-trivial topology this transition occurs for much higher interaction energies, around  $U = 32$ . In a way, topology protects the material from becoming a Mott insulator

In figure 4.21 one can see a similar behaviour to the case without spin orbit coupling. At the critical  $U$  value the material density of states seems to be metallic, since there are a lot of states around zero frequency. However, due to the issues connected to analytical continuation, it is not guaranteed that the result at the transition represents the correct solution.

Since due to the large interaction the material becomes a Mott insulator, it obviously has to effect the topological  $\mathbb{Z}_2$  invariant. In order to prove this, one can apply the Z2pack on the DMFT results for different interaction values. In figure 4.22 it can be easily observed that the material is topologically non-trivial over a wide range of interaction energies. However, above the critical value near  $U = 32$  the topology in the Mott state is trivial with a vanishing  $\mathbb{Z}_2$  invariant. As already mentioned in the previous subchapter, with interactions at hand the topological effects are enhanced. This is also the reason why the Mott transition takes place for much higher interaction values than it does for Bismuthene without spin-orbit coupling. With increasing interaction also the effective SOC is increased and therefore, the topology is protected.



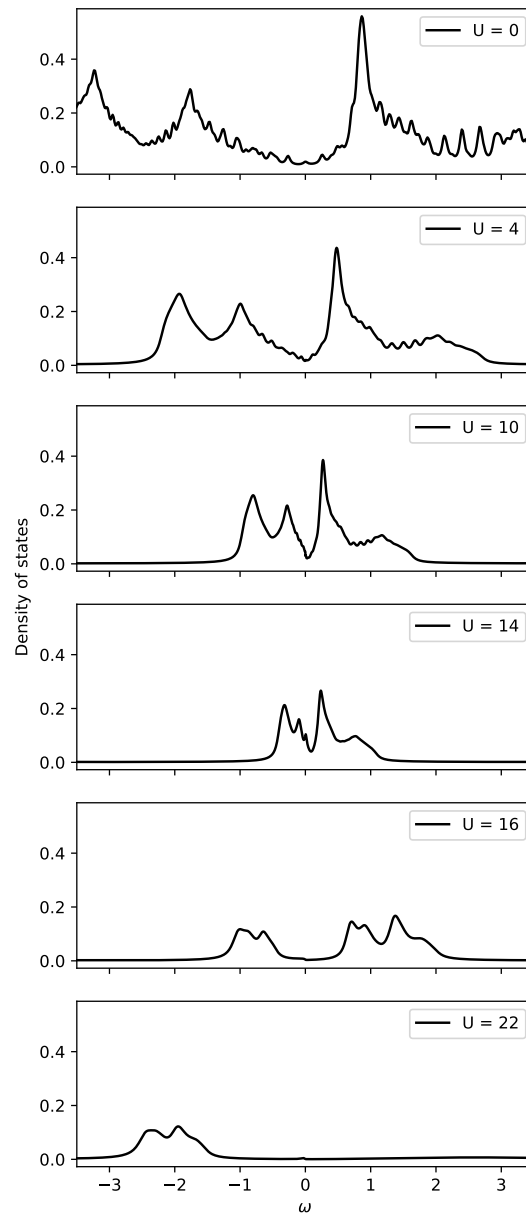


**Figure 4.20:** The density of states of Bismuthene without spin-orbit coupling plotted for increasing interaction values  $U$  and  $J = 0.2U$ .

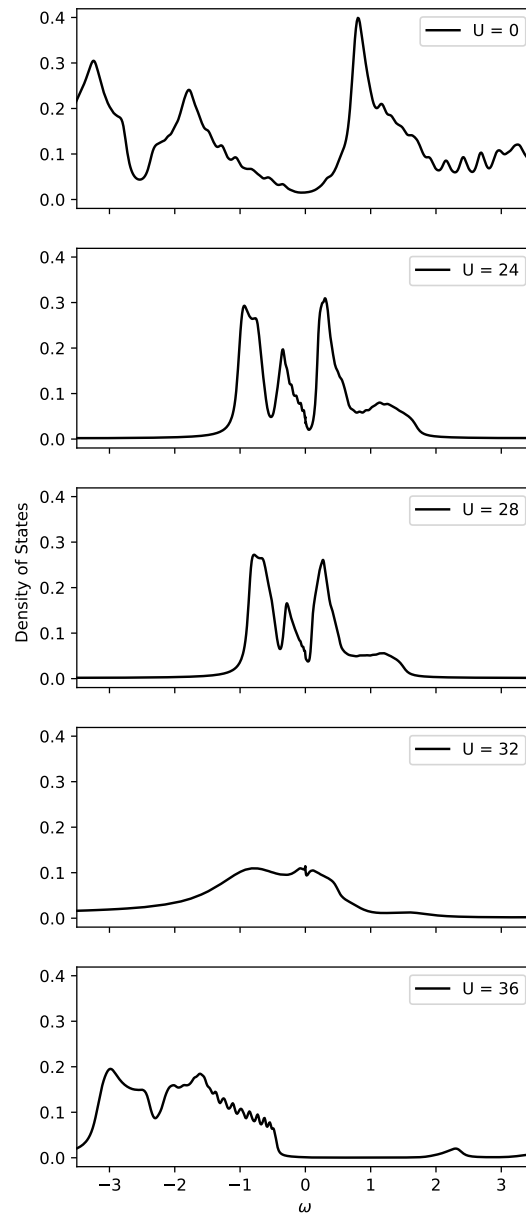


**Figure 4.21:** The density of states of Bismuthene with spin-orbit coupling plotted for increasing interaction values  $U$  and  $J = 0.2U$ .

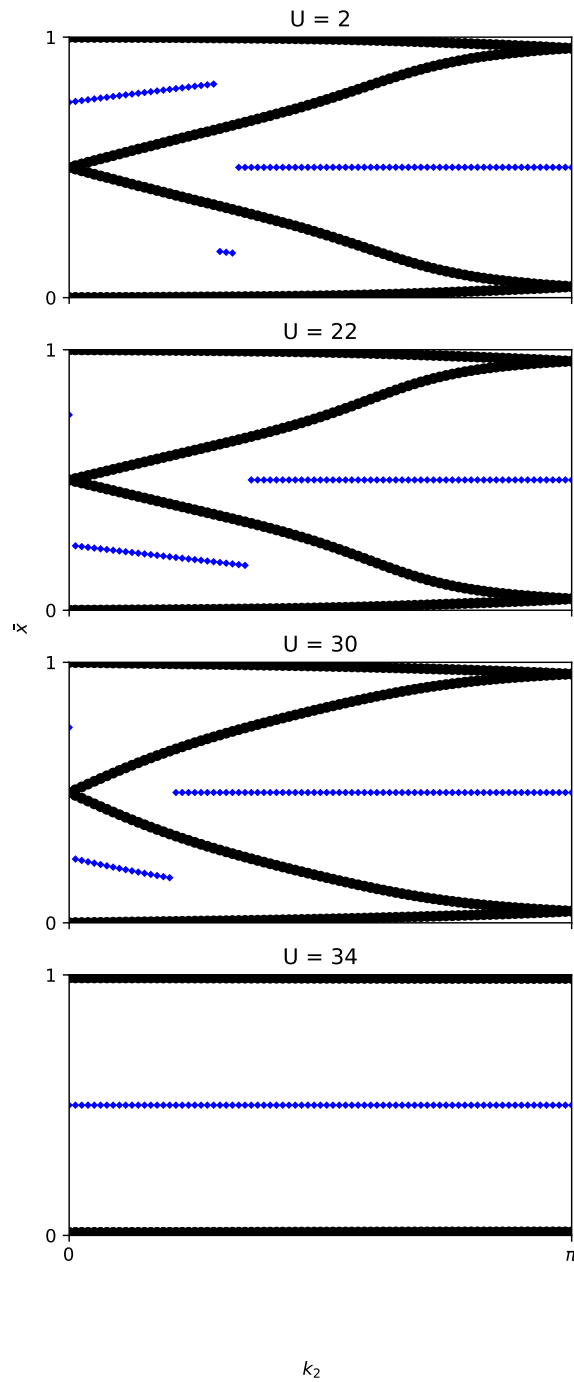


**Figure 4.22:** Wannier charge centers for increasing  $U$  values and  $J = 0.2U$ . Above the critical interaction parameter  $U = 32$  the topology becomes trivial.

# Conclusion

In this thesis the two band  $p_x$ - $p_y$ -model as an example of Bismuthene has been investigated. After setting up the prerequisites to perform the DFT + DMFT calculations with the help of the one band toy model, a two band model has been prepared. This was done by passivating a sheet of Bismuthene atoms with the help of additional Hydrogen atoms, that shifted the  $p_z$ -orbitals away from the Fermi level. As a result the  $p_x$ - $p_y$ -model is obtained.

The DFT+DMFT calculations of this model show that the bands are half filled, even though they are not symmetric around the Fermi level. This can be seen both in  $G(\tau)$  and in the density of states. The correlation effects due to electron-electron interactions are very small since the  $p_x$ - and the  $p_y$ -orbitals form hybrid orbitals. Only with artificially increased interaction parameter  $U$  one can observe a Mott transition. However, this transition occurs at interaction values only relevant in theory but not for the real material of Bismuthene.

When spin-orbit coupling is added to the two-band model, correlations start to become in a sense more relevant, since the effective SOC-constant also depends on the self-energy of the off-diagonal terms that arise due to SOC. Therefore, with larger electron-electron interaction the effective SOC gets bigger. With the spin-orbit coupling the system becomes topological non-trivial. This state is even further ensured when the interactions are increased. The system performs a Mott transition at a sufficiently large interaction parameter, however, this does not happen until the interaction parameter takes values that are no longer relevant to describe the nature of Bismuthene.

In this thesis two different approaches have been implemented to include SOC. Both ways, including SOC at the DFT-level or adding a local SOC-term to the Wannier Hamiltonian of a non-SOC DFT calculation, lead to very similar results in the DMFT calculations. They only differ in the magnitude of self-energy in the off-diagonals, which gives rise to different effective SOC parameters.

We used two different approaches to calculate the topological invariants of interacting systems. On the one hand the approach of using a non-interacting Hamiltonian and adding the self-energy obtained from DMFT calculations and on the other hand the method where the inverse impurity Green's function of a converged DMFT calculation is used as an interacting Hamiltonian. It was shown that the same results are obtained from both methods.

# Bibliography

- [1] Freitas R. R. Q., Rivelino R., de Brito Mota F., de Castilho C. M. C., Kakanakova-Georgieva A., and Gueorguiev G. K. Topological Insulating Phases in Two-Dimensional Bismuth-Containing Single Layers Preserved by Hydrogenation. *The Journal of Physical Chemistry C*, 119(41):23599–23606, 2015. ISSN 1932-7447. doi: 10.1021/acs.jpcc.5b07961. doi: 10.1021/acs.jpcc.5b07961.
- [2] F. Reis, G. Li, L. Dudy, M. Bauernfeind, S. Glass, W. Hanke, R. Thomale, J. Schäfer, and R. Claessen. Bismuthene on a SiC substrate: A candidate for a high-temperature quantum spin Hall material. *Science*, 357(6348):287–290, 2017. ISSN 0036-8075.
- [3] Gerd Czycholl. *Theoretische Festkörperphysik Band 1*. Springer Spektrum, 2016.
- [4] W. Kohn. Nobel Lecture: Electronic structure of matter—wave functions and density functionals. *Rev. Mod. Phys.*, 71:1253–1266, Oct 1999. doi: 10.1103/RevModPhys.71.1253. URL <https://link.aps.org/doi/10.1103/RevModPhys.71.1253>.
- [5] P. Hohenberg and W. Kohn. Inhomogeneous Electron Gas. *Phys. Rev.*, 136:B864–B871, Nov 1964. doi: 10.1103/PhysRev.136.B864. URL <https://link.aps.org/doi/10.1103/PhysRev.136.B864>.
- [6] W. Kohn and L. J. Sham. Self-Consistent Equations Including Exchange and Correlation Effects. *Phys. Rev.*, 140:A1133–A1138, Nov 1965. doi: 10.1103/PhysRev.140.A1133. URL <https://link.aps.org/doi/10.1103/PhysRev.140.A1133>.
- [7] Nicola Marzari, David Vanderbilt, Arash A. Mostofi, Jonathan R. Yates, and Ivo Souza. Maximally localized Wannier functions: Theory and applications. *Rev. Mod. Phys.* 84, 1419, 2012.

- 
- [8] Jacques Des Cloizeaux. Energy Bands and Projection Operators in a Crystal: Analytic and Asymptotic Properties.
- [9] Nicola Marzari and David Vanderbilt. Maximally localized generalized Wannier functions for composite energy bands.
- [10] Ivo Souza, Nicola Marzari, and David vanderbilt. Maximally localized Wannier functions for entangled energy bands.
- [11] Arash A. Mostofi, Jonathan R. Yates, Giovanni Pizzi, Young-Su Lee, Ivo Souza, David Vanderbilt, and Nicola Marzari. An updated version of wannier90: A tool for obtaining maximally-localised Wannier functions.
- [12] Gernot J. Kraberger. *Development of a full matrix ab-initio scheme for materials with strong spin-orbit coupling and Coulomb interactions*. PhD thesis, Graz University of Technology, 2018.
- [13] Robert Triebl. *Interplay of spin-orbit coupling and strong electronic correlations in multiorbital systems and topological insulators*. PhD thesis, Graz University of Technology, 2018.
- [14] Antoine Georges, Gabriel Kotliar, Werner Krauth, and Marcelo J. Rozenberg. Dynamical mean-field theory of strongly correlated fermion systems and the limit of infinite dimensions. *Rev. Mod. Phys.*, 68:13–125, Jan 1996. doi: 10.1103/RevModPhys.68.13. URL <https://link.aps.org/doi/10.1103/RevModPhys.68.13>.
- [15] Jamie H. Warner, Franziska Schäffel, Alicja Bachmatiuk, and Mark H. Rümmeli. *Graphene: Fundamentals and emergent applications*. 2013.
- [16] James D. Bjorken and Sidney D. Drell. *Relativistic Quantum Mechanics*. 1964.
- [17] Charles Lewis Kane. *Topological Insulators, Chapter 1 - Topological Band Theory and the  $\mathbb{Z}_2$  Invariant*. Elsevier, 2013.
- [18] M. V. Berry. Quantal phase factors accompanying adiabatic changes. *Proceedings of the Royal Society of London. A. Mathematical and Physical Sciences*, 392(1802):45-57, 1984.
- [19] Yoichi Ando. Topological Insulator Materials. *J. Phys. Soc. Jpn.* 82, 102001, 2013.

- 
- [20] Mahito Kohmoto. Topological invariant and the quantization of the Hall conductance. *Annals of Physics*, 160(2):343 – 354, 1985.
- [21] M. Z. Hasan and C. L. Kane. Colloquium: Topological insulators. *Rev. Mod. Phys.*, 82:3045–3067, Nov 2010. doi: 10.1103/RevModPhys.82.3045. URL <https://link.aps.org/doi/10.1103/RevModPhys.82.3045>.
- [22] Qian Niu, D. J. Thouless, and Yong-Shi Wu. Quantized Hall conductance as a topological invariant.
- [23] C. L. Kane and E. J. Mele. Quantum Spin Hall Effect in Graphene.
- [24] D. N. Sheng, Z. Y. Weng, L. Sheng, and F. D. M. Haldane. Quantum Spin-Hall Effect and Topologically Invariant Chern Numbers. *Phys. Rev. Lett.*, 97:036808, Jul 2006.
- [25] Liang Fu and C. L. Kane. Time reversal polarization and a  $Z_2$  adiabatic spin pump. *Phys. Rev. B*, 74:195312, Nov 2006. doi: 10.1103/PhysRevB.74.195312. URL <https://link.aps.org/doi/10.1103/PhysRevB.74.195312>.
- [26] Alexey A. Soluyanov and David Vanderbilt. Computing topological invariants without inversion symmetry. *Phys. Rev. B*, 83:235401, Jun 2011. doi: 10.1103/PhysRevB.83.235401. URL <https://link.aps.org/doi/10.1103/PhysRevB.83.235401>.
- [27] Robert Johannes Triebl. Wannier charge centers and the calculation of topological invariants: Application to the Kane-Mele-Hubbard model. Master’s thesis, Graz University of Technology, 2015.
- [28] V. Gurarie. Single-particle Green’s functions and interacting topological insulators. *Phys. Rev. B*, 83:085426, Feb 2011.
- [29] Zhong Wang and Binghai Yan. Topological Hamiltonian as an exact tool for topological invariants. *Journal of Physics: Condensed Matter*, 25(15):155601, mar 2013.
- [30] Zhong Wang, Xiao-Liang Qi, and Shou-Cheng Zhang. Topological invariants for interacting topological insulators with inversion symmetry.
- [31] Zhong Wang and Shou-Cheng Zhang. Simplified Topological Invariants for Interacting Insulators.



- [32] FIZ Karlsruhe Leibnitz-Institut für Informationsinfrastruktur GmbH. Online, April 2019. URL [http://www2.fiz-karlsruhe.de/icsd\\_legal\\_notices.html](http://www2.fiz-karlsruhe.de/icsd_legal_notices.html).
- [33] John P. Perdew, Kieron Burke, and Matthias Ernzerhof. Generalized Gradient Approximation Made Simple. *Phys. Rev. Lett.*, 77:3865–3868, Oct 1996. doi: 10.1103/PhysRevLett.77.3865. URL <https://link.aps.org/doi/10.1103/PhysRevLett.77.3865>.
- [34] P. Blaha, K. Schwarz, G. K. H. Madsen, D. Kvasnicka, J. Luitz, R. Laskowski, F. Tran, and L. D. Marks. *An Augmented Plane Wave + Local Orbitals Program for Calculating Crystal Properties*. WIEN2k. 2018. ISBN ISBN 3-9501031-1-2.
- [35] G. Kresse and J. Furthmüller. Efficient iterative schemes for ab initio total-energy calculations using a plane-wave basis set.
- [36] G. Kresse and D. Joubert. From ultrasoft pseudopotentials to the projector augmented-wave method.
- [37] Priyanka Seth, Igor Krivenko, Michel Ferrero, and Olivier Parcollet. TRIQS/C-THYB: A continuous-time quantum Monte Carlo hybridisation expansion solver for quantum impurity problems. *Computer Physics Communications*, 200:274–284, 2016. ISSN 0010-4655. doi: 10.1016/j.cpc.2015.10.023. URL <http://www.sciencedirect.com/science/article/pii/S001046551500404X>.
- [38] Markus Aichhorn, Leonid Pourovskii, Veronica Vildosola, Michel Ferrero, Olivier Parcollet, Takashi Miyake, Antoine Georges, and Silke Biermann. Dynamical mean-field theory within an augmented plane-wave framework: Assessing electronic correlations in the iron pnictide LaFeAsO. *Phys. Rev. B*, 80:085101, Aug 2009. doi: 10.1103/PhysRevB.80.085101. URL <http://link.aps.org/doi/10.1103/PhysRevB.80.085101>.
- [39] Dominik Gresch, Gabriel Autès, Oleg V. Yazyev, Matthias Troyer, David Vanderbilt, B. Andrei Bernevig, and Alexey A. Soluyanov. Z2Pack: Numerical implementation of hybrid Wannier centers for identifying topological materials. *Phys. Rev. B*, 95:075146, Feb 2017. doi: 10.1103/PhysRevB.95.075146. URL <https://link.aps.org/doi/10.1103/PhysRevB.95.075146>.

- 
- [40] Alexey A. Soluyanov and David Vanderbilt. Computing topological invariants without inversion symmetry. *Phys. Rev. B*, 83:235401, Jun 2011. doi: 10.1103/PhysRevB.83.235401. URL <https://link.aps.org/doi/10.1103/PhysRevB.83.235401>.
- [41] Gernot J. Kraberger, Robert Triebl, Manuel Zingl, and Markus Aichhorn. Maximum entropy formalism for the analytic continuation of matrix-valued Green's functions. *Phys. Rev. B*, 96:155128, Oct 2017.